Innovative Method dedicated to the development of a ferrite-pearlite grade regarding its MAChinability

(IMMAC)

FINAL REPORT

European Commission

Research Fund for Coal and Steel

Innovative Method dedicated to the development of a ferrite-pearlite grade regarding its MAChinability

(IMMAC)

Enrico D'Eramo, Amandine Roth
ASCO INDUSTRIES - Avenue de France, FR-57301 HAGONDANGE CEDEX

Sébastien Allain
INSTITUT JEAN LAMOUR (UNIVERSITÉ DE LORRAINE) - 2 allée André Guinier, FR-54011 NANCY CEDEX

Diego Herrero Villalibre, Jacinto Albarran
SIDENOR INVESTIGACIÓN Y DESARROLLO S.A. - Barrio Ugarte s/n, ES-48790 – BASAURI

Mustapha Abouridouane
RHEINISH WESTFAELISCHE TECHNISCHE HOCHSHULE AACHEN - Templergraben 55, DE-52062 AACHEN

Pedro J. Arrazola, Daniel Soler, Patxi X. Aristimuno,
Mikel Saez de Buruaga, Inaki M. Arieta
MONDRAGON GOI ESKOLA POLITEKNIKOA - Loramendi 4, ES-20500 ARRASATE/GIPUZKOA

Eva Butano, Flavia Gili, Valter Polignano
CENTRO RICERCHE FCA - Strada Torino 50, IT-10043 ORBASSANO

Cédric Courbon, Joël Rech
ECOLE NATIONALE D'INGENIEURS DE SAINT ETIENNE - Rue Jean Parot 58, FR-42023 SAINT ETIENNE CEDEX 2

Taina Vuoristo, Niclas Stenberg
SWEREA KIMAB AB - Isaf Jordsgatan 28A, SE-16407 KISTA

Final report

Directorate-General for Research and Innovation

<p style="text-align:center">Table of contents</p>

1. <u>Final summary</u>

Ferrite-pearlite (FP) steels are the most common material for engineering and automotive industries (gear box parts, crankshaft, connecting rods, injection parts…). Without any extensive research, considering the different morphology of ferrite-perlite possible to achieve, it may be assumed that the machining performances are highly dependent on the FP parameters. Nevertheless, even now, we observe larger tolerances on requirements specification on FP steels which cause variability on microstructure morphology not always perceptible with standard metallurgical characterizations.

In some case, the technical specification causes complex customer complaints between steelmakers and their customers: the microstructure seems as expected but unacceptable variability in machinability is observed. IMMAC project aims to develop a numerical method to predict the machining performances of designed FP steels depending on their microstructural parameters; and to use this method as a flexible steel development strategy to better design the machinability-improved grades tailored according to the part and its machining range. Three cutting technologies were studied: turning, drilling and broaching. The figure below shows a scheme of the research approach with proposed work packages (WP) interrelation. D0, D1 and D2 are main deliverables of the project.

Research approach of the project
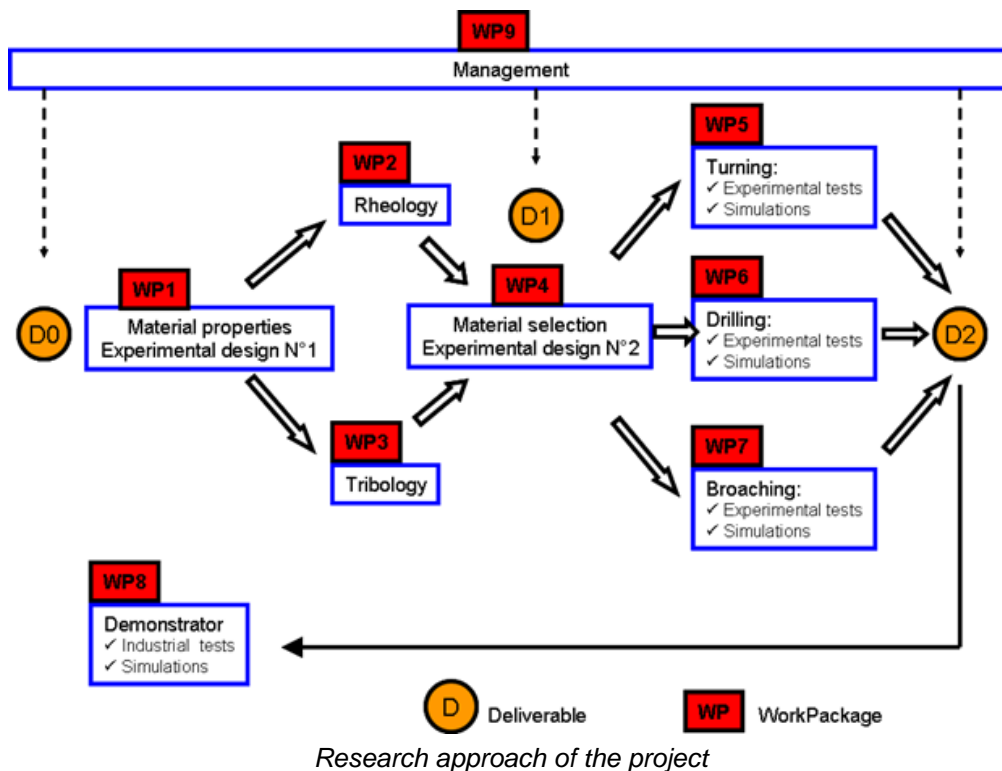
WP1: Steel manufacturing - metallurgical analysis for experimental design N°1

Objectives:
- Manufacturing of required steels variants for experimental design N°1
- Fine description of microstructures of steel variants to have useful metallurgical data which will be exploited in the machining and the modelling works.
- Thermal properties of steel variants and tool materials which will be used in modelling tasks.

TASK 1.1 Steels selection & manufacturing for experimental design N°1:

Four steel grades (16MnCr5, 27MnCr5, C45 and C60), each of them in different microstructural states obtained after the corresponding heat treatment were produced. Additionally, C70 after an isothermal annealing was also considered as example of 100% pearlitic steel. Taking into consideration that, among the considered heat treatments, the only standardized ones are the isothermal and globular annealing, the other two had to be experimentally designed before their industrial execution.

TASK 1.2 Steel variants heat treating for experimental design N°1:
The heat treatments were performed to achieve the following microstructural characteristics in the steel:
- **R**: reference microstructure with homogeneous ferrite-pearlite (FP) distribution (isothermal annealing); well-done considered for each steel.
- **CG**: FP microstructure with coarser pearlite grains (modified isothermal annealing); big pearlite grains for C45 and C60; association of small pearlite grains and big pearlite grains for 16MnCr5 and 27MnCr5
- **GP**: FP microstructure with a significant percentage of globular pearlite (modified isothermal annealing or globular annealing); well-done considered , except for steel 27MnCr5
- **WB**: FP microstructure with a high banding level (modified isothermal annealing); well-done considered, except for steel 27MnCr5

The table below shows the codification of each steel variant applied in the project:

STEEL GRADES	STRUCTURE STATUS			
	Standard	Coarse pearlite grain	Globular pearlite	With more bands
16MnCr5	16R	16CG	16GP	16WB
27MnCr5	27R	27CG	27GP	27WB
C45	45R	45CG	45GP	45WB
C60	60R	60CG	60GP	-
C70	70R			

TASK 1.4 and 1.6 Chemical composition and inclusion studies
The chemical composition was analysed in all the variants in order to identify any difference that could lead to dissimilar machinability performances. The inclusions population showed that about 90% of the total amount of inclusions was MnS. The differences in the Al contents observed between the steels produced by Sidenor (C45 and C60) and Ascometal (16MnCr5 and 27MnCr5) are due to the different deoxidation process followed by each steelmaker, based in Si addition (Sidenor) or in Al addition (Ascometal). This information can partly explain the results obtained in the turning tests where the performance of the reference C45 (45R) was a little bit better than expected (task 5.2).

TASK 1.5 Microstructural studies
A large amount of work was dedicated to perform a detailed assessment of all the useful microstructural aspects of the manufactured FP steels variants in order to be considered in the machining and modelling tasks: %ferrite, % lamellar pearlite, % globular pearlite, ferrite and pearlite grain size, and interlamellar spacing of pearlite (two tables below).

Variants	% ferrite	%lamellar perlite (LP)	% globular pearlite (GP)	Ratio GP/LP (%)	Interlamellar spacing / std deviation (nm)	Ferrite grain size (µm)	Bands
16R	58	37	5	12	190 / 65	10	B
16CG	56	33	11	25	222 / 65	12	B
16GP	53	12	35	75	204 / 69	12	A-B
16WB	59	35	6	15	146 / 41	12	B
27R	40	54	6	10	285 / 74	14	B
27CG	52	43	5	10	229 / 59	15	B
27GP	45	55	0	0	197 / 56	12	B
27WB	44	56	0	0	202 / 51	12	B
45R	25	56	19	25	293 / 82	17	A
45CG	15	81	4	5	366 / 170	30	A
45GP	10	0	90	100	632 / 192	10	n/a
45WB	20	64	16	20	326 / 116	19	B-C
60R	14	65	21	24	372 / 135	11	A
60CG	6	89	5	5	306 / 79	17	A
60GP	14	21	65	75	623 / 186	10	n/a
70R	0	100	0	0	206 / 70	-	-

Pearlite grain size (P GS):

P GS (µm)	16MnCr5	27MnCr5	C45	C60	C70
R	13-15 few 22	15 few 89-177	22-27 and 62-89	31 and 62	-
CG	< 11 few 31-62	11 few 62-89	76-89	125-500	-

TASK 1.7 Mechanical properties

The main mechanical properties of the steels were also tested. Coherent values of hardness, toughness and strength were obtained for all the evaluated variants.

TASK 1.8 Thermal properties of steels and cutting tools

The thermal characterization of the selected steels and the tool materials used were developed. The following properties were studied: specific heat, density, thermal diffusivity and thermal conductivity. Overall, similar trends were observed for each of the characterized thermal properties for all the variants.

Due to the different cutting technologies studied in the project, thermal properties of two tool materials were characterized: a high speed steel material referring to broaching studies, and a tungsten carbide material referring to turning and drilling studies. The evolutions of thermal properties regarding temperature are very different. All these data will be employed in Finite Element models in order to better predict heat flow and temperature distribution, in one hand, for the chip and workpiece, and on the other hand, in the cutting tool.

WP2: Rheology – indentification of constitutive models

Objectives:

The ultimate objective of WP2 was to propose a rheological model that describes the deformation behavior of the studied steels variants at strain rates and temperatures relevant to three different machining operations; in order to take into account the impact of microstructure variations in machining simulations. To achieve that goal, a vast experimental campaign was performed on the different steel grades studied in the project. The objective was to obtain a large amount of rheological data that allow improving the understanding of deformation mechanisms of the steels as well as the influence of the different microstructural parameters for an accurate identification of the model parameters.

Task 2.1 Definition of the matrix of the tests

For development of the rheological model, an extensive testing program including compression Gleeble testing at strain rates between $0.5 \ s^{-1}$ and $50 \ s^{-1}$; compression Split Hopkinson Pressure Bar (SHPB) testing at strain rates between 500 and $5000 \ s^{-1}$ as well as tensile testing at about $1 \ s^{-1}$ was developed and carried out. Room temperature, 500 and 680 °C were chosen as temperatures for all the strain rates. The above testing parameters were validated by the partners in charge of the process modeling to be relevant with machining operations studied, and taking into account the limitations of testing devices.

Task 2.2 and 2.3 Characterization of steel behaviour for low, medium and medium strain rates

The experimental results from WP2 include very extensive characterization of the mechanical behavior of the steel grades and their microstructural variants with a more than 300 combinations of material, temperature and strain rate. A phenomenon that was observed in the results was Dynamic Strain Aging (DSA) that is evidenced by the rather anomalous temperature dependence of flow stress.

Task 2.4 Identification of the parameters of the constitutive model

A constitutive model based on the microstructure-based behavior law developed for composite ferrite-lamellar pearlite steels by Bouaziz et al. and the physically-based description of the strain rate sensitivity of ferritic steels proposed by Allain et al. was developed in this work.

The model takes into account the abovementioned deformation mechanisms and the microstructural parameters for an accurate description of the main tendencies of experimental data. Model parameters for each steel grade and microstructural variant based on the experimental data were identified. The developed model has been implemented using Excel and allows an easy extraction of interesting values as an input in finite element models for cutting simulations. The model also contains a term to account for the DSA. The main inaccuracies regarding the model are the applicability at high plastic strains that lack experimental data or at high temperature where the experimental data is affected by thermal (adiabatic) softening.

Conclusions

The characterization of the thermo-mechanical behavior and modeling work made in WP2 of IMMAC Project were a keystone for the work done in subsequent WPs. A huge amount of data emerged from the experimental characterizations. The data has been treated to extract the most representative configurations of cutting conditions. Besides, the interesting feature of Dynamic Strain Aging (DSA) has been highlighted in the behavior of all the steel grades.

The rheological model developed in this project shows good results and is successful to capture the main tendencies of the experimental data taking into account the microstructure of the steel grades. However some improvements can be considered for a better agreement with the experimental data. The influence of the strain rate on the flow stress could potentially be improved with an adapted description of the homogenization law at low and high strain rate. By the way, to be able to accurately describe the influence of temperature, softening should be taken into account including a deeper analysis of the microstructure during and after the compression tests.

The experimental results obtained can be used for further development of constitutive equations to describe viscoplastic behavior of ferritic pearlitic steels. The material models developed in the project can be used to model different machining processes to evaluate the effect of microstructure on the process parameters.

WP3: Tribology – identification of contact laws

Objectives:
- Identify the effect of the microstructure on the tribological properties of the investigated variants.
- Investigate friction coefficients, heat partition and wear tendency under a large range of contact conditions corresponding to the targeted processes.

Task 3.1 Experimental tests in dry conditions

The first experimental campaigns were performed on an open tribometer under dry conditions and relevant ones compared to those existing in a turning and broaching process. These experiments were important as they provided the first fundamental data regarding the effects of a given microstructure on the tribological behaviour without the effect of a third body at the interface (lubricant).

In a turning context, they highlighted that friction is drastically dependent on the sliding velocity and decreases when increasing the sliding velocity. Moreover, it was shown that changing the microstructure to coarser pearlite grains (CG) reduces friction whereas a globular pearlite (GP) or a banded structure (WB) tends to increase it at low and medium sliding velocity. Sliding velocity was found to be the main parameter affecting heat transfer at the contact interface.

In a broaching context, applying a TiN coating on the pin significantly improve the friction stability and lower the friction level and remained the main influencing factor. Sliding velocity slightly affected the frictional behaviour over the selected range.

Task 3.2 Contact mechanisms

In order to understand how the microstructure could affect the tribological behaviour, contact zones on the pins and contact tracks on the workmaterials were analysed on the "turning oriented" tribological tests. Optical microscopy revealed that low carbon variants lead to less stable frictional behaviours at low sliding velocities. Transfer mechanisms were thoroughly analysed on the tests performed at high sliding velocity using Energy Dispersive X-ray spectrometry (EDX) as friction values were really similar from one variant to another (around 0.22) whereas the morphology of the contact areas was significantly different. These analyses proved that the ferrite ratio is the key parameter governing the adhesion tendency of a given grade.

Task 3.3 Mechanical and thermal models

In this task, the objective was to identify contact models that could be later implemented in the different numerical models developed in WPs 5-6-7.

Results obtained in Task 3.1 were plotted versus several microstructural parameters. The most relevant one appeared to be the ferrite ratio. A clear trend could be extracted and showed that friction coefficient clearly increases when increasing the ferrite content. This effect was however limited when increasing the sliding velocity.

This task resulted in the development of three key contact models: (i) two friction models relating the friction coefficient to the sliding velocity and ferrite content in dry turning and dry broaching conditions, (ii) a heat partition model only depending on the sliding velocity in dry turning conditions.

Task 3.4 Influence of lubricant

The tribological investigations performed in this task were related to the broaching process under straight oil and the drilling process under Minimum Quantity Lubrication (MQL). Consistent material pairs (substrate/coating) were selected accordingly to the targeted process.

In both campaigns the use of a lubricant drastically reduces the friction level and completely erases the differences between the variants, proving the larger contribution of the lubricant.

In a drilling context, larger pin wear was detected when increasing the carbon content under the higher velocities (> 150 m/min).

From a more scientific point of view, the work done in this WP3 improved the fundamental understanding of the tribological behaviour of FP steels variants studied. Nevertheless, important aspects such as local wear and material transfer phenomena would have deserved more time than what was possible, but it emphasized several promising perspectives.

WP4: Steel manufacturing and testing devices for experimental design N°2

Main objectives:
- Selection and production of steel variants
- Definition of tools and cutting parameters.

Task 4.1 Production process analysis
With information given by FCA and state of the art, the manufacturing line were analyzed in term of machining operations, parameters, cutting tools and lubricant, in order to define the laboratory tests in the WPs 5-6-7. For turning and drilling, the cutting conditions replicate those applied on a crankshaft. For broaching, the cutting conditions are representative to those applied on a steering rack.

Task 4.2 Selection of tools and cutting conditions

Cutting operation	Tool	Lubricant conditions	Task concerned	Leader
Turning	Coated cemented carbide	Dry	5.2	SIDENOR
			5.3	MGEP
Drilling	Coated cemented carbide	Emulsion 10%	6.2	WZL
Broaching	Coated and uncoated HSS	Dry and Oil	7.2	ENISE

Task 4.3 Steel variants selection for machining tests
Taking into account the results of Deliverable D1 (work on WPs 1,2 and 3), we selected 8 steel variants that demonstrated interesting rheological and/or tribological and/or thermal mechanisms. The tables below summarize the selection of variants and the microstructural impacts studied:

STEEL GRADES	STRUCTURE STATUS			
	Standard	Coarse pearlite grain	Globular pearlite	With more bands
16MnCr5	16R	-	16GP	-
27MnCr5	27R	-	-	-
C45	45R	-	45GP	45WB
C60	60R	60CG	-	-

Microstructures	Impacts	Machining operation to observe close up
16R – 27R – 45R – 60R	Ferrite/pearlite ratio	All
16R – 16GP	Pearlite in a way of globulization	Broaching
45R – 45GP	High globalization of pearlite	Drilling and turning
45R – 45WB	Bands	All
60R – 60CG	Pearlitic grain size	Drilling
16GP – 45GP	Level of pearlite globulized	All

Task 4.4 Steel variants manufacturing and heat treatment for experimental design N°2
For each steel variant selected, it was necessary to treat additional bars from the heats produced in the quantity required for each specific machining characterisation.

Task 4.5 Material supply
Initially, it was planned to study 6 steel variants for experimental design N°2. As we decided to select 2 added variants, the delivery of these steel variants has been delayed.

WP5: Turning operation

Main objectives:
- Experimental tests in 3D and 2D turning
- 2D fundamental studies of chip formation process
- 2D modelling investigations taking into account FP microstructure parameters

Task 5.1 2D Finite Element Numerical FE model
An orthogonal 2D cutting model under the Arbitrary Lagrangian Eulerian (ALE) formulation was developed for the machinability prediction. The input parameters, the flow stress model and the friction behaviour, were set depending on the composition of the steels and the microstructure parameters of ferrite-pearlite fraction, interlamellar spacing and ferrite grain size.

The proposed numerical model was able to predict the main trends observed in the empirical orthogonal tests. However, there were still large gaps in the quantitative prediction of variables such as contact length and feed forces. Nevertheless, this seemed reasonable, as experimentally the measured contact length corresponds to that of the maximum length, in which the full contact and the stick-slip of the chip are considered, and in the FE model this stick-slip effect is not simulated. A further improvement of the flow stress at the high temperature domain might also help to improve this under predictions. Despite this drawback, the prediction of non-measurable variables such as contact pressures and shear stresses were identified to be accurate when evaluated with the weighted point method and when compared to experimental evaluations.

Task 5.2 Machinability tests in turning
Eight FP steel variants were chosen to evaluate the machining during turning operation (standard wear test ISO 3685 – V20 index). Comparing the results of these tests, the influence of the main microstructural aspects on the machinability was established. It was observed that the main metallurgical parameters driving the V20 value is the macro hardness obtained in the steel variants after the different heat treatments; % Carbon, %lamellar pearlite, %globular pearlite and pearlite grain size play an important role; the higher the hardness, the lower the V20 value is. The dominating wear mechanism is abrasion. A machining ranking was created in order to be compared with the results provided by the turning simulation and thus validate the developed model.

Task 5.3 Fundamental study of chip formation process
Two techniques were developed for a scientific analysis of the cutting process, both in orthogonal cutting conditions. The first consisted of an advanced orthogonal cutting set up to analyse the influence that the steels grades and variants had on cutting and feed forces, tool side temperature, chip thickness and tool chip contact length. The second approach was mainly focused on the high-speed filming of the orthogonal cutting with the objective of measuring the strain and strain rates occurred in cutting region. These results were related to the abovementioned machinability tests.

Concerning the fundamental variables, in general, clear differences among variants were only observed for the C45 and C60 grades. The most significant differences between grades, and between the variants of the C45 and C60, were observed in chip thickness, tool-chip contact length and feed force measurements. It is worth noting that the measurements of cutting forces did not differ between all the 16 tested steels. Thus, it was suggested that the calculation of average contact pressures could be a better indicator to test machinability.

The ferrite-pearlite fraction, which was linked to C (carbon) content, was identified as the most influencing microstructure property. From the macroscopic point of view, CG and GP were the variants that differ in a greater manner from the standard grade.

The high-speed filming of the chip formation while orthogonal cutting presented several difficulties. Although the obtained images where of high quality, the deformations in the shear zone were so significant that avoided measurements on the primary shear zone. Some improvements were proposed for future essays such as lens with higher depth of field or the use of two cameras that would enable the measurement of the deformation in the transversal axis.

Task 5.5 Tool wear and tool-chip contact zone studies in turning
The tool-chip contact length on the rake face side of cutting tools was obtained by orthogonal face turning tests. The motivation of the work was to provide further understanding of the material dependent chip curl of the steels included in the project. At first glance the tool-chip contact numbers are linked to the steel hardness. That can be explained by the belief that the tool-chip contact zone reflects the chip curl, which in turn relies partly on the chip temperature. The more heat that is generated in the secondary shear zone of the tool-chip contact the more curls the chip gets, due to the thermal expansion of the underside, as compared to the not sheared upper side of the chip.

Task 5.6 Machinability prediction
A weighted point evaluation method was assessed to give accurate machinability predictions. This was tested from both empirical and numerical point of view, and was validated through the comparison of experimental machinability V20 tests carried out in task 5.2. The evaluation resulted in the following machinability ranking: 16R, 45GP, 27R, 45R, 45CG, 60R.

WP6: Drilling operation

Objectives:
The main objective of WP6 is the development and validation of a microstructure based computation tool capable to predict and optimize the machinability of ferritic-pearlitic steels by drilling including:

- Determination and classification of the machinability of ferritic-pearlitic steels in drilling tests:
  - Quantification of cutting phenomena that occur during drilling process (chip formation, feed force, cutting torque, tool wear mechanisms, …)
  - Machinability classification by means of the weighted point evaluation method
  - Determining a correlation between the microstructure and the machinability
- Development and validation of 3D FE models for twist drilling ferritic-pearlitic steels:
  - Modelling investigation at the macro range (drill diameter d = 8 mm, isotropic material model)
  - Modelling investigation at micro range (drill diameter d = 1 mm, heterogeneous material model)
- Optimisation criteria for ferrite-pearlite microstructure design derived from cutting simulation with respect to higher machinability performance.

Task 6.1 Modelling investigation at the macro range
A 3D FE computation model for twist drilling at the macro has been developed and successfully validated for the ferritic-pearlitic grades selected: 16R, 27R, 45R, 45CG, 45GP and 60R. The developed FE model can predict the drilling process values feed force, cutting torque, chip compression ratio, maximal normal pressure and temperature (on the rake face of the tool), which will be used to compute the machinability of the investigated grades.

Task 6.2 Machinability of ferritic-pealitic steels in twist drilling tests
The Machinability of the investigated grades is characterized by means of tool life tests:
- The pearlite volume fraction controls in a nice manner the cutting forces when drilling the reference grades 16R, 27R, 45R and 60R.
- The grades with globular pearlite (GP) show the highest values of feed force and torque due to the dominant material adhesion on the tool cutting edge during drilling.
- The feed force and cutting torque increase with the number of the drilled holes due to the progressive wear of the used drill.
- Regarding the chip form, independent of the drilled grade, short chips are detected and the chip size decreases with the volume fraction of pearlite.
- The tool flank wear of the used drills correlates well with the measured torque and is more pronounced in the case of the more ductile steel variants 45GP, 60GP and 16R due to the formation of material adhesion.
- The wear behavior of the cutting edges is controlled by the wear mechanism abrasion when drilling the reference grades 27R, 45R and 60R. This abrasive wear has led to coat spalling on the cutting edge. In the case of the grades 45GP, 60GP and 16R, the dominating wear mechanism is, as expected, adhesion.

Task 6.3 Machinability classification by means of the weighted point evaluation method
The classification of the machinability when drilling of the investigated grades 16R, 27R, 45R, 45CG, 45GP and 60R is performed by means of the weighted point evaluation method:
- The evaluation results in the following machinability ranking: 45R, 27R, 45CG, 60R, 16R, 45GP.
- The ranking of the first 4 variants is obtained by the wear mechanism abrasion. The variant 45R with moderate lamellar pearlite content (56%) shows the best machinability.
- The variant 16R and 45GP with predominant adhesion wear mechanism show the worst machinability.

Task 6.4 Determining correlation between the microstructure and the machinability
Based on the machinability classification (Task 6.3) and the results performed in WP1, a qualitative correlation between microstructure and machinability could be deduced.

Task 6.5 Modelling investigation at the micro range
The quality of the developed material and friction laws has been checked successfully by drilling at the micro range.

Task 6.6 Indentification of the microstructure parameters driving the machinability performances in drilling
The machinability of the investigated grades could be empirically and numerically predicted and compared with the experimental measured machinability:
- The microstructural parameters driving the machinability performance in drilling are the pearlite volume fraction, the pearlite grain size, the pearlite interlamellar spacing and the globular pearlite volume fraction.

- An empirical formulation for the machinability has been developed based on the microstructure.
- A machinability index could be defined with help of the weighted point evaluation method.
- Both the FE drilling simulation and the empirical model predict adequately the machinability classification of the investigated grades.

WP7: Broaching operation

Main objectives:
- Mechanical behavior and machinability determination of FP steels in broaching tests
- Development and validation FE models for broaching FP steels taking into account FP microstructure parameters

Task 7.1 2D/3D modelling
The broaching process can be seen as a plane strain deformation process. The difference between 2D assumptions and 3D actual situation is smaller than in other processes like longitudinal turning and drilling. Thus, a 2D ALE model was developed to perform the broaching simulations. It enables a more physical material separation around the tool cutting edge without damage or element deletion compared to the model developed during the first year. Most of all, the same approach is used in WP5 by MGEP allowing a joint work on the modelling part and leading to an interesting and relevant comparison between results from WP5 and WP7. Data from WP2 and WP3 were implemented and consistent numerical outputs were defined to be compared with the experimental data.

Task 7.2 Experimental broaching device
A dedicated experimental set-up fitted on a 3+1 axis machine was used and upgraded to investigate broaching in a "simplified" configuration. A strain gauge dynamometer was used to record online the machining forces. A holding system was developed to set a microscope or more advanced camera (high speed or infrared) in front of the cutting tool. Following preliminary tests, a second version of the set-up had to be designed as the spindle and corresponding slidings were not stiff enough to avoid a slight bending of the workmaterial specimen leading a fluctuating depth of cut, unstable cutting phenomena and a high deviation on the results. High speed imaging under those conditions did not make sense and had to be stopped. Instead, chips were carefully collected and analysed and roughness of the machined surface was measured for each experiments.

Task 7.3 Influence of microstructural parameters
This task aimed at determining the influence of different microstructural parameters on the macroscopic outputs of the broaching process, i.e. machining forces, chip curvature and breakability as well as surface roughness. Experiments were carried out under dry and lubricated conditions using 3 different tool configurations: an uncoated broaching tool, a fully TiN coated tool and a partially TiN coated (flank only) tool mimicking an industrial broaching tool.
In dry conditions, surprisingly, forces and roughness were found to increase as the ferrite content increases. Increasing the ferrite content has been proved to increase friction and adhesion at the tool-chip interface, showing an interesting correlation with the WP3 findings. This is confirmed by the fact that, as the lubricant is applied, both forces and roughness drastically decrease. However, if the effect of the coating is relatively weak under dry conditions, the combination of fully coating and lubricant have a major effect leading to the lowest cutting force and Ra roughness.

Task 7.4 Cutting mechanisms
Chips were collected during the previous experiments, embedded in resin, polished, etched and analysed. The objective was to observe the deformed microstructure and measure the average chip thickness. The microstructure was found to be highly deformed with, even under lubricated conditions, an intense shear occurring at the tool-chip interface. A pronounced serration was visible on the globular pearlite GP variant which was related to the amplified sticking behaviour characterising these type of microstructure as seen in WP3. Increasing the ferrite content increases the chip thickness under dry conditions whatever the tool configuration. The GP variants exhibited the thickest chips, whereas using a lubricant limited it to a threshold value whatever the ferrite content. Both findings were in good agreement with the findings from WP3 (larger friction) and proved the important contribution of the tribological aspects in broaching.

Task 7.5 Microstructural parameters driving broaching
This task was devoted to the correlation between the numerical and the experimental results in order to identify the influential parameters and the capability of the simulation to take them into account. The weighted point evaluation method proposed in Task 6.3 was applied to assess the agreement level between the simulation and the experiments on the selected variants. If large discrepancies were observed regarding the 16R and to a lower extent the C45GP, the simulation was in good agreement as far as the other variants were concerned. The evaluation resulted in the following machinability ranking: 60R, 45CG, 45R, 27R, 45GP, 16R. For grade C45, the model was able to predict the main trends when changing from a R to CG and R to GP microstructure.

It emphasized the remaining challenge: to properly model the tribological behaviour of FP steels under so complex conditions leading to a predominant contribution of adhesion and material transfer, difficult to implement in the modelling.

WP8: Demonstrator

Main objectives:
- Dissemination : establish an appropriate communication of the project results
- Machining tests: perform industrial tests on an optimized FP microstructure steel variant and on damaged FP microstructure variants
- Validation of the numerical approach: compare the machinability classification obtained with industrial tests, with the machinability classification obtained with the numerical simulations.

Task 8.1 Dissemination

One of the objectives of WP8 was to establish an appropriate and effective communication of the project works, developments and results to potential users and interested parties. The dissemination of the project results were undertaken by all consortium partners. The goal of the dissemination was to create a series of actions able to share IMMAC challenge, approach and results during the project and beyond to appropriate stakeholders. Publications in scientific journals and the project site, presentations at international and national scientific conferences, congress, seminars and the final Workshop in CRF at the end of the project represented effective tools to disseminate. The Workshop, in particular, took place at Centro Ricerche FCA on November 29th,2017, during which there was space for comments and speeches from the different guests as tool supplier (Walter, Sandvik, Guhring), Academia (Arts et Métiers de Cluny, Ecole Nationale Supérieure des Mines de Nancy), industries (CIE automotive forging and Zanardi steelmaker) and FCA automotive end user. After the Workshop a questionnaire was sent to each participant due to their expert and specialized support in the technical/scientific field of material, process/treatment, machining and industry: the survey aim was done to understand stakeholder technical involvement and satisfaction and to effectively gauge and give rise to a constructive reflection on the work done in IMMAC during the project period. The comments, regarding the organization, the materials, the machinability, the forging process, underlined new aspects not developed in the project. Have put in dialogue the different industrial experiences and resonances encouraged both new possibilities about model simulation development for other materials and product machinability improvement in new studies and praised the IMMAC approach about the simulation effort and regarding the classification of steel variants.

Task 8.2 Choice of an optimized FP grade to validate the numerical approach

Based on the results obtained in the previous WP, the microstructure of the variant 45R was seen as an optimized steel solution for the component oriented machining tests (task 8.5). The machining performances of this reference were compared with those of damaged structure variants 45CG and 45GP in order to make a classification with an industrial point of view.

Task 8.3 Rheology and tribology

Models from WP2 and WP3 were used.

Task 8.4 Numerical simulation

FE simulations and empirical models from WP5, WP6 and WP7 were used.

Task 8.5 Description of component oriented machining tests

Turning and drilling operations were tested in semi-industrial components, which were simulated by workpieces with similar dimension or shape. In particular, the crankshaft has been identified as the most appropriate automotive component because includes in the manufacturing cycle both operations and the actual reference material of end-user partner (FCA) comprises a medium-high carbon content, similarly to the chosen steel for the IMMAC tests. For the component oriented broaching test, the steering rack was identified. Turning and drilling operations were performed through specific tests at CRF Advanced Machining Laboratory, equipped with machines comparable to industrial machines. In both cases insert tool life was observed, cutting forces, insert wear and piece roughness according to the industrial drawing specifications were measured. In the industrial crankshaft the main bearing journal and the crankpin bearing journal are turned. The internal ducts for the oil passages are manufactured through deep drilling. The bars were turned and drilled in transversal direction, as in crankshaft, using specific operation cycle parameters.

Turning tests:

The automotive crankshaft manufacturing process presents different turning operations starting from roughening of the forged component to the finishing; in order to represent one of the turning step, the **finishing operation OP150** has been chosen. In this operation two crank cheek together per time with two inserts are turned in a transversal direction; to reproduce and simulate

the OP150 in laboratory only one insert work was considered, using a coated carbide insert from Sandvik Coromant**.**

Important point, compared to turning tests carried out in the WP5, the depth of cut (ap) chosen was significantly lower (ap=0.25 mm – finishing step). In WP5, ap was 1 or 2 mm. In the production line, the tool change frequency is made each 125 turned crankshaft (representing 4500 mm machined). The turning tests were performed using this limit. After 4500 mm machined, the tool wear generated in the tools was difficult to estimate and seemed very low. Thus, the evolution of roughness was chosen as the parameter that distinguished the steel variants best. With this criterion, the microstructures of 45R and 45CG show the best machinability for turning. This result can be attributed to a suitable tool-chip contact (little or no adhesive phenomenon).

Drilling tests:

The deep drilling operation of internal oil ducts is named OP70. The bars were drilled in transversal direction taking into account the plant and the tool supplier (Guhring) suggestions. The tool was a deep carbide drill with coating. The cutting speed and the feed are similar to those used in the WP6, but the cutting length and the lubricating mode are different: MQL (minimum quantity lubricant) instead of emulsion. To set up the test two different drill diameters were used, Ø5mm and Ø8mm, due to an average crossing length through the bar diameter. Considering the drills with Ø8mm, feed force and torque acquisition during the tests were carried out. The feed force is a little higher for 45CG and similar for the other C45 variants (around 1050 – 1080 N). The torque of 45GP (globular perlite) is 10 to 15% higher compared to other variants (adhesive effect); same trend was observed in WP6 work. Considering the drills with Ø5mm, tool life tests were performed in order to analyse the flank wear of drill. It was decided to perform the test until a cutting life of 60 meters drilled (usual industrial cutting life for carbide drill). Following the flank wear behaviour during the test for each C45 variants, the results highlighted that the microstructures of 45R and 45WB (with a good pearlite ratio Lamellar P/Globular P) have the better and similar deep drilling performances with industrial conditions applied in FCA production line (around 57 m drilled). For 45GP, the test was stopped at 17 meter drilled due to the material gluing along the chip evacuation channels (adhesive mechanism observed in WP6 machining tests). For 45CG (coarse perlite grain), the tool life was very short (< 2 m drilled) due probably to the abrasive effect generated by the higher percentage of lamellar perlite (80%). This effect was not noticeable on tool life with the WP6 drilling conditions (short drill – emulsion); only the roughness of hole was significantly different between 45R and 45CG (friction aspect to study between the different lubricating modes).

Broaching tests:

In broaching, semi-industrial tests were performed on the set-up presented in Task 7.2. A specimen mimicking a steering rack was used and single tooth broaching tests were carried out in order to assess the tool life under similar cutting conditions and under dry condition. A partially TiN coated tool was employed and machining forces, chips and surface roughness were again monitored. Trends observed in the Task 7.3 were found again, but with the cutting conditions used, no significant difference in terms of wear was observed on the tool's flank face between all the C45 variants after 75 meters machined. It is certainly due to a too low cutting speed applied (20 m/min).

Task 8.6 Validation of the numerical approach

Regarding the different C45 steel variants studied, the models developed in the project for the 3 cutting technologies clearly target the reference 45R as the microstructure involving the greater chance to obtain the better "global" machining performances. The table below recalls the classification of the C45 variants, the cutting conditions on which the models were built and those applied for oriented component tests. We also underline the predominant tool-chip contact or tool-material contact mechanism concerned for each case.

Cutting technology	End-use application	Cutting conditions	Classifications	Contact mechanism (main behaviour involved)
High speed Dry Turning	Crankshatf	ap : 1 to 2 mm	Simulation : 45GP > **45R** > 45CG	Abrasion (Tribology)
		ap : 0.25 mm (OP150)	Industrial tests : 45CG > **45R** > 45GP (but incomplete results regard with tool wear)	Abrasion-adhesion (rheology and tribology)
Medium speed Lubricated Drilling		Drilling Emulsion 10%	Simulation : **45R** > 45CG >> 45GP	Abrasion-adhesion (rheology and tribology)
		Deep drilling MQL (OP70)	Industrial tests : **45R** > 45GP >>> 45CG	
Low speed Dry Broaching	Steering rack	V : 20 m/min RPT : 40 µm	Simulation : 45CG>**45R**>>45GP	Adhesion (rheology++ and tribology)
			Industrial tests : Incomplete results	Abrasion-adhesion (rheology and tribology)

The component oriented turning tests (OP150) shown that the globular microstructure (45GP) demonstrates the worst results, contrary to his positioning with simulation. This result can be explained by the criteria used for classifying the C45 variants: the roughness after 4500 mm machined, with tools slightly worn (very low depth of cut). The current turning model has integrated data acquired through more severe operating conditions and without any link with roughness of the steel variant machined. To validate this model, the cutting life of the tools should be extended. Nevertheless, within the context of the **choice of one optimized microstructure for crankshaft application** (turning and deep drilling operation are concerned), the component oriented tests have shown that deep drilling tools are highly sensitive to microstructure variations. Coarse pearlite grain and globular pearlite presents important risk of worsening performance of the drill. The drilling model proposed in WP6 reflects well this risk, and for this end-use application, is predominant than turning model for the definition of the most appropriate ferrite-pearlite microstructure: the homogeneous FP microstructure here represented by variant 45R. We are unfortunately not able to validate the classification propose by the broaching model. Additional tests are needed with higher cutting speed.

<u>Conclusion</u>

In the framework of IMMAC project, a better understanding of thermal stress-strain behaviors, contact mechanisms and thermal properties of FP microstructures and material cutting tool have been achieved. The main parameters of FP microstructure and the main contact mechanisms driving the machinability performances were identified for each cutting operation. Related model parameters identified through the rheological and tribological tests were used in numerical models to predict qualitative machinability performances of FP steels variants. Moreover, an interesting empirical formulation, only for the drilling, has been developed based on FP microstructure parameters. With the help of numerical and empirical models, **an optimized microstructure for crankshaft application could be predicted,** and component oriented machining tests carried out by the partner end-user have confirmed this microstructure solution. As said in introduction, we observe now larger tolerances on requirements specification on FP steels which cause variability on microstructure morphology not always perceptible with common metallurgical characterizations. It is mainly linked to the fact that the methods to identify the FP parameters (grain size, pearlite globalization, banding level…) are not standardized. The interpretations are made with by comparison with standard images. This qualitative approach can be considered subjective. The numerical methodology proposed in IMMAC could be used by end-users and steelmakers as a basis to renew their manufacturing methods, define the associated cutting conditions and specify in a clearer and more robust way the material "specifications/requirements" for each functional component. The tribological effect of lubricant processes (MQL, emulsion) and the numerical modelling of the tribological behaviour of steels leading to a predominant contribution of adhesion remain areas for improvement.

2. Scientific and technical description of the results

2.1 Objectives of the project

FP steels as multiphase materials:

Ferrite-pearlite (FP) steels are the most common material for engineering and automotive industries (gear box parts, crankshaft, connecting rods, injection parts…). FP steels can be seen as multiphase materials. It mainly consists of a ferritic matrix with embedded islands of a hard second phase (pearlite). Pearlite is a two-phase material with hard and brittle cementite lamellae embedded in a ferrite matrix. These lamellae are arranged in colonies within which the orientation of the cementite is (ideally) constant. Increasing the volume fraction of hard phase generally increases the strength, while ferrite provides a good ductility. Controlling this combination enables to reach higher ultimate tensile strengths and work-hardening rates than conventional steels of similar yield strength. This appears as one growth way to develop optimized grades with improved mechanical properties and/or forming capabilities.

Even if steels with a FP structure are among the most common materials, they are not at the very least the easiest materials to machine. More precisely, the machining performance appears to be highly dependent on the microstructural parameters [1]. During machining, the low deformability and greater hardness of pearlite cause, on the one hand, significant abrasive wear and high resultant forces [2][3]. On the other hand, pearlite reduces the adhesion tendency and the formation of built-up edges of ferrite [4], promotes the formation of favourable chip forms, causes less burr formation on the workpiece and improves the surface quality [4][5]. Under a certain scale, the material clearly cannot be assumed as homogeneous and isotropic [6][7].

Nevertheless, even now, we observe larger tolerances on requirements specification on FP steels which cause variability on microstructure morphology not always perceptible with standard metallurgical characterizations. In some case, the technical specification causes complex customer complaints between steel-makers and their customers: the microstructure seems as expected but unacceptable variability in machinability are observed.

With reference to FP steels, no study has yet clearly reported the exact contribution of ferrite/pearlite ratio, morphology of the pearlite, interlamellar spacing or even grain size on the machining performance. The thermal stress-strain behaviours and the contact mechanisms seem to be not completely understood.

Numerical simulation as a flexible tool to design steel grade with optimized FP microstructure for machining a dedicated part:

In industry, numerical simulation is mainly used for casting, forging, rolling or heat treating. This is not the case for machining. Therefore, a need of industrial flexible and predictive support tools is clearly rising in order to limit the experimental campaigns, optimize the use of existing steels but also to help steelmakers in designing optimized grades tailored to a particular component manufacturing. The numerical simulation appears as a relevant tool that matches these criteria. The will to model multiphase materials is growing for more than ten years now with studies mainly focused on the micromechanical behaviour [8][9][10][11] and some applications in machining [12][13][14][15]. However, they still present a complex and CPU consuming approach rather hard to implement in an industrial context.

Simple constitutive and cutting models considering the microstructure are still highly required. Such physically based models are available at room temperature for ferrite-pearlite steel [16] including pearlite volume fraction, interlamellar spacing, ferritic grain size with a viscoplastic law for ferrite validated using a large data base taking into account the effect of strain rate and of temperature. This modelling approach was selected for the project to incorporate the influence of ferrite-pearlite microstructure parameters into rheological models.

Based on these statements, IMMAC project was proposed for:
- The development of a numerical method to predict the machining performance of designed ferritic-pearlitic steels depending on microstructural parameters
- The use of this method as a flexible steel development strategy to design new machinability-improved grades tailored according to the part and its machining range.

Three cutting technologies were studied: turning, drilling and broaching.

2.2 Description of activities and discussion

The Figure 1 below reminds the research approach with proposed work packages (WP).
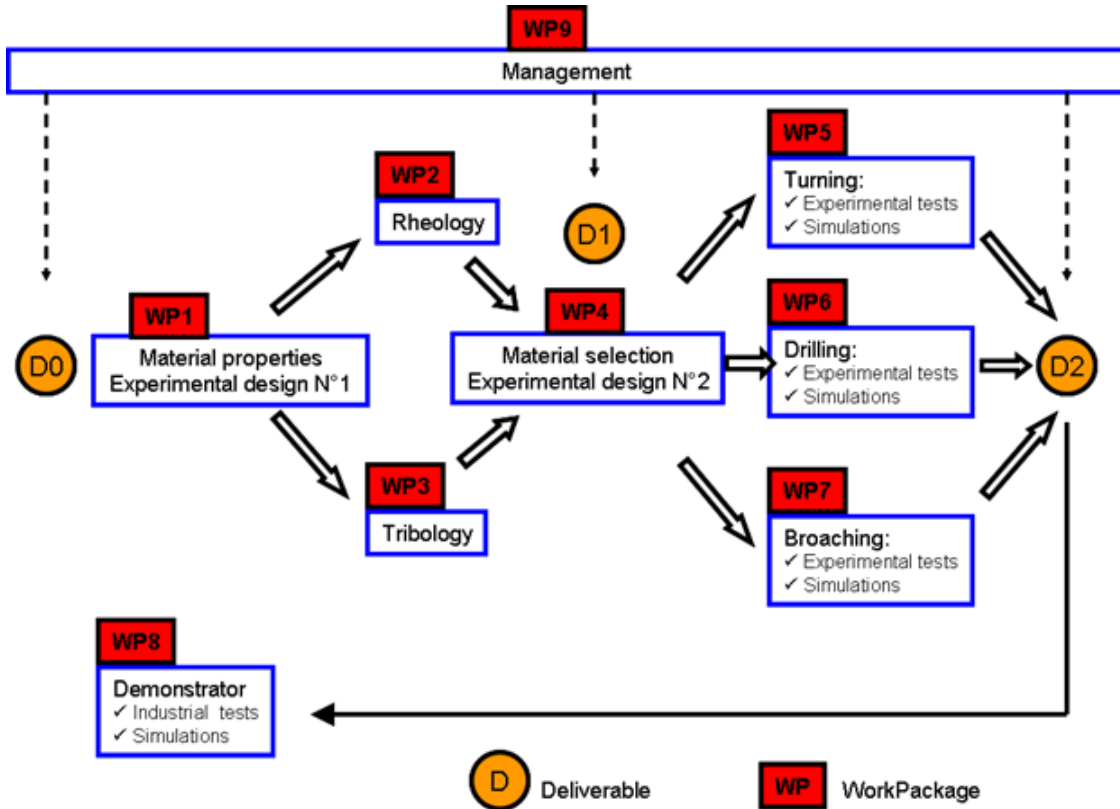D0, D1 and D2 are the main deliverables of the project.

Figure 1 : Research approach of the project

2.2.1 WP1: steel manufacturing and metallurgical characterization – experimental design N°1

Task	Title	Initial plan	Work accomplished	Note
Task 1.1	Steel selection	Three variants of the C60 were considered	Three variants of C60 and C70 only in the reference condition were evaluated	(1)
	Number of variants	The study of 15 variants was initially expected	Finally, 16 steel variants were considered	(2)
	S content	All the variants with similar S content (0,020-0,040% S)	C70 variant had higher S content (0,065% S)	(3)
Task 1.2	Heat treatment	The treatment of 15 variants was initially expected	Finally, 16 steel variants were considered	(2)

For the other tasks, there has been no major deviation from the original project plan.

The main goals of this WP are:
- To propose different available manufacturing routes for FP steels that lead to different cutting behaviours.
- To manufacture the material which has been studied along the project.
- To generate all the metallurgical information from the manufactured steels that could be needed to interpret the results generated in the other WPs and to feed the simulation models developed during the project.

TASK 1.1 Steels selection & manufacturing for experimental design N°1

Note 1: in the project proposal four steel grades were chosen: 16MnCr5, 27CrMn5, C45 and C70. Although at the beginning of the project, it was decided to replace the C70 by a C60 because of manufacturing program issues, a variant (obtained after an isothermal annealing) of this C70 was decided to be kept in the researching program to have a reference of a 100% pearlitic steel.

The production of the chosen steels was distributed between the two steelmakers involved in the project as follows: 16MnCr5 (Ascometal), 27MnCr5 (Ascometal), C45 (Sidenor), C60 (Sidenor) and reference variant of C70 (Ascometal).

Each of the four selected steel grades was manufactured in four different microstructural states:

- A **reference microstructure** variant (**R**): Homogeneous FP microstructure obtained after an isothermal annealing.
- A **damaged microstructure** with coarse pearlite grain size (**CG**): the goal is to obtain a variant with a coarser pearlite grain with regards to the reference variant. A specific heat treatment was designed to attain the desired results.
- A **damaged microstructure** with globular pearlite (**GP**): the aim is to transform a significant percentage of the lamellar pearlite into globular one. This transformation takes place during a globulization annealing.
- A **damaged microstructure** with a higher banding level (**WB**): to increase the banding level of FP microstructures a modified isothermal annealing was carried out. This heat treatment, as in the case of CG variants, was specifically designed to reach the desired microstructural state.

Note 2: due to the high carbon content of the C60 is not possible to manufacture the more bands variant, the ferrite amount is not enough to create bands. Furthermore, as previously stated, an isothermal annealed C70 was also evaluated. Thus, the following 16 variants were studied during the project (Table 1)   :

Steel Grades	Reference	Coarse pearlite grains	Globular pearlite	High banding level
16MnCr5	16R	16CG	16GP	16WB
27MnCr5	27R	27CG	27GP	27WB
C45	45R	45CG	45GP	45WB
C60	60R	60CG	60GP	-
C70	70R	-	-	-

Table 1 : Steel variants studied

TASK 1.2 Heat treatments for experimental design N°1

The heat treatments utilized to produce the variants R (isothermal annealing) and GP (globulization annealing) are commonly employed in the steelmaking process. However, for the other two variants (CG and WB), there was not any developed heat treatment through which the desired microstructural characteristics could be attained. Hence, in the IMMAC project specific heat treatments were designed to reach the required properties (Figure 2).
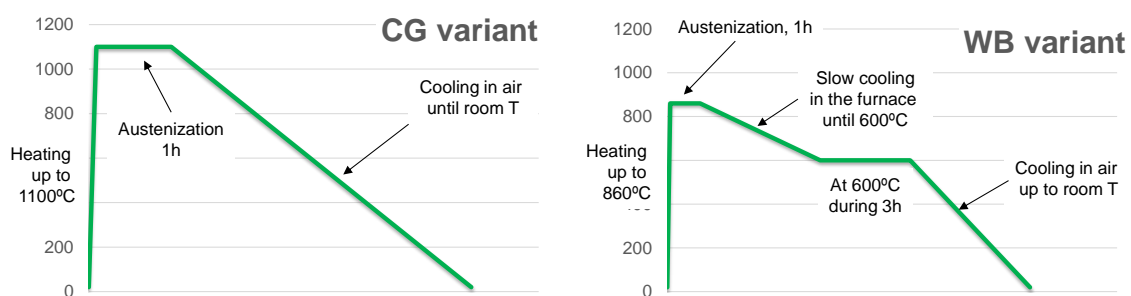

Figure 2 : Heat treatment cycle for CG and WB microstructures

To obtain the coarse pearlitic grains the austenization temperature was increased up to 1100ºC, then, after 1 h, the cooling was conducted in air until reaching room temperature.

To produce the variant with high banding level an isothermal annealing was taken as reference. After the austenization, instead of performing a quick cooling, the temperature was slowly reduced (maintaining the bars in the furnace) until 600ºC. The rest of the process was the same than the followed in the isothermal annealing. Taking into consideration that both, coarse pearlite grain and high banding level, are considered to be detrimental for the steel performance (they commonly appear as consequence of any problem during the heat treatment). The production of steels with these characteristics was not possible through conventional heat treatments. Therefore, the development of these two thermal cycles was very important for the project development given that they allowed to obtain in a controlled way the microstructures defined in the project proposal.

TASK 1.4 and TASK 1.6 Chemical compositions and inclusion studies

The chemical composition and the inclusionary state were analysed in all the variants in order to identify any difference that could lead to dissimilar machinability performances. The chemical composition of the different heats (Table 2) was measured on the rolled bars. All the variants of each grade were manufactured from the same heat.

Grade	C	Si	Mn	S	P	Ni	Cr	Mo	Cu	Al
16MnCr5	0,19	0,17	1,23	0,028	0,016	0,19	1,03	0,07	0,17	0,020
27MnCr5	0,25	0,24	1,19	0,033	0,009	0,09	1,06	0,04	0,11	0,032
C45	0,45	0,33	0,78	0,025	0,014	0,09	0,12	0,02	0,11	0,007
C60	0,61	0,28	0,65	0,027	0,016	0,14	0,11	0,04	0,24	0,005
C70	0,71	0,21	0,57	0,065	0,007	0,06	0,15	0,02	0,03	0,002

Table 2 : Chemical composition

The C content was a bit high in the 16MnCr5 and a bit low in the 27MnCr5, in the rest of the grades, the carbon content was the expected one. The differences detected in the Al content were due to the different deoxidation methods used to manufacture the steels. C45, C60 and C70 were deoxidized with Si, while the 16MnCr5 and the 27MnCr5 were deoxidized with Al (this is the reason for their higher Al content). This higher Al content will lead to different inclusions populations which may affect the steel machining performance.

Note 3: the high S content of the 70R was because Ascometal does not manufacture the C70 grade with lower S.

The inclusionary studies were conducted using SEM-EDS with the Inca Feature software. The inclusions were sorted out in different classes: sulphides, oxides, complex inclusions and carbo-nitrides. The main conclusions that can be extracted from the results of this inclusions assessment are the following ones:

- The inclusions population showed that about 90% of the total amount of inclusions was MnS. Nevertheless, the different deoxidation method used by the steelmakers leads to higher Si content in the inclusions present in the steels manufactured by Sidenor and to higher Al in the inclusions of the Ascometal steels.
- The 16MnCr5 and 27MnCr5 were subjected to a Ca treatment at the final stage of the metallurgy to improve their castability. The top slag of these steels was based on Al_2O_3, as given by the characteristics of the inclusions present in them.
- The C45 steel was produced using SiO_2 top slag, with Ca addition to improve the castability, that had formed CaS.
- The top slag of C60 was partly based on SiO_2, as given by the relatively high amount of oxides. The oxides content in the C60 grade was almost the double than in the C45, this was expected because the O content in the C60 was also higher.

The information generated in the analysis of the chemical composition and in the inclusionary studies can be helpful for the interpretation of results obtained in machinability tests.

TASK 1.5 Microstructural studies

The main aim of this assessment is to provide all the microstructural information required to feed the numerical models that were developed in the project. During the project, apart from all the microstructural parameters mentioned in the proposal, some additional aspects were evaluated, i.e. the fraction of globular pearlite in each of the variant.

The reference variants of all the steel grades (Figure 3) had homogeneous FP microstructure. The 27R was the only one with some bands (Level B according the standard Renault 1194).

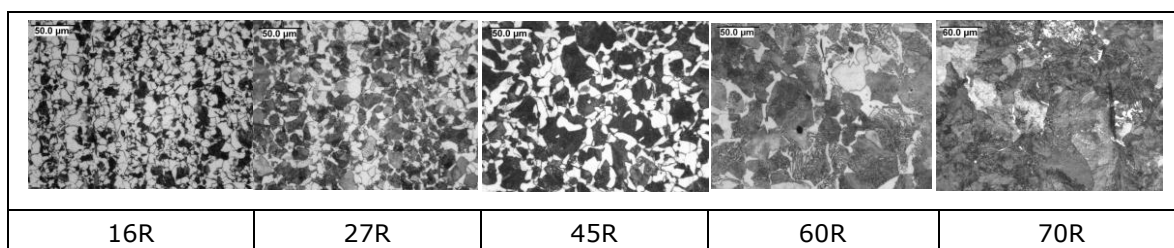| 16R	27R	45R	60R	70R

Figure 3 : R variants

Regarding the CG variants (Figure 4) as expected the morphology of this structure is different between low carbon steels (16CG and 27CG) and high carbon steels (45CG and 60CG). For low carbon steels, there are some pearlitic coarse grains (ASTM 5) in the ferrite-pearlite structure; the rest of pearlitic grains were quite fine (ASTM 10). For high carbon steels (lower ferrite content), the size of all the pearlitic grains increased, reaching ASTM 3-4.
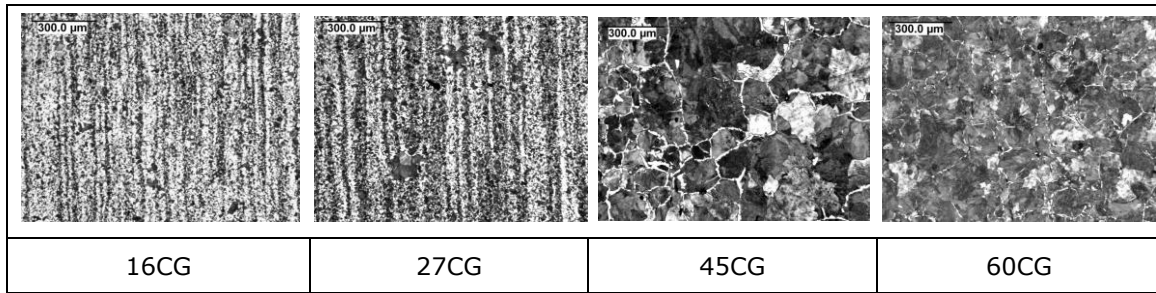
Figure 4 : CG variants

In the case of the GP variants (Figure 5), the heat treatment defined in the variant 27GP didn't generate globular perlite. For variant 16GP approximately 75% of the pearlite is in the way of globulization (broken pearlite). For the 45GP and 60GP the pearlite is quite completely globulized; 100% and 75% of globular pearlite was respectively achieved for 45GP and 60GP.
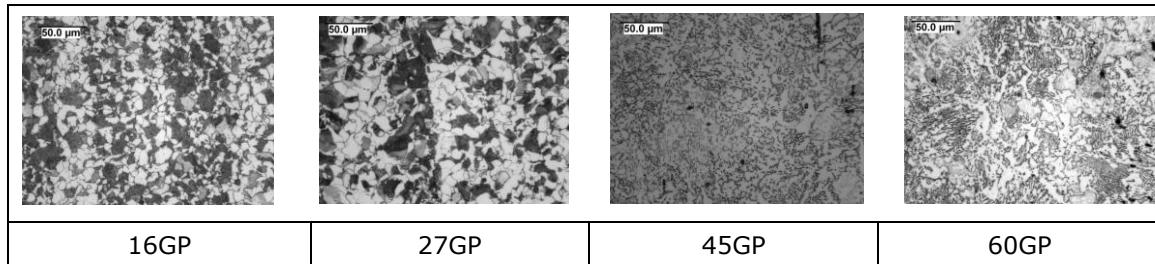

Figure 5 : GP variants

The level of bands (Figure 6) attained with the two low C steel grades (16MnCr5 and 27MnCr5) was lower than expected (in the best of the cases level B according to the Renault standard 1194). On the contrary, for the 45WB the goal of obtaining a more banded microstructure was reached given that a banding level B-C (according to the standard Renault 1194) was attained.
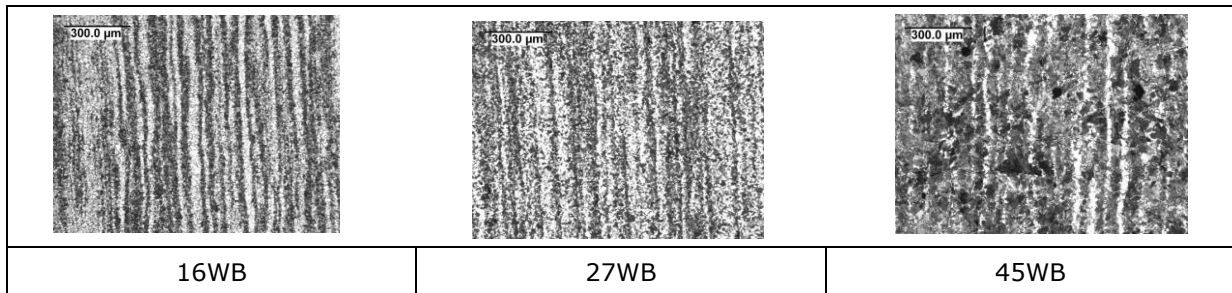
Figure 6 : WB variants

Additionally, and to fulfil the needs of the rheological modelling work, two variants of C70 were also analysed; one 100% pearlitic and the other one with 100% of globular pearlite (Figure 7).
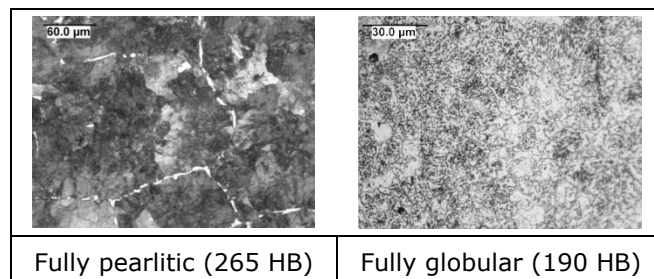

Figure 7 : Microstructures obtained for the C70 grade (for rheology measurements only)

Apart from the general characterization shown above, many other microstructural aspects such as ferrite/pearlite ratio, grain size, interlamellar spacing… were evaluated for each of the manufactured FP steels in order to be considered in the modelling tasks.
Proeutectoid ferrite was measured using statistical image analysis. Each value was obtained using 30-40 images (magnification 200X), using 10 random targets.

The formation of ferritic-pearlitic bands in low C grades is strongly related to the cooling rate between the austenization and the isothermal annealing temperatures. This parameter was hardly controllable, as it is mainly influenced by the sample dimensions. The relatively large thickness of the steel bars did not allow reducing the banding below level B. For the variant 45WB, the proposed heat treatment allowed the modification of the microstructure compared to the reference 45R.

The ferritic grain size was measured by comparing with reference pictures. The measurement can be performed only when proeutectoid ferrite exhibits a nodular aspect. In all the C60 variants, as well as in the 45CG, the ferrite is present at prior austenite grain boundaries only. In the globular variants 45GP and 60GP, proeutectoid ferrite nodules could not be identified.

Pearlitic grain sizes were also measured by comparison with reference pictures. The min-max values are given in the Table 3 below, since pearlitic grain size was not homogeneous for all the samples. The 60CG variant exhibits the highest pearlitic grain size (P GS).

P GS (µm)	16MnCr5	27MnCr5	C45	C60	C70
R	13-15 few 22	15 few 89-177	22-27 and 62-89	31 and 62	-
CG	< 11 few 31-62	11 few 62-89	76-89	125-500	-

Table 3: pearlitic grain size

The proportion of globular pearlite was evaluated using the Renault 1193 method. This method consists in a comparison with reference pictures and provides an evaluation of the globular pearlite from 0 to 100%.

Average interlamellar spacing (Figure 8), as well as standard deviation, was measured at ASCO for the variants of the 16MnCr5 and 27MnCr5 and at Sidenor for the variants of the C45 and C60. Given that different methods were employed, the interlamellar spacing of the 60R variant was evaluated with both attaining similar results. For the 16GP no lamellar pearlite was detected, all was broken. As explained before, this means that the pearlite started to be globulized.
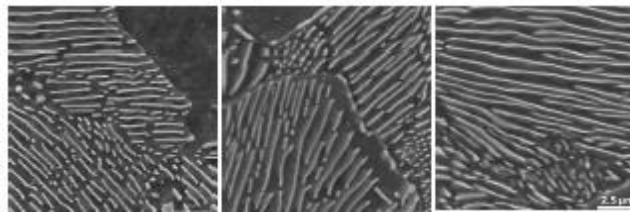

Figure 8 : image of pearlite lamellar

All the results of these detailed studies (except pearlitic grain) are shown in the Table 4. These useful metallurgical data were exploited in the machining and the modelling works.

23

Variants	% ferrite	%lamellar perlite (LP)	% globular pearlite (GP)	Ratio GP/LP (%)	Interlamellar spacing / std deviation (nm)	Ferrite grain size (μm)	Bands
16R	58	37	5	12	190 / 65	10	B
16CG	56	33	11	25	222 / 65	12	B
16GP	53	12	35	75	204 / 69	12	A-B
16WB	59	35	6	15	146 / 41	12	B
27R	40	54	6	10	285 / 74	14	B
27CG	52	43	5	10	229 / 59	15	B
27GP	45	55	0	0	197 / 56	12	B
27WB	44	56	0	0	202 / 51	12	B
45R	25	56	19	25	293 / 82	17	A
45CG	15	81	4	5	366 / 170	30	A
45GP	10	0	90	100	632 / 192	10	n/a
45WB	20	64	16	20	326 / 116	19	B-C
60R	14	65	21	24	372 / 135	11	A
60CG	6	89	5	5	306 / 79	17	A
60GP	14	21	65	75	623 / 186	10	n/a
70R	0	100	0	0	206 / 70	-	-

Table 4: Useful metallurgical data of the different steel variants.

TASK 1.7 Mechanical properties

In the following Table 5 a summary of the results obtained for the main mechanical properties evaluated in the project are depicted. UTS values were well correlated to hardness. The results obtained in the tensile and toughness tests (conducted at room temperature) were in-line with the fracture mechanics. As expected, toughness was lower for the highest UTS values.

Variant	Tensile test				Toughness	Hardness
	UTS (MPa)	YS (MPa)	El (%)	RoA (%)	KU (J)	HB
16R	NR	NR	NR	NR	NR	162
16CG	603	403	27	73	70	162
16GP	544	375	30	73	79	160
16WB	544	306	30	72	76	162
27R	610	367	33	66	60	163
27CG	636	394	24	69	66	168
27GP	645	408	28	69	68	174
27WB	642	410	27	69	66	178
45R	667	361	18	48	20	185
45CG	747	399	19	37	17	198
45GP	623	306	31	62	16	143
45WB	623	328	29	44	17	165
60R	699	372	17	34	12	188
60CG	842	454	15	41	8	225
60GP	574	299	26	56	18	148
70R	924	502	12	22	8	265

Table 5 : Mechanical properties of the different steel variants

TASK 1.8 Thermal properties

The thermal characterization of the considered steel variants was performed evaluating the following properties: specific heat (Cp), density (ρ), thermal diffusivity (α) and thermal conductivity (λ).

For all the variants a variation on the measured density (Figure 9) was observed at T 700-800ºC due to a phase change on the material (austenite transformation). The density values decreased from approximately 7800 to 7400 kg/m^3 when moving from room T to 800ºC. Density differences were found between some of the studied variants: 16GP (lower values) and 45GP (higher dispersion).
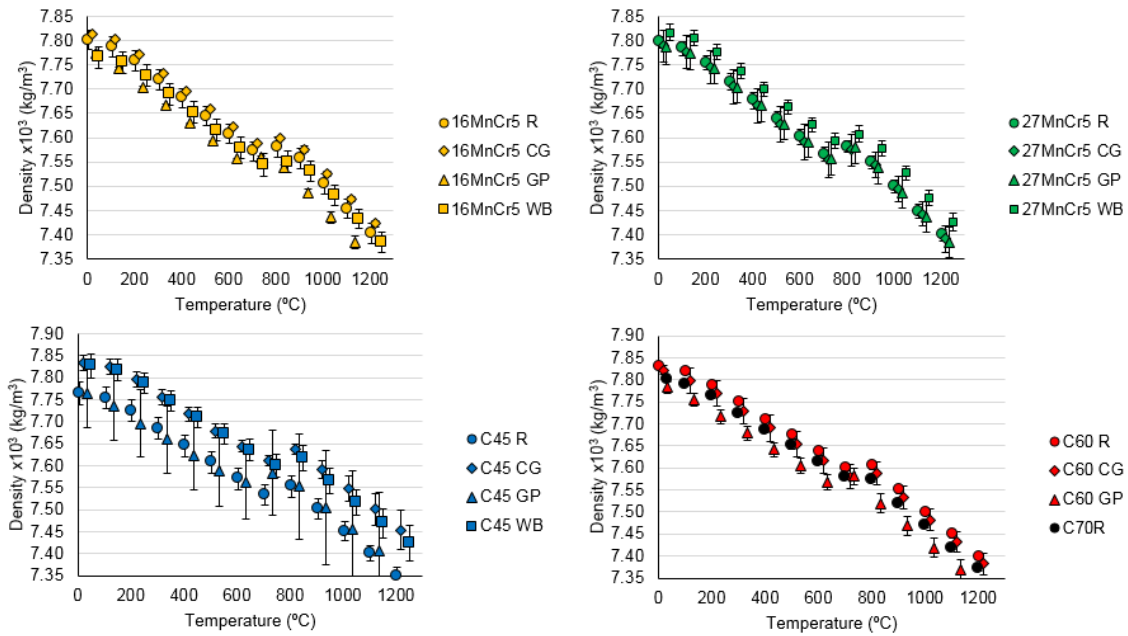
Figure 9 : Density of the different steel variants

Regarding the diffusivity (Figure 10), the values decreased with the increase of the T in all the studied steels. The results obtained for the variants 27GP, 45GP and 60GP clearly differ from the results of their respective reference.
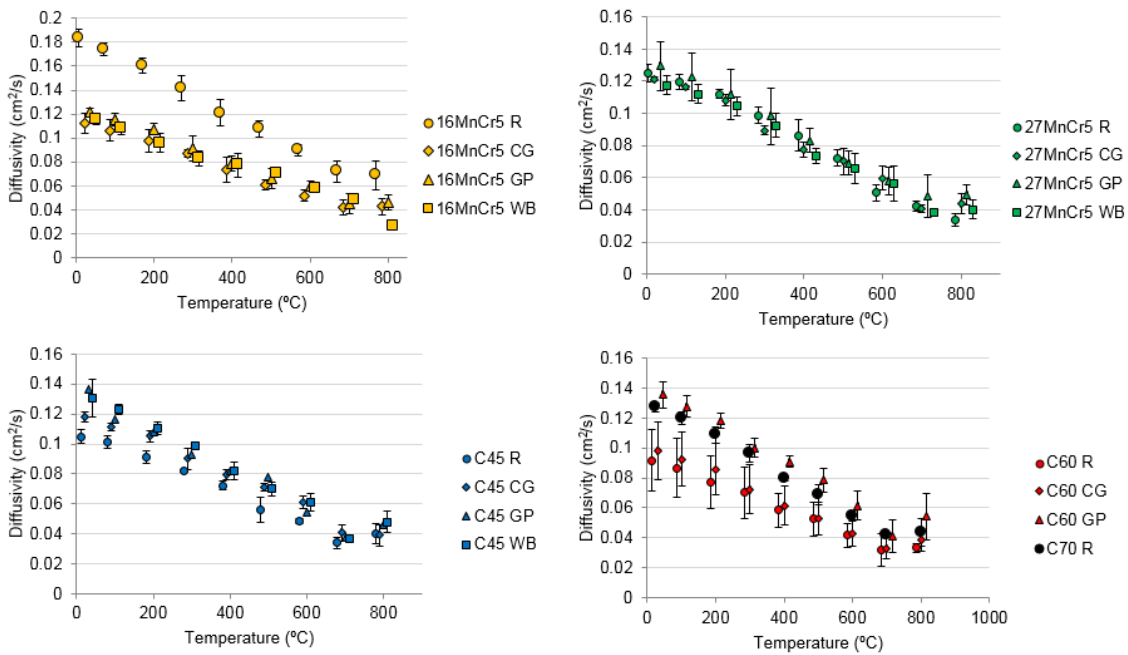

Figure 10 : Diffusivity of the different steel variants

The specific heat tests (Figure 11) showed the same absolute values and trends for all the steel grades. Results increased from 400 to 800 J/kgK with the increase from room T to 800ºC. Some measurements at 800ºC showed a discrepancy due to limitations of the measurement equipment (these results were not taken into consideration).
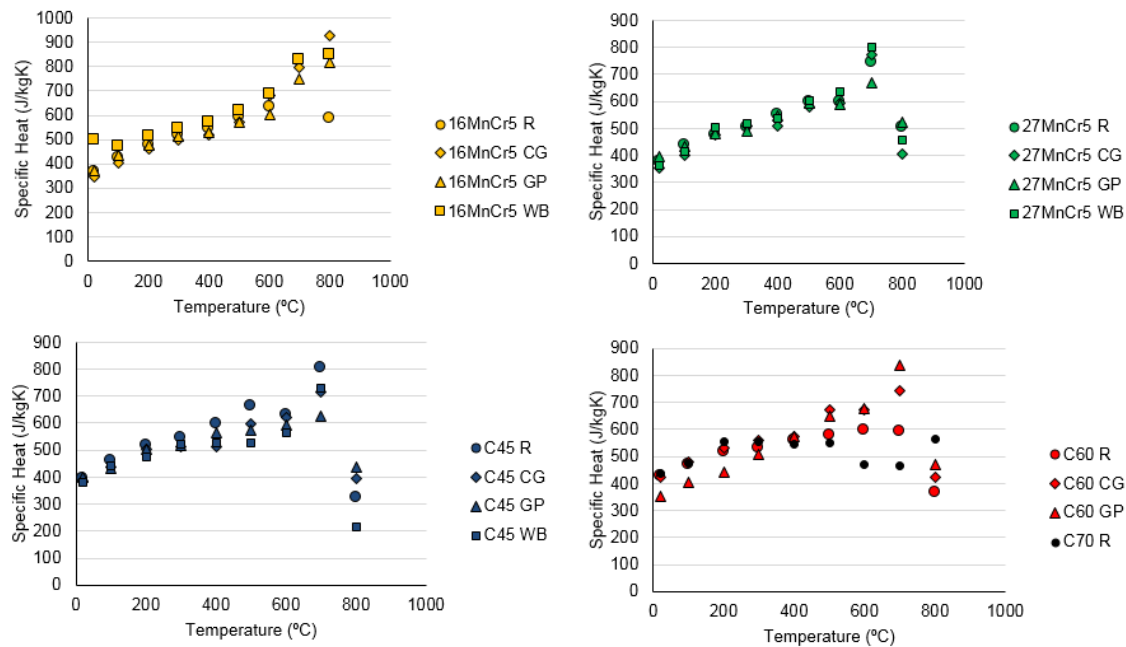
Figure 11 : Specific heat of the different steel variants

Conductivity results Figure 12 showed a decrease with the increment of T. This trend was observed for all the studied steels except for the 16MnCr5. This aspect may be due to the variations detected in the diffusivity measurements. The 60GP variant differed once again from the reference (60R).
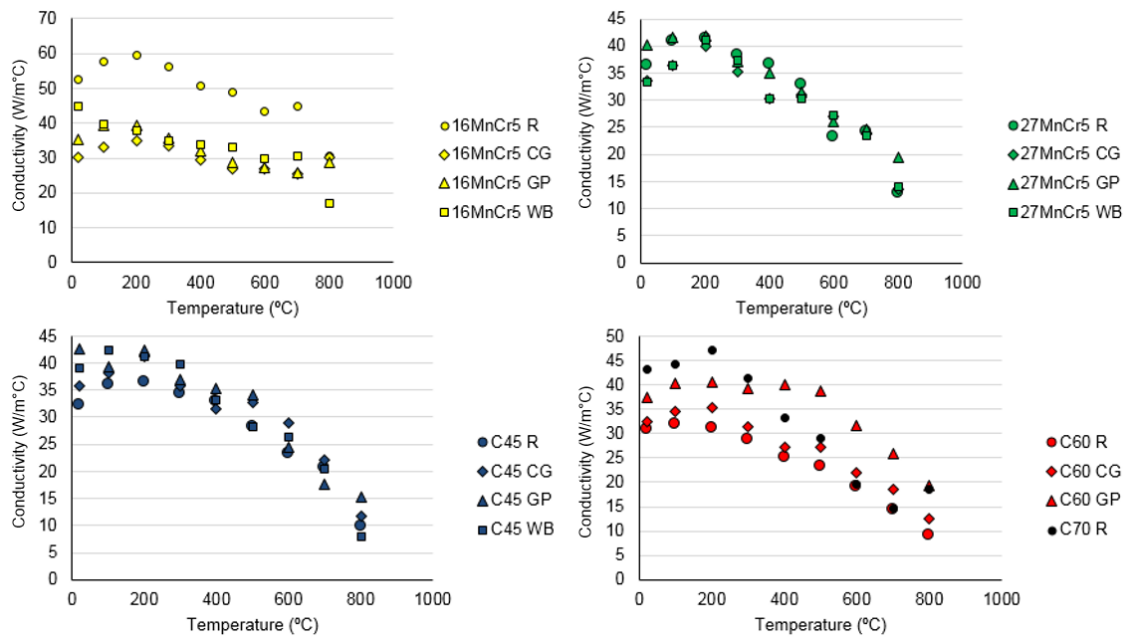
Figure 12: Conductivity of the different steel variants

Same trends of the characterized thermal properties were found for all the grades and variants. Regarding the absolute values, the clearest differences were achieved for the case of density and thermal diffusivity results. In the case of the density, GP variants obtained the higher values in comparison with the reference grade. Focusing on diffusivity results, the highest values were obtained for the GP and WB variants. The resultant thermal conductivity only showed significant differences among the different variants for the grades 16MnCr5 and C60.

Thermal properties of two tool materials were also characterized (Figure 13). A high-speed steel (M35) and an uncoated carbide (H13A). Density of carbide H13A doubled the one of the M35 with values of 15000 and 8000 kg/m^3 respectively. Thermal conductivity maintained constant along the analysed temperature for the M35 with a value of 17 W/m°C. In contrast the one of the H13A lowered from 112 to 28 W/m°C when temperature varies from 20 to 800°C.Diffusivity of H13A had also a decreasing tendency (0.37-0.16 cm^2/s) while in the case of the M35 remained constant at 0.05 cm^2/s. Specific heat of M35 doubled the one of H13A with a value of 425 and 206 J/kgK respectively.
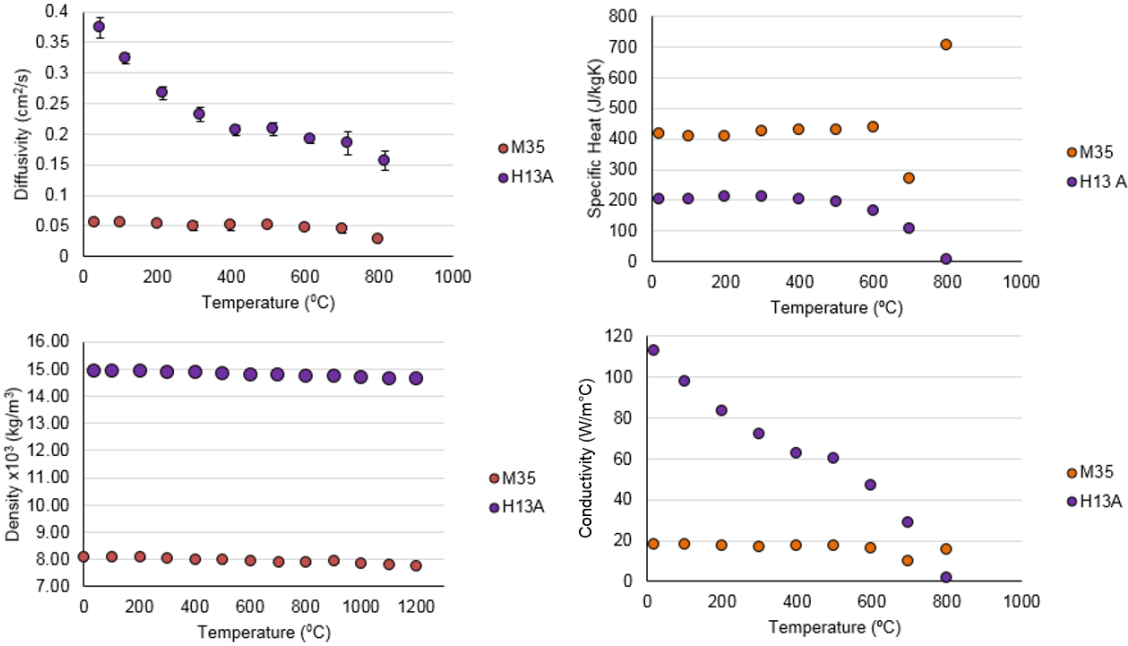
Figure 13 : Thermal properties of tool materials

All these data were employed in finite element models in order to better predict heat flow and temperature distribution, in one hand for the chip and the workpiece, and the other hand in the cutting tool.

2.2.2 WP2: Rheology – identification of constitutive models

Task	Title	Initial plan	Actual plan	Note
Task 2.1	Matrix of tests	Do a matrix of test for all the selected steel grades for the two experimental devices	For all the 16 steel variants defined, a matrix of compression tests was performed with 18 conditions per grade in all	(1)
Task 2.2	Characterization of steel behaviour for low and medium strain rates	Compression tests on a Gleeble: - up to five temperatures (from 20°C to 850°C) - up to five strain rates (from 0.01m/s to 1m/s) Optical observations and EBSD analysis	Additional tests were performed at an extra strain rate of 0.001 s^{-1} especially for C70 grade Deformed specimens were only few characterized (observation of interlamellar spacing of pearlite after the tests).	(1) (2)
Task 2.3	Characterization of steel behaviour for high strain rates	Crash testing rig tests: - up to five temperatures (from 20°C to 850°C) - up to five strain rates (from 1m/s to 20m/s) - the deformation mode : tensile, compression or shear test. Optical observations and EBSD analysis	The experimental work was finally subcontracted to Tampere University of Technology using the split Hopkinson bar method. The deformation mode was only compression. The mechanism of dynamic strain ageing (DSA) was evidenced. Deformed specimens were not characterized since this task was not considered of primary importance for the description of the model.	(1) (3)
Task 2.4	Identification of the parameters of the constitutive model	Description of the viscoplastic behavior of ferrite-pearlite steels In the three types of machining simulations, a simpler material model in needed.	The behavior of pearlite was totally identified from experimental data, in particular with interlamellar spacing and globules size measurements for lamellar and globular pearlite respectively. The developed model has been implemented using Excel. Thermal softening was not taken into account in the model.	(4) (5) (6)

TASK 2.1 Definition of the matrix of the tests

Note (1): The objective of WP2 was to propose a rheological model to be able to simulate machining operations taking into account the microstructure of the steel grade and its variations. Three machining operations are studied:

- Turning
    - Strain: 200 – 500 %
    - Strain rate: 10^4 s^{-1} – 10^5 s^{-1}
    - Temperature: 20 – 1000°C

- Drilling
  - Strain: 100 – 500 %
  - Strain rate: 10^4 s^{-1} – 10^5 s^{-1}
  - Temperature: < 500°C
- Broaching
  - Strain: 80 – 150 %
  - Strain rate: < 10^4 s^{-1}
  - Temperature: 20 – 500°C

For each machining operation, the typical ranges of local temperature-strain-strain rate conditions undergone by an elementary volume of material in the process zone have been indicated. These ranges have been defined by the partners of the project in charge of process modeling.

To obtain a large amount of rheological data, numerous experiments were performed on the different steel grades studied in the project.

- Compression tests at low strain rate were performed at CREAS on the Gleeble machine; compression tests at higher strain rate were performed by a subcontractor to KIMAB (Tampere University of Technology) using the split Hopkinson bar method.

- For each chosen grade, compression tests were performed at 20°C, 500°C and 680°C. Gleeble tests were carried out at 0.5 s^{-1}, 5 s^{-1} and 50 s^{-1} (0.0075 m/s – 0.75 m/s); additional tests were performed at an extra strain rate of 0.001 s^{-1} especially for C70 grade (100% pearlite) for a better identification of the pearlite behavior in the quasi-static state.

- Split Hopkinson bar (SHPB) tests were carried out at the same temperatures, at strain rates of 500 s^{-1}, 2000 s^{-1} and 5000 s^{-1}. Because of the limits of this device, the chosen strain rate were a bit different (3 m/s – 40 m/s) from the one planned (1 m/s – 20 m/s).

- Extra tensile tests at a strain rate of 0.7 s^{-1} were carried out at KIMAB at temperatures 20°C, 500°C and 680°C for all the steel grades.

TASK 2.2 and TASK 2.3 Characterisation of steel behavior

Analysis of the experimental curves

The development of behavior laws always requires experimental results even if they are supposed to be physically-based. They always account to parameters that must be carefully adjusted. This a reason why many experimental mechanical tests have been carried out in the project to explore the wide range of temperatures and strain rates necessary to model machining operations.
For all the studied steel grades (16MnCr5, 27MnCr5, C45 and C60), the influence of microstructural variants at each temperature and strain rate is highlighted. At low strain rate (0.5 – 50 s^{-1}), all the variants show a positive strain rate sensitivity in the considered strain rate range, *i.e.*, an increasing flow stress with increasing strain rate. The evolution of the flow stress with the temperature is typical thermally activated behavior with decreasing flow stress with increasing temperature. This appears less obvious for the curves at high strain rates. An overview of the experimental curves is given in appendices 7.1.1 and 7.1.2 at low and high strain rates for C45 grade.

For each grade the influence of microstructural variants is globally the same at each temperature and strain rate, *i.e.,* from the softest to the hardest GP, WB, R and CG.

The model proposed is based on an accurate description of the behavior of the different phases: ferrite, lamellar and globular pearlite. The ferritic phase has already been well described in the literature in a wide range of temperatures and strain rates.
Note (2): In the present experimental work, the characterization of the behavior of 100% (lamellar) pearlitic C70 was of prime importance for the identification of the pearlitic behavior with strain rate and temperature dependency to feed the model. Figure 14 shows the tensile curves of C70 steel in the temperature range considered and at low strain rates (0.001 s^{-1} – 50 s^{-1}).
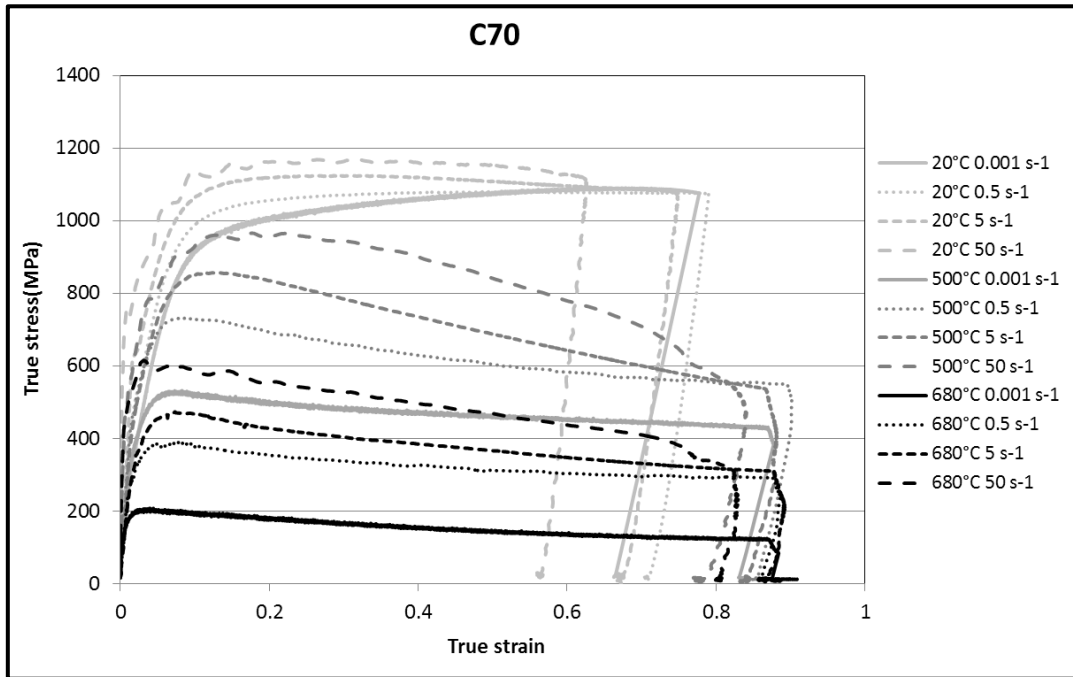
Figure 14 : Experimental compression curves describing the behavior of C70 steel.

To accurately describe the globular pearlite behavior, C70 material was heat-treated to obtain 100% globular pearlite. The curves are presented in Figure 15.
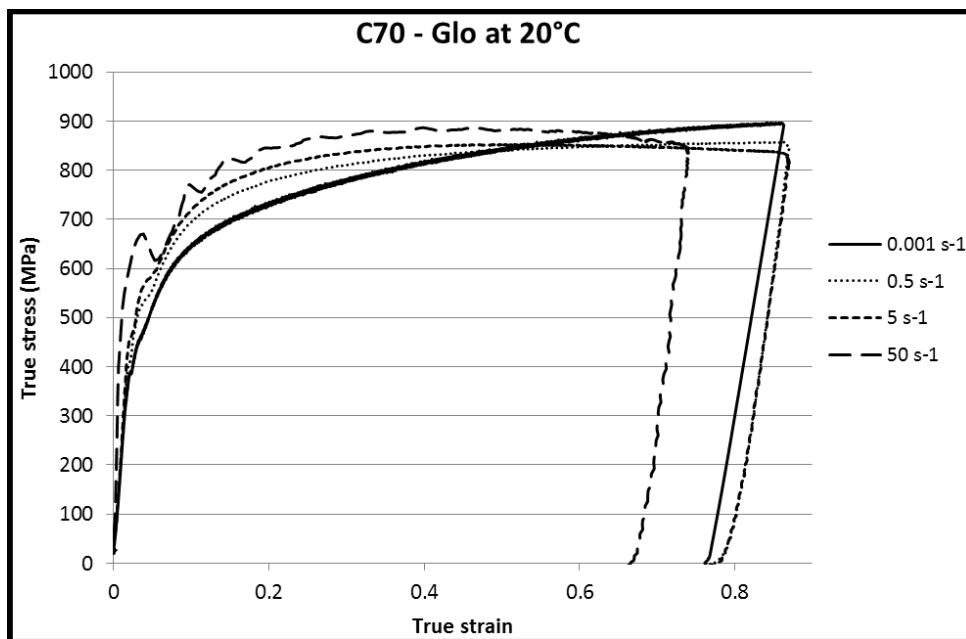

Figure 15 : Flow curves of 100% globular pearlite C70 at room temperature.

Influence of variants on reference grades

Based on the experimental data, the variants of 16MnCr5 and 27MnCr5 grades showed no significant differences in their deformation behavior within the wide range of strain rates studied here. Both the grades have a low and close pearlite fraction and a very small variation of pearlite content between R, CG, GP and WB variants. On the contrary, the compression curves of C45 and C60 grades with higher pearlite content were more sensitive to the changes in the microstructure. That is explained by a (lamellar) pearlite content that varies within 10-15% between the microstructural variants.

The fraction of pearlite is thus the key parameter controlling the flow stress properties of these steels.

The sensitivity of flow stress to microstructural changes for each grade has been quantified and is reported in Table 6 and Table 7. The impact of microstructural variant is calculated from the reference value which has been taken arbitrarily at 0.1 plastic strain for low strain rate and at 0.02 for high strain rate (because of limitations of the SHPB-device).

Grades/variants	Reference value (MPa) at 0.1 plastic strain	Effect of variant (%)		
	R	CG	GP	WB
16MnCr5	619	+7	-2	+1
27MnCr5	681	+3	+3	+0.9
C45	769	+16	-24	-14
C60	816	+24	-16	
C70	1025			

Table 6 : Summarization of the impact of variant compared to reference grade at 20°C - 0.5 s^{-1}

Grades/variants	Reference value (MPa) at 0.02 plastic strain	Effect of variant (%)		
	R	CG	GP	WB
16MnCr5	608	+5	+2	-2
27MnCr5	670	-2	+2	+10*
C45	745	+18	-17	-8
C60	760	+29	-19	
C70	1050			

Table 7 : Summary of the impact of microstructure compared to reference grade at 20°C - 500 s^{-1}.
* Value considered with caution because of possible artifacts.

Both tables show that the effect of microstructure on the flow behavior is more pronounced for the grades with high pearlite content (C45 and C60), and that the tendency is the same both at low and high strain rates.

Thermal softening

A significant softening was observed on Gleeble flow curves at high temperatures (higher than 20°C) for every grade and variant at all the studied strain rates. This is consistent with what has already been observed in the PhD thesis of C. Courbon [17] and also in the literature [18]. To evaluate whether this phenomenon is representative of the real behavior of the materials (dynamic recovery or recrystallisation), or related to self-heating (due to plastic deformation) or other experimental artifacts, complementary experiments were carried out.

Multistep Gleeble tests were performed on C70 grade: the first trials consisted in heating a Gleeble specimen at 500°C at 5°C/s heating rate and keeping it at 500°C during 1 minute. Then the compression test is performed at 0.5 s^{-1}, without simultaneous heating until a deformation of 10 % is reached. The specimen is then heated to 500°C again and held at that temperature during 1 minute followed by a second compression step to 20 % deformation without heating. These steps are then repeated until a total deformation of 80% is reached in order to compare the curves obtained in the initial test with one-step compression. In that way, the temperature of the sample has time to homogenize and thermal gradient effects should be prevented. The results indicate self-heating as the mechanism to explain the decrease in flow stress observed in Gleeble tests. The results were further confirmed in additional two-step Gleeble tests for C70 and 16MnCr5 R where the specimens were first pre-strained at 500°C, then cooled down to 20°C, and strained again. The results show that the behavior of both grades is different at room temperature (but the same that in tests made completely at RT) than at 500°C, hence confirming that the softening is from thermal origin.

Dynamic strain aging

Note (3): The temperature sensitivity in the high strain rate tests particularly caught our attention. Classically, the flow stress decreases with increasing temperature, as it was the case at low strain rate. At high strain rate, however, a bell shaped flow stress–temperature curve appeared, with first a decreasing flow stress with increasing temperature followed by an increasing flow stress with further increase in temperature until a peak value is reached. This feature is characteristic of a Dynamic Strain Ageing (DSA) phenomenon. The same feature has been observed for all steel grades and variants, independently of their ferrite/pearlite ratio.

DSA is due to recurrent pinning of dislocations while arrested at obstacles during their motion that results in plastic straining [19]. The phenomenon is attributed to the additional resistance of dislocation motion produced by the mobility of solute atoms (e.g., C and N for steels) that can diffuse to dislocations above a certain temperature while the dislocations are waiting at their short range barriers. As the solutes catch up with moving dislocations and pin them down, the flow stress increases. With increasing strain rates, higher temperatures are required to make the solute atoms to diffuse on dislocations at sufficient speeds. Thus, both plastic deformation behavior and DSA are dependent on both temperature and strain rate.

This feature was interesting from the material behavior point of view, and relatively easily integrated in the model. Nonetheless, it was demonstrated further (by cutting simulations with finite elements) that its integration in the behavior law had no influence on the cutting results.

TASK 2.4 Identification of the parameters of the constitutive model

Rheological model

As explained and described in detail above, the behavior of ferrite-pearlite steels strongly depends on different microstructural parameters such as phase fraction and probably also globular particle and grain size of pearlite, and on external loading conditions, such as strain rate and temperature. Moreover, during machining, elementary volume in the process zone experiences very high strain levels.

According the knowledge of the authors, no behavior law that could fulfill the requirements was available in the literature before this project. Therefore, new models have been developed in this project based on:

- the microstructure-based behavior law developed for composite ferrite-lamellar pearlite steels by Bouaziz et al [20]. This law has been developed to model cold-rolling of hot-bands in the flat steel product sector. As a consequence, it is restricted to room temperature deformation and to limited strain (up to 60%)
- the physically-based description of the strain rate sensitivity of ferritic steels proposed by Allain et al. [21].This law has been developed to model crash behavior of steels at room temperature. Its validity has been demonstrated only at low homologous temperatures up to 200°C and for strain rates up to 1000 s^{-1}.

These two models are the basis of our framework in which we have incorporated further mechanisms and improvements:

- An extended empirical description of work-hardening (stage IV [22]) in both phases to cover the interesting range of strains as listed before.
- An empirical hardening contribution of DSA to reproduce the flow stress peaks observed in certain temperature/strain rate ranges
- The behavior of globular pearlite as a new phase in the composite microstructure.

We have been obliged also to implicitly extend the validity of the previous models to other working conditions, for instance:

- physically-based description of the strain rate sensitivity which has been applied to pearlite and to strain rates higher than 1000 s^{-1}.
- microstructure-based models for lamellar components at high temperatures

In the following, the constitutive equations as well as the adjustment procedures of the parameters will be described in detail.

The macroscopic behavior is deduced from a homogenization law based on the iso mechanical work (iso-W) of each phase and given by equation (1) knowing the behavior of each constituting phase, *i.e.,* ferrite and lamellar pearlite in reference steels:

$$\sigma = F \cdot \sigma^{\mathrm{pearlite-dynamic}} + (1 - F) \cdot \sigma^{\mathrm{ferrite-dynamic}} \qquad (1)$$

Where :

- σ is the macroscopic flow stress of the ferrite-pearlite steel
- F is the pearlitic phase volume fraction
- $\sigma^{pearlite-dynamic}$ is the temperature/strain rate dependent flow stress of the pearlitic phase
- $\sigma^{ferrite-dynamic}$ is the temperature/strain rate dependent flow stress of the ferritic phase

Contrary to face-centered cubic (FCC as copper for instance), body centered cubic (BCC) metals whose strength is mainly due to forest obstacles to dislocation glide inside grains, body-centered cubic metals present an additional obstacle to dislocation glide which comes from lattice friction. Dislocation movement necessitates to overcome energetic barriers introduced by the periodicity of the lattice. This mechanism is thermally activated which means that the higher the temperature, the easier will the dislocation overcome the barriers. It also appears that edge parts of dislocations move faster than their screw parts. At sufficiently low temperature, dislocations in BCC structure

move by the creation of double-kinks of edge type along their screw parts. To account for this particular elementary mobility mechanism, a first formulation was proposed by Edgar Rauch [23]. The description has been used and developed in the work of Allain and Bouaziz ([21],[24]) and does refer to a "dynamic" behavior since it takes into account both the influence of temperature and strain rate on the flow stress. The dynamic behavior for each phase is given by the same formulae based on the work, initially developed for 100% ferritic steels. It is given by equation (2) with the addition of the term DSA when compared to the original formulation of Allain and Bouaziz:

$$\sigma^{dynamic} = \left(\sigma_0 \cdot \frac{\mu(T)}{\mu^0}\right) + \frac{\sigma^*}{2} + \frac{1}{2}\sqrt{(\sigma^*)^2 + 4(\sigma_i)^2} + DSA \tag{2}$$

With

$$\sigma_i = \sigma^{static} - \left(\sigma_0 \cdot \frac{\mu(T)}{\mu^0}\right) \tag{3}$$

The different terms are explained below:

σ₀   Contribution of the lattice friction at room temperature and the effects of solid solution hardening. Its value depends on the content of alloying elements: Mn, Si, Cu, Ni, Cr, B, Mo and Al. For the considered grades, it varies between 100 and 200 MPa. This contribution is weighted by a temperature dependent term $\mu(T)/\mu^0$.

σ*   Effective stress necessary for dislocations to overcome local obstacles (thermally activated mechanism), i.e., the double-kink mechanisms

σᵢ   Long-range internal stress that hinders dislocation glide (structural hardening). It sizes with the elastic shear modulus.
σ_i describes the work-hardening behavior at low strain rate, i.e., the quasistatic behavior.

μ(T)   Shear modulus; the evolution of μ with temperature is taken from the literature [25]. At RT, $\mu(T)$ is called μ^0

DSA   Contribution of Dynamic Strain Ageing (DSA) that depends on temperature and strain rate.

The DSA contributions have been determined using an empirical approach adjusted on experimental results, inspired from literature [26]:

$$DSA^{pearlite} = \sigma^{max} \cdot exp\left(-\left(\frac{\left(T - \left(T_C + A \cdot (log(\dot{\varepsilon}^{pearlite}) + B)\right)\right)^2}{\Delta T^2}\right)\right) \tag{4}$$

With:

σᵐᵃˣ   Maximum stress for DSA

T_C   Temperature of DSA peak at low strain-rate

A and B   Two calibrating parameters

ΔT   Temperature range where DSA does occur

These parameters have been identified for model 100% lamellar pearlitic steel (C70).

Pearlitic and ferritic phases follow different quasi-static behavior laws. Their sensitivities to temperature and strain rate are not necessarily similar, neither are their effective stresses. The effective stress to overcome local obstacles derives from a general formulation [27] based on Orowan's mobility relation and is given by equation (5):

$$\sigma^* = \left[\frac{k_B T}{V^* b^3} \cdot asinh\left(\frac{\dot{\varepsilon}}{2M\rho_m \nu_{Debye} b^2 exp\left(-\frac{\Delta G_0}{k_B T}\right)}\right)\right] \tag{5}$$

The meaning and value of the different parameters are given in Table 8:

Parameter	Definition	Value	Unit
k_B	Boltzmann constant	1.38E-23	$[J.K^{-1}]$
V^*	Activation volume	3.5 for pearlite 5.0 for ferrite	b^3
b	Burgers vector	$2.5.10^{-10}$	$[m]$
ρ_m	Density of mobile dislocations	1.10^{10}	$[m^{-2}]$
ν_{Debye}	Debye frequency	1.10^{13}	$[s^{-1}]$
M	Mean Taylor factor	3	$[-]$
ΔG_0	Activation energy	0.27 for pearlite 0.22 for ferrite	$[eV]$

Table 8 : Physical parameters related to the effective stress σ^* equation.

Equation (5) contains only two unknown parameters, V^* and ΔG_0, which are linked to the thermally activated gliding mechanism. These parameters are independent of the temperature, and are different for ferrite and pearlite. They have been identified for the pearlitic phase (C70 grade: 100% pearlitic) from the experimental data of the flow stress evolution with strain rate. The parameters of the ferritic phase have then been fitted to be suitable for the ferrite-pearlite grades. The orders of magnitude are similar to those proposed by Allain et al. [21].

The plastic strain rate $\dot{\varepsilon}^p$ is calculated for each increment of plastic strain $d\varepsilon^p$ and is different for the pearlite and ferrite phases (equation (6) and (7)). In fact, as the phase does not have the same flow stress, iso-W assumption imposes that ferrite phase deforms more than pearlite phase.

$$d\varepsilon^{p-pearlite} = d\varepsilon^{p-ferrite} \cdot \frac{\sigma^{ferrite-dynamic}}{\sigma^{pearlite-dynamic}} \tag{6}$$

$$d\varepsilon^{p-ferrite} = \frac{d\varepsilon^p}{(1-F) + F \dfrac{\sigma^{ferrite-dynamic}}{\sigma^{pearlite-dynamic}}} \tag{7}$$

Description of the ferritic phase

The evolution of the flow stress of the ferritic phase is based on the forest hardening model proposed by Mecking, Kocks, Estrin and Bergström [28]-[30]:

$$\sigma^{ferrite-static} = \sigma_0 \cdot \frac{\mu(T)}{\mu^0} + X^{ferrite} + \alpha M \mu(T) b \sqrt{\rho^{ferrite}} + \theta^{IV} . \varepsilon^{ferrite} \tag{8}$$

The different terms are explained below:

$X^{ferrite}$ Kinematic hardening which increases with the density of geometrically necessary dislocations. This contribution is related to **the key parameter d** which is the ferritic grain size.

α Constant related to the forest dislocations hardening for the ferrite phase; α is typically taken equal to 0.4

$\rho^{ferrite}$ Statistically stored dislocation density in ferrite; it grows with increasing plastic strain towards a saturating value. This contribution is also related to the **key parameter d** which is the ferritic grain size.

θ^{IV} Stage IV, saturating, of work-hardening; Θ^{IV} was taken equal to 100 MPa.

The evolution of $X^{ferrite}$ is given by the following equation:

$$X^{ferrite} = \frac{M\mu(T)b}{d \cdot 10^{-6}}\left(n_0\left(1 - \exp\left(-\frac{\lambda \cdot \varepsilon^{p-ferrite}}{n_0}\right)\right)\right) \quad (9)$$

Where two parameters, fitted from Bauschinger effect measurements on ferritic steels [32] are introduced:

n_0   Threshold density of geometrically necessary dislocations (GND); in the present model: $n_0 = 2.82$

λ   Density of shear bands; in the present model: $\lambda = 34.5$

d in this model is given in micron.

Development made for the pearlitic phase

Note (4): The description of the behavior of lamellar pearlite comes from an empirical formulation, taken from Allain et al. [32]. In pearlitic steels the yield stress increases with decreasing interlamellar spacing ([33]-[36]). This law is based on saturation Voce's law which does not contain an explicit term related to dislocation density contrary to the scheme suggested by Mecking, Kocks and Estrin ([28],[29]). The initial flow stress for pearlite is controlled by **the key parameter s**, which is the interlamellar spacing of lamellar pearlite, and by plastic work-hardening, considered here as fully isotropic. It is given by the following equation:

$$\sigma^{pearlite-static} = \left(\sigma_0 + \frac{M\mu b}{s.10^{-9}} + \left(\frac{K}{g}\cdot\left(1 - \exp\left(\frac{\varepsilon^{pearlite}.g}{2}\right)\right)\right) + \theta^{IV}.\varepsilon^{pearlite}\right)\cdot\frac{\mu(T)}{\mu^0} \quad (10)$$

Where the following parameters are introduced:

s   Interlamellar spacing of pearlite; depends on the microstructure of each grade; it is kept constant along the deformation, given in micron.
K   Empirical constant hardening parameter which describes the initial slope of work-hardening
g   Empirical hardening parameter which depends on the temperature
θ^{IV}   Stage IV, saturating of work-hardening; θ^{IV} was taken equal to 100 MPa.

The comparison between the model after adjustment and the experimental results of lamellar C70 give satisfactory results in quasi-static conditions, as shown in Figure 16
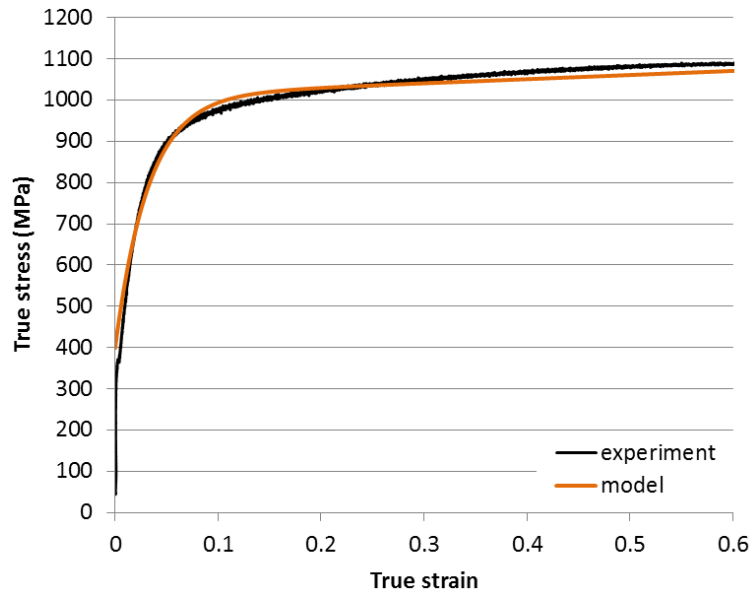
Figure 16: Comparison between the modeled and the experimental data for 100% (lamellar) pearlitic C70 steel at 20°C and 10^{-3} s^{-1}.

Globular pearlite

The different microstructural variants (Reference, Coarse Grain, Wide Bands and Globular Pearlite) are only distinguished in the model by the three parameters, the volume fraction of pearlite, the ferritic grain size and the interlamellar spacing of lamellar pearlite, as mentioned above. For the description of GP grades, the interlamellar spacing of broken pearlite (relatively high) was first taken into account. To allow a more appropriate description of the globular pearlite behavior (cementite carbides in a ferritic matrix), a specific formulation is now proposed.

Introducing the description of the globular pearlite, equation (1) becomes:

$$\sigma = F \cdot \sigma^{pearlite-dynamic} + F_G \cdot \sigma^{pearlite\ G-dynamic} + (1 - F - F_G) \cdot \sigma^{ferrite-dynamic} \tag{11}$$

With:

F_G The fraction phase of globular pearlite
$\sigma^{pearlite\ G-dynamic}$ The evolution with temperature and strain rate of the globular pearlite

Equations (2) - (5) are also valid for globular pearlite, associating the appropriate strain rate $\dot{\varepsilon}^{pearlite\ G}$.

Only the formulation of the quasi-static behavior is different and given by equation (12). This formula is adapted from the formulation proposed for dual phase steels (ferrite steel with low fraction of hard martensite) which is assumed to be similar to the ferrite steel hardened by coarse granular carbides [37].

$$
\begin{aligned}
\sigma^{pearlite\ G-static} = &\left(\sigma_0 + \alpha M \mu \sqrt{b} \sqrt{\frac{1 - \exp\left(-f_G M(\varepsilon_G{}^{pearlite})\right)}{f d^{\alpha G}} + 8\left(\frac{F_m}{d_m}\right) \cdot \frac{1 - \exp\left(-r M(\varepsilon_G{}^{pearlite})\right)}{r}} \right. \\
&\left. + M \mu \sqrt{b} \cdot \left(\frac{F_m}{d_m}\right) \sqrt{\frac{1 - \exp(-r' M \varepsilon_G{}^{pearlite})}{r'}} + \theta^{IV} \cdot \varepsilon_G{}^{pearlite} \right) \cdot \frac{\mu(T)}{\mu^0}
\end{aligned} \tag{12}
$$

With:

$d^{\alpha G}$ Ferritic grain size in globular pearlite

F_m Fraction of cementite carbides ; taken constant at 0.12 (12 % of cementite inside pearlite) at equilibrium

d_m Size of cementite carbides

f_G Dynamic recovery; fitting parameter: $f_G = 1.7$

r Saturating parameter of isotropic hardening ; fitting parameter: $r = 14$

r' Saturating parameter of kinematic hardening ; fitting parameter: $r' = 14$

Parameters $d^{\alpha G}$, F_m and d_m are determined from the microstructure analysis of globular C70.

Compression tests at low strain rate (Gleeble) and at room temperature have been performed on 100% globular pearlite C70 as mentioned earlier. The comparison between the model after adjustment and the experimental results of globular C70 gave satisfactory results in quasi-static conditions.

Solver algorithm

An overview of the different equations presented above is given in Appendix 7.1.3. It shows the way they interact together to obtain the behavior law (in terms of plastic strain and flow stress for each F+P material) which will be integrated in the cutting simulation.

Analysis of the microstructure to feed the model

The analysis of microstructural parameters was a time-consuming and key task of WP2 for the validation of the model with the experimental data. The ferritic grain size and the fraction of phases were determined by optical analyses of the microstructure. The interlamellar spacing was determined by SEM analyses. It is important to mention that the uncertainties in microstructure measurements are a possible source of discrepancies between modelled and experimental results that should be considered carefully in the analysis.

Results of modelling

Note (5): The developed model has been implemented using Excel. All differential equations have been integrated following a purely explicit method. An Excel folder has been produced for each microstructural variant. One sheet must be used for every tested temperature and strain rate condition. In each sheet, the macroscopic flow stress (equation (1)) and the flow stresses of each phase (equation (2), (8) and (10)) can be plotted versus the macroscopic plastic strain or the plastic strain of phases. A table with the different interesting values can easily be extracted from the Excel files to be integrated as input in the finite element models for cutting simulation (implementation by tabulated values in Abaqus).

Modeling C70 grade

The results of the model for C70 are presented in Figure 17. As the physical aspect of the model is limited to low strains, only the first 20 % of strain are represented below and compared with the experimental data at 20°C and 500°C, for each strain rate.
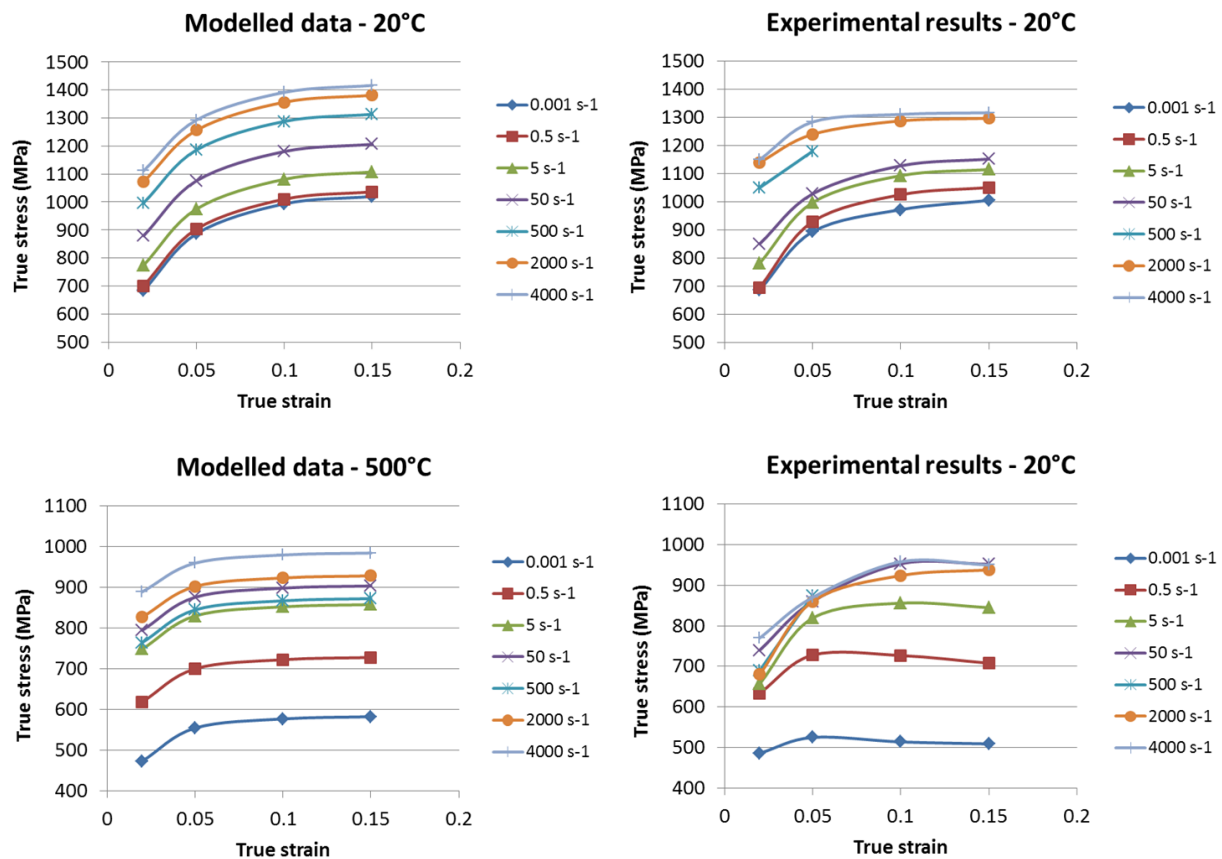
Figure 17: Comparison between the modelled and the experimental results for C70 at different strain rates 20°C (up) and 500°C (bottom).

The modelling results are consistent with the experimental data, with a very accurate description of the stress levels and of the influence of strain rate at 20°C, except for the highest strains at very high strain rate, where the plateau observed cannot be caught by the model.

Note (6): The description of the behavior at 500°C is also consistent with the tendencies observed in terms of strain rate; the main difficulty lies in the presence of softening in the experimental data, especially visible for 0.0001 s^{-1} and 0.5 s^{-1} from 0.05 strain, which cannot be captured by the actual model.

Influence of strain rate and temperature

Two examples of the modelling results for ferrite-pearlite grades are given in appendices (7.1.4 and 7.1.5). As for C70, these results are focused on the first 20% of strain, where a good correlation between the model and the experimental results is obtained. At higher strain, the modelled flow stress is continuously increasing due to the addition of stage IV hardening, the softening (due mainly to self-heating) observed experimentally on every grade is not taken into account (appendix 7.1.6). It can be noticed that the main tendencies are well captured.

Influence of variants

The flow stress of C45 and C60 grades which have the highest pearlite content show the most highest sensitivity to microstructure. Appendix 7.1.7 presents the comparison between the modelled and the experimental data for these two grades, at 20°C and 0.5 s^{-1}. As mentioned earlier in the report, some parameters have been adjusted for the ferritic phase (activation energy and volume, DSA parameters) after the identification on C70 for the pearlitic phase. This work has been done on the reference grades, C45R and C60R. This figure displays good agreement for these variants between the modelled and the experimental data. In the model, the different variants are only distinguished by the different microstructural parameters (phase ratio, ferritic grain size, interlamellar spacing, cementite carbide size for globular pearlite). The results of this figure show that the tendency is rather well described by the model, although the experimental and modelled stress levels are not always in agreement.

CONCLUSION

The characterization of the thermos-mechanical behavior and modeling work made in WP2 of IMMAC Project were a keystone for the work done in subsequent WPs. A huge amount of data emerged from the experimental characterizations. These data have been treated to extract the most representative configurations of cutting conditions. Besides, the interesting feature of Dynamic Strain Aging (DSA) has been highlighted in the behavior of all the steel grades.

The rheological model developed in this project shows good results and is successful to capture the main tendencies of the experimental data taking into account the microstructure of the steel grades. However some improvements can be considered for a better agreement with the experimental data. A list of the parameters of the model is given in a table in appendix 7.1.8, reminding their meaning, specifying if they are physical or empirical and suggesting possible improvement.

The influence of the strain rate on the flow stress could potentially be improved with an adapted description of the Iso W homogenization law at low and high strain rate.

To be able to accurately describe the influence of temperature, softening should be taken into account including a deeper analysis of the microstructure during and after the compression tests.

2.2.3 WP3: Tribology – identification of contact laws

Task	Title	Initial plan	Actual plan	Note
Task 3.1	Experimental tests in dry conditions	Tests with 2 tests rigs: open & close contact Open tests with various normal load 1 tool system (substrate+coating)	Dry tests with the open configuration only 4 different tool systems, consistent with the investigated cutting processes Constant normal load	(1) (2)
Task 3.2	Contact mechanisms	No change compared to the initial plan		
Task 3.3	Mechanical and thermal models	Friction model depending on sliding velocity, contact pressure, microstructural parameter Heat partition model depending on sliding velocity, contact pressure, microstructural parameter	Friction model depending on sliding velocity and ferrite ratio Heat partition model depending on sliding velocity	(3)
Task 3.4	Influence of the lubricant	Lubricated tests on 3 selected variants in open and close configurations	Lubricated tests on 14 variants and 2 contact conditions in close configuration Lubricated tests on 8 variants and 2 tool systems in open configuration	(4)

The objective of WP3 was to identify the effect of the microstructure on the tribological properties of the investigated variants. Measuring friction coefficients, heat partition and getting trends in terms of wear were of interest from a practical and numerical point of view.

Note (1): CRF faced difficulties in running the tribological tests under dry conditions due to excessive heat generation, material transfer and vibrations of the experimental set-up.
Therefore, the two partners decided to focus their experimental campaign on a dedicated cutting operation as presented in Figure 18. Attention has been paid to use friction pins made of the same substrate and coating as in the final cutting operation.

ENISE carried out two campaigns, one focused on "Turning" using TiN coated tungsten carbide friction pins (WC-Co + TiN) under dry conditions and on "Broaching" using uncoated and TiN coated M35 High Speed Steel friction pins (HSS) both under dry and lubricated (oil) conditions.
In order to perform tests closer to the drilling operation performed in FCA production line under Micro Quantity Lubrication (MQL), CRF carried out a campaign on a close tribosystem, more suitable to simulate the contact between the drill (margins) and the workpiece, under lubricated conditions (same oil used for MQL) and WC-Co + TiAlN friction pins.
A detailed description of each experimental setup is described in appendices 7.2.1 and 7.2.2.

The friction coefficient is calculated based on the tangential force recorded during a tribological test under a given normal force and sliding velocity. Each test approximately lasts 10s and the friction coefficient values displayed in the figures is the average over approximately 7s of steady state sliding. More details can be found in appendices 7.2.

Partner	ENISE	CENTRO RICERCHE FIAT
Operation	Turning	Broaching	Drilling
Pin VS Tool	WC-Co + TiN	Uncoated HSS & HSS + TiN	WC-Co + TiAlN
Lubrication		Straight oil	MQL
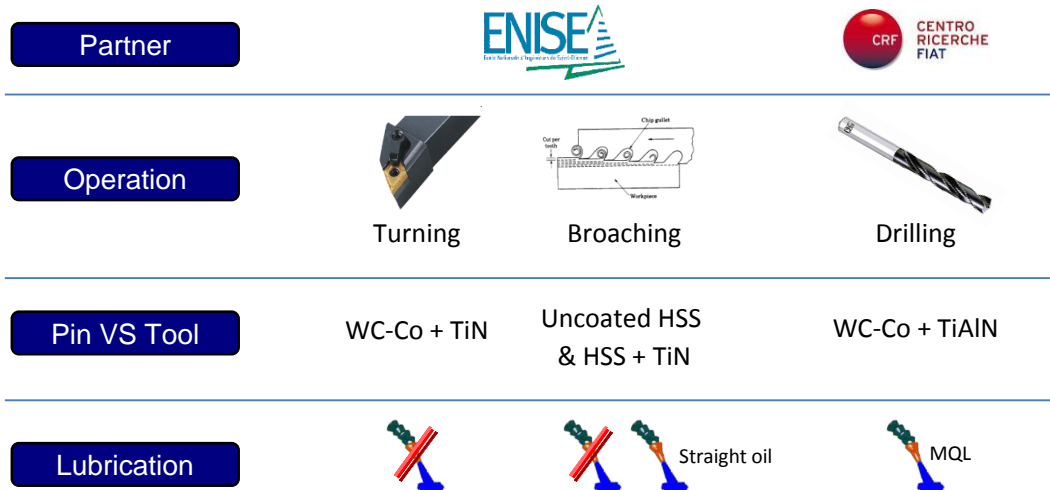
Figure 18: Strategy developed in WP3 and consistency between the tribological tests and the concerned cutting operations.

TASK 3.1 Experimental tests in dry conditions

This task aimed at providing quantitative data to be input in the numerical models but also to gain a fundamental understanding of how microstructural parameters can affect the tribological behaviour when in contact with a coated carbide pin. Three different sliding speeds were selected: 10, 100 and 300m/min to cover the mechanisms that could appear at high speeds but also at lower sliding velocities. Three repetitions were performed for each sliding conditions and sometimes one more leading a total of 140 experiments. In the figures, the results for the tests performed at 10, 100 and 300m/min have been displayed by slightly spreading/spacing each data point in order to make it easier for the reader. The data points on the left were all performed at 10m/min, those in the centre at 100m/min and those on the right of the plot at 300m/min.

Note (2): After performing some preliminary tests at 300 and 1000 N, it was decided to perform the whole set of experiments only at 1000 N as no drastic difference has been observed between these two normal loads. 1000 N also enables to perform the tests at a contact pressure of approximately 1.2 GPa which is consistent with what is expected to occur at most of the tool-chip interface.

a) Results with WC-Co + TiN pins (Dry turning)

The first campaign (C1) with the coated tungsten carbide pins focused on conditions similar to a turning operation. The Figure 19 shows the summary of the experimental results.
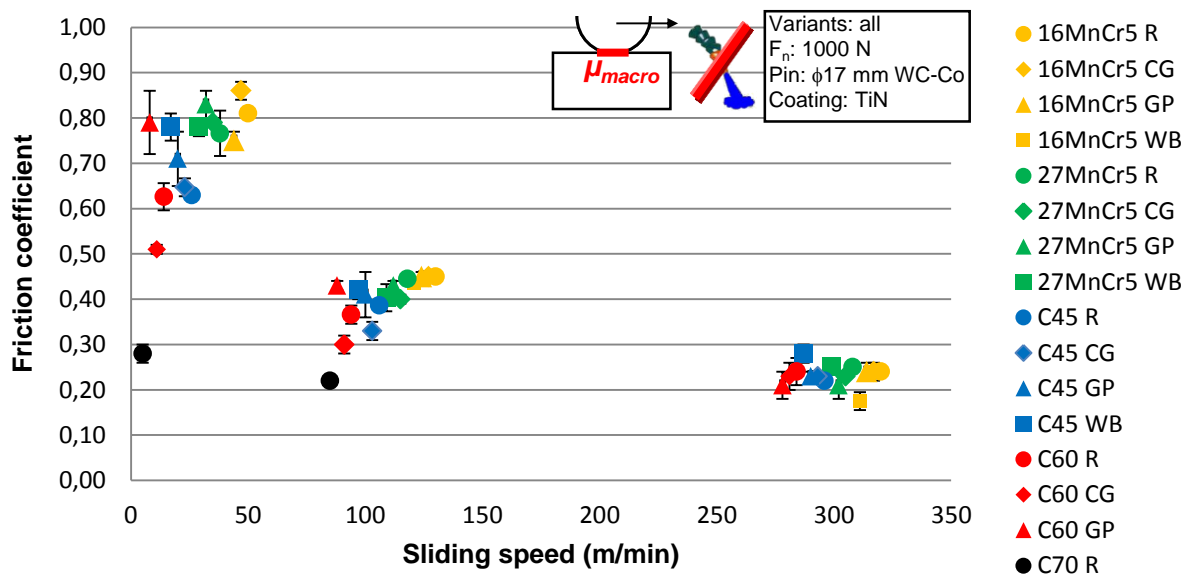
Figure 19: Updated evolution of the macroscopic friction coefficient with sliding velocity for each variant.

40

Analysing separately the contribution of the different microstructure morphologies leads us to the Figure 20 which concludes on the main trends that have been observed regarding the frictional behaviour:

- The friction coefficient is above all dependent on the sliding velocity;
- Changing the microstructure to coarser pearlite grains (CG) reduces friction;
- A globular pearlite (GP) increases friction at low and medium sliding velocity;
- A banded structure (WB) seems to increase friction but to a lower extent;
- Increasing the pearlite content is leading to a lower friction coefficient.
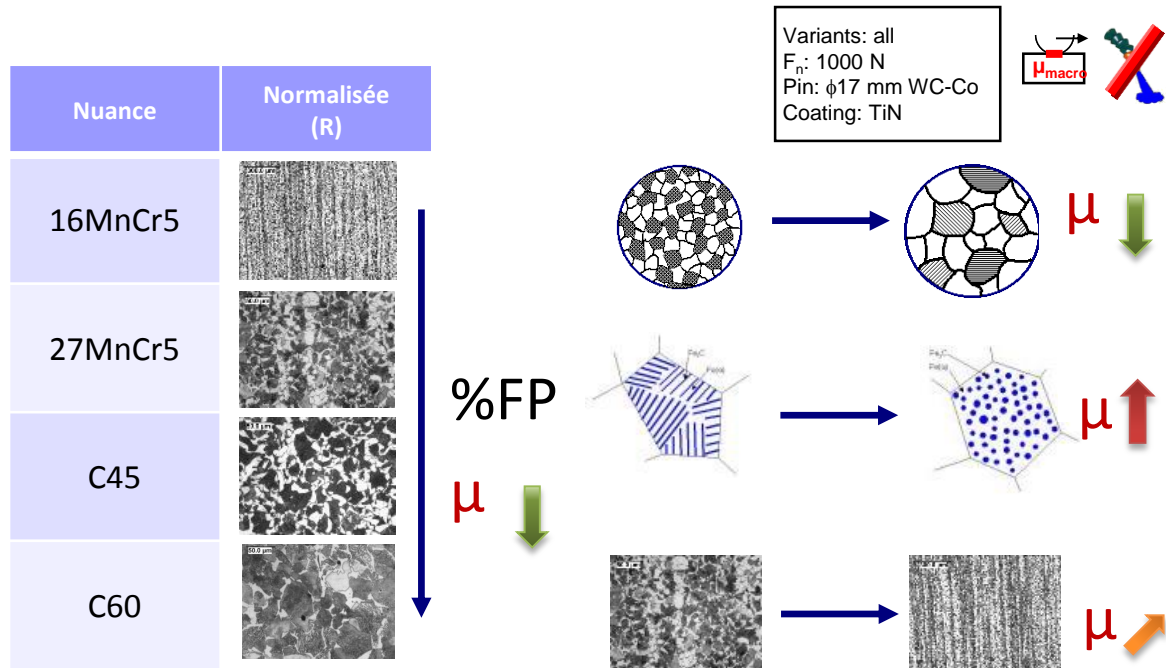
Figure 20: Trends observed compared to the standard variant when using TiN coated WC-Co pins.

Regarding heat partition coefficient, the Figure 21 shows that the heat partition coefficient depends to a great extent on the sliding velocity. Most of the energy is transmitted to the carbide pin with a maximum of 30% with the C45 CG at 10 m/min. This amount is decreasing from a factor 3 to 6 when increasing the sliding velocity, i.e. more energy is transmitted to the workpiece.
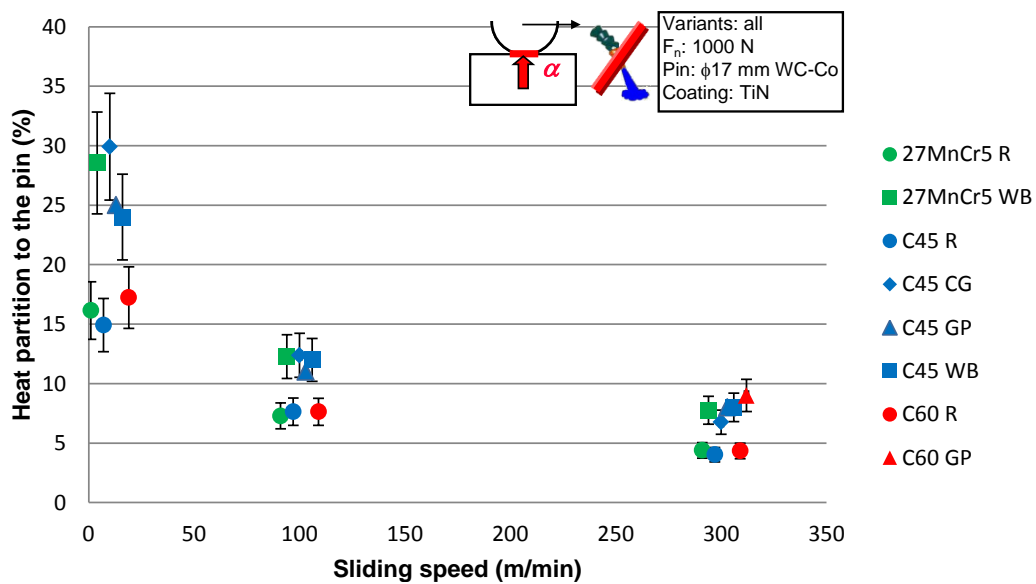
Figure 21: Evolution of the heat partition to the pin with sliding velocity for each variant.

Note (3): Considering the observed deviation and the precision of the measurement technique itself, the authors do not think that the variants can really be dissociated based on these results. Moreover, the instrumentation of the pin holder has been damaged and sent for maintenance with a different temperature sensor implemented (thermocouple instead of thermistor). Based on these considerations and assumptions, it won't be possible to dissociate the effect of the variants on heat partition coefficient.

b) Results with Uncoated HSS & HSS + TiN pins (Dry broaching)

The second campaign (C2) focused on dry contact under broaching conditions using uncoated and TiN coated High Speed Steel (HSS) pins. All the tests were performed in dry conditions to amplify the possible differences between the variants and not to introduce a third body at the interface.

The summary of the recorded friction coefficients is presented in Figure 22 depending on the sliding velocity and keeping the agreed colour code. The following conclusions could be drawn:

- The effect of the sliding velocity is less predominant that in C1. However, the friction coefficient with the uncoated pins seems to decrease when increasing the sliding speed from 2 to 60 m/min.
- The effect of the carbon content (ferrite-pearlite ratio) can again be seen at the lowest speeds. Experiments performed at 60 m/min with the uncoated pins exhibited a lot of wear which can affect the interpretation of the results;
- Applying a TiN coating (Figure 22b) lowers the friction coefficient mainly at 2 m/min and at 20 m/min to a lower extent. Adhesion is drastically reduced which leads to a better stability of the friction tests.

The Figure 23 graphically summarises the main trends observed on the uncoated HSS pins exhibiting the largest differences in terms of microstructure

Note (3) : Considering the large deviation observed in the friction coefficient, it did not really make sense to calculate the heat partition coefficient as presented in the previous subsection.
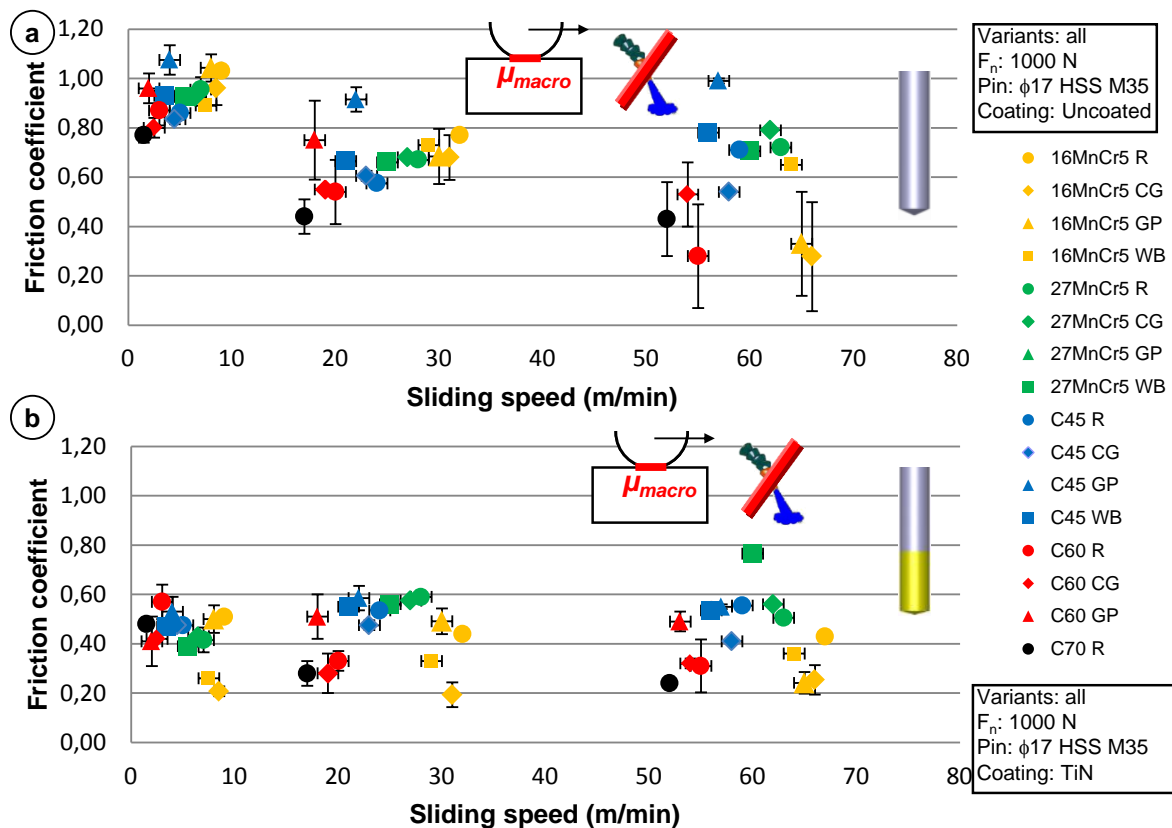
Figure 22: Evolution of the macroscopic friction coefficient with sliding velocity for each variant with a) uncoated HSS pins and b) TiN coated HSS pins.
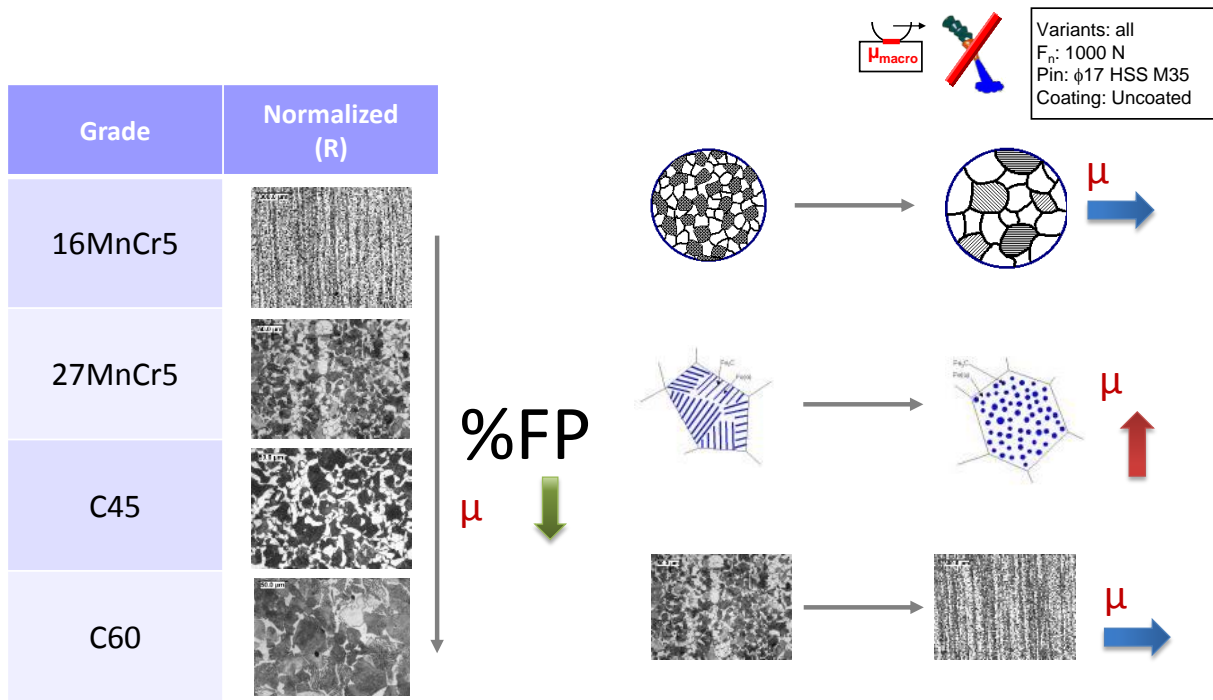
Figure 23: Trends observed compared to the standard variant when using uncoated and HSS pins.

TASK 3.2 Contact mechanisms

These analyses were focused on the coated carbide pins (C1) and on some selected variants and/or sliding conditions. Analysing the contact tracks (Figure 24) shows that low carbon variants lead to less stable frictional behaviours at low sliding velocities (stick-slip phenomenon). The topography of the contact tracks presents some wavelets whereas increasing the carbon content (C45 and C60) or increasing the velocity limits the occurrence of this phenomenon.
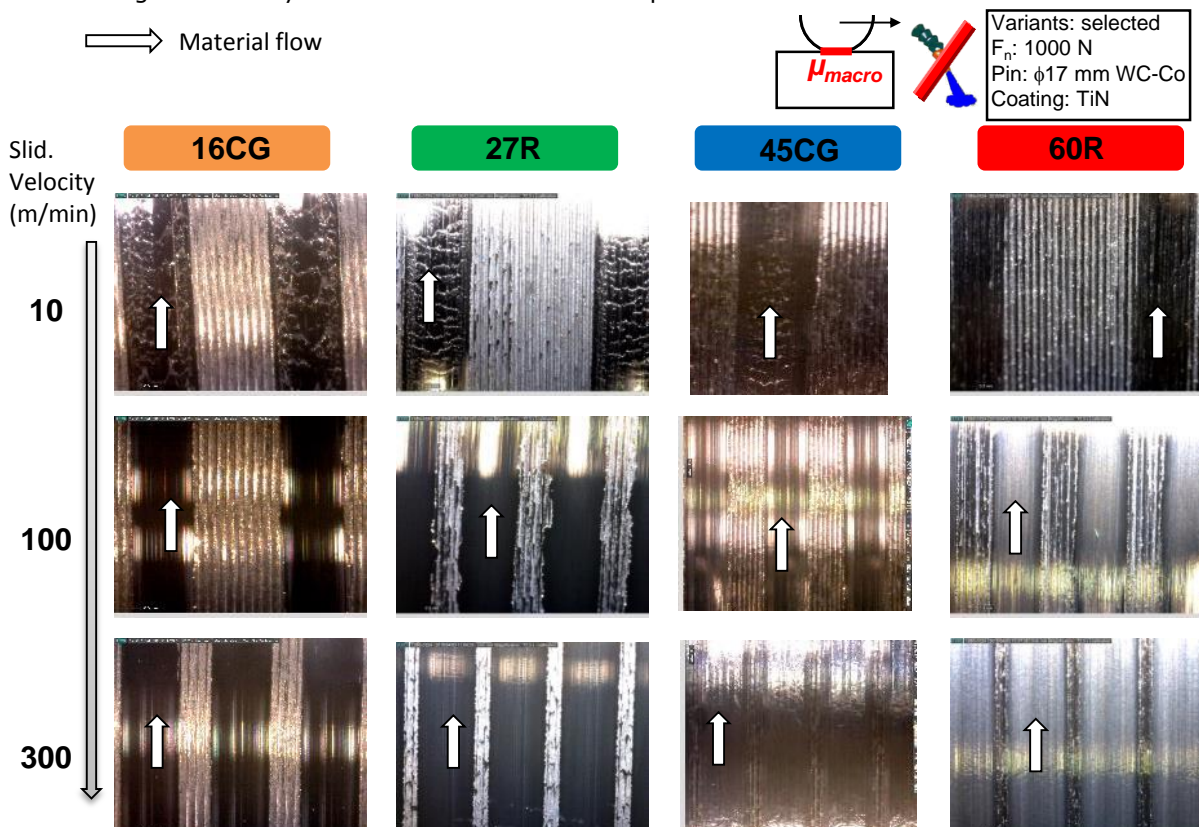
Figure 24: Examples of contact tracks observed on the workmaterial in C1 at different sliding velocities and for some selected variants – WC-Co+Tin pins.

Transfer mechanisms were thoroughly analysed on the tests performed at 300 m/min using Energy Dispersive X-ray spectrometry (EDX). It was shown that both the size and morphology of the contact area depend on the carbon content and microstructure. From a general point of view, variants of the 16MnCr5 and 27MnCr5 exhibit a more intense material transfer than C45 and C60. Figure 25a illustrate this finding at two different sliding velocities for two representative grades and selected variants whereas Figure 25b-c prove that the adhesion tendency is mainly directed by the ferrite pearlite ratio instead of the hardness as expected.
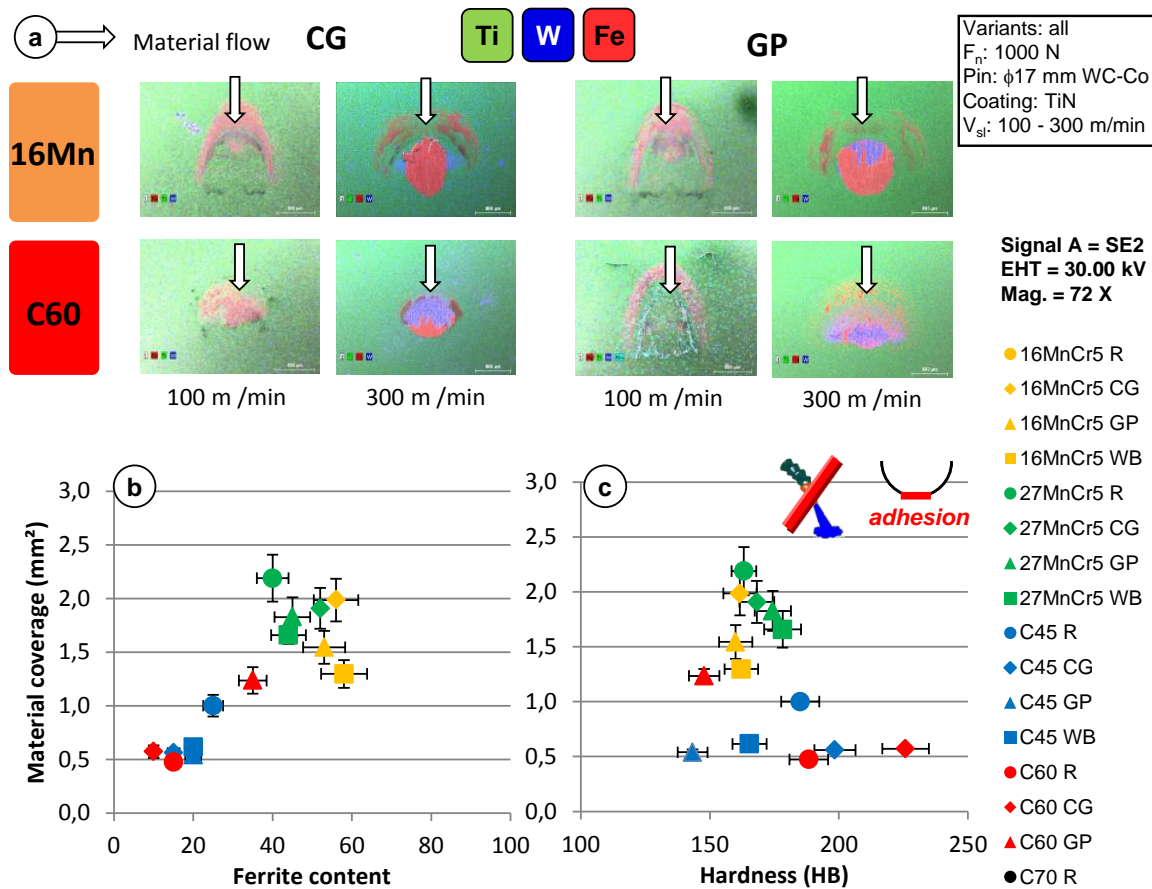
Figure 25 : a) Material transfer observed on the WC-Co + TiN coated pins at 100 and 300 m/min, b-c) Evolution of material coverage on the pins with the microstructural parameters.

Different wear mechanisms were observed on the friction pins at this sliding velocity. Low carbon grades lead to an intense material transfer within the contact zone but also a severe delamination of the coating all around the entrance of the contact. When increasing the carbon content, the dominant wear mode changed to abrasive wear. Abrasive grooves could be clearly seen the C60 variants whereas material transfer was found only at the back of the contact. Details can be found in appendix 7.2.3.

TASK 3.3 Mechanical and thermal models

Note (3): Results were thus plotted versus several material parameters. The large deviation observed on the interlamellar spacing did not enable to properly identify a friction model pendent on this parameter. Detailed results are presented in appendix 7.2.5; a fitting procedure has been developed and the following equation (13), relating the friction coefficient to the sliding velocity (V_{sl}) and ferrite content (%F), has been fitted on the obtained results.

It has been generally observed that the friction coefficient decays exponentially from a static value **µs** to the kinetic value **µk** according to the equation 13. For each variant, a least square method using the simplex algorithm has first been used to identify the parameters **µs**, **µk** and **dµ** leading to the best fit of the friction coefficient versus the sliding velocities. Then these triplets were plotted versus each of the microstructural parameter in order to check if a possible trend/correlation could be observed. The power laws and polynomial equations given in the Table 9 were found to be the expressions fitting the best the evolution of **µs**, **µk** and **dµ** versus the ferrite content.

The same methodology was then applied to identify the **correcting factor K** for CG and GP variants: relative differences compared to the standard variants were plotted versus the microstructural parameters and polynomial expressions fitted on the given data.
The Table 9 summarizes the coefficients identified for the main two different tool systems.

$$\mu(V_{sl}) = \left(\mu_k + (\mu_s - \mu_k) \times \exp(-d_\mu \|V_{sl}\|) \right) \times (1 + K(\|V_{sl}\|)) \tag{13}$$

Tool	μ_k	μ_s	d_μ	$K_{CG}(\|V_{sl}\|)$	$K_{GP}(\|V_{sl}\|)$
WC-Co + TiN	$0.25 \times \%F^{-0.06}$	$0.26 \times \%F^{0.32}$	$2.2\ 10^{-4} \times \%F^2$ $-0.015 \times \%F$ $+ 0.963$	$(-2\ 10^{-5} \times \|V_{sl}\|$ $-5.8\ 10^{-3}) \times \%F$ $+ 7\ 10^{-4} \times \|V_{sl}\|$ $- 0.239$	$(3\ 10^{-5} \times \|V_{sl}\|$ $-7\ 10^{-3}) \times \%F$ $- 1.5\ 10^{-3}$ $\times \|V_{sl}\| + 0.355$
Uncoated HSS	$0.37 \times \%F^{0.17}$	$-2.8\ 10^{-4} \times \%F^2$ $-1.15\ 10^{-2} \times \%F$ $+ 1.37$	25	$(-2\ 10^{-5} \times \|V_{sl}\|$ $-5.8\ 10^{-3}) \times \%F$ $+ 7\ 10^{-4} \times \|V_{sl}\|$ $- 0.239$	$(3\ 10^{-5} \times \|V_{sl}\|$ $-7\ 10^{-3}) \times \%F$ $- 1.5\ 10^{-3}$ $\times \|V_{sl}\| + 0.355$

Table 9: Identified coefficients of the friction models depending on the selected tool system (K_{CG} and K_{GP} correction factors with uncoated HSS tools are only valid between 2 and 20 m/min and for the grades C45 and C60)

Nevertheless, these models do not take into account the friction modification when changing the structure to a banded structure as the trends were not that obvious. Instead, tabular data directly provided by the tribological tests could be used and implemented in the different numerical models. According to the large deviations observed with the uncoated HSS with the 16MnCr5 variants and at the highest sliding velocity, the proposed model for the CG and GP variants (KCG and KGP correction factors) is only valid between 2 and 20 m/min and for the grades C45 and C60. Comparison with the experimental results is shown in appendix 7.2.6.

Note (3): Regarding heat partitioning to the friction pin, no clear correlation to the microstructural parameters could be extracted due to the large deviations already observed on the heat flux. Therefore, the following heat partition model (equation (14)) only depending on the sliding velocity (V_{sl}) could be proposed to be implemented in the turning FE simulations (WC-Co + TiN tool system):

$$\alpha(V_{sl}) = \alpha_k + (\alpha_s - \alpha_k) \times exp(-d_\alpha \|V_{sl}\|)$$

$$\alpha_k = 6,4 \ - \ \alpha_s = 25 \ - \ d_\alpha = 0,98$$

(14)

TASK 3.4 Influence of the lubricant

a) Drilling oriented tests with oil used for MQL

Note (4): Compared to the initial plan, 14 variants were investigated under 2 different sliding conditions (26 and 147 m/min) leading to a full comparison between all the variants under drilling conditions.
Long friction tests were performed in this campaign (respectively 2.5 hours at 26 m/min and 30 min at 147 m/min) in order to assess the wear tendency (Figure 26). In the following bar charts, the friction coefficient is reported as the average value from ½ test duration to test end, pin wear is reported as an average value over the two test repetitions and results are displayed according to increasing wear track width.
Friction was found to be extremely low, especially at the highest sliding velocities. No clear trend was observed neither depending on grade nor on microstructure as friction values lied all between 0.12 and 0.14 at 26 m/min and 0.04-0.05 at 147 m/min.
When considering wear of the pin, the experiments performed at 147 m/min showed that wear tendency could somehow follow the evolution of the carbon content. This was not the case at the lowest sliding velocity of 26 m/min.
Friction pins resulting from the experiments performed at the highest sliding velocity were analysed using SEM/EDX. The figure in appendix 7.2.4 shows an example of the results obtained for a low and medium carbon steels. No adhesion phenomena on pins were observed in these tests; counterpart steel disc traces (Fe – red) were detected outside the wear track, along the track boundaries, mixed to cooling fluid (C –yellow) deposits. In some cases a complete worn off of the coating was observed (blue color inside the wear track), even if not for the full length of the track; at 147 m/min in general less pin wear could be noticed for lower carbon content steel disc mates, but a clear tendency concerning steel microstructure wasn't identifiable.
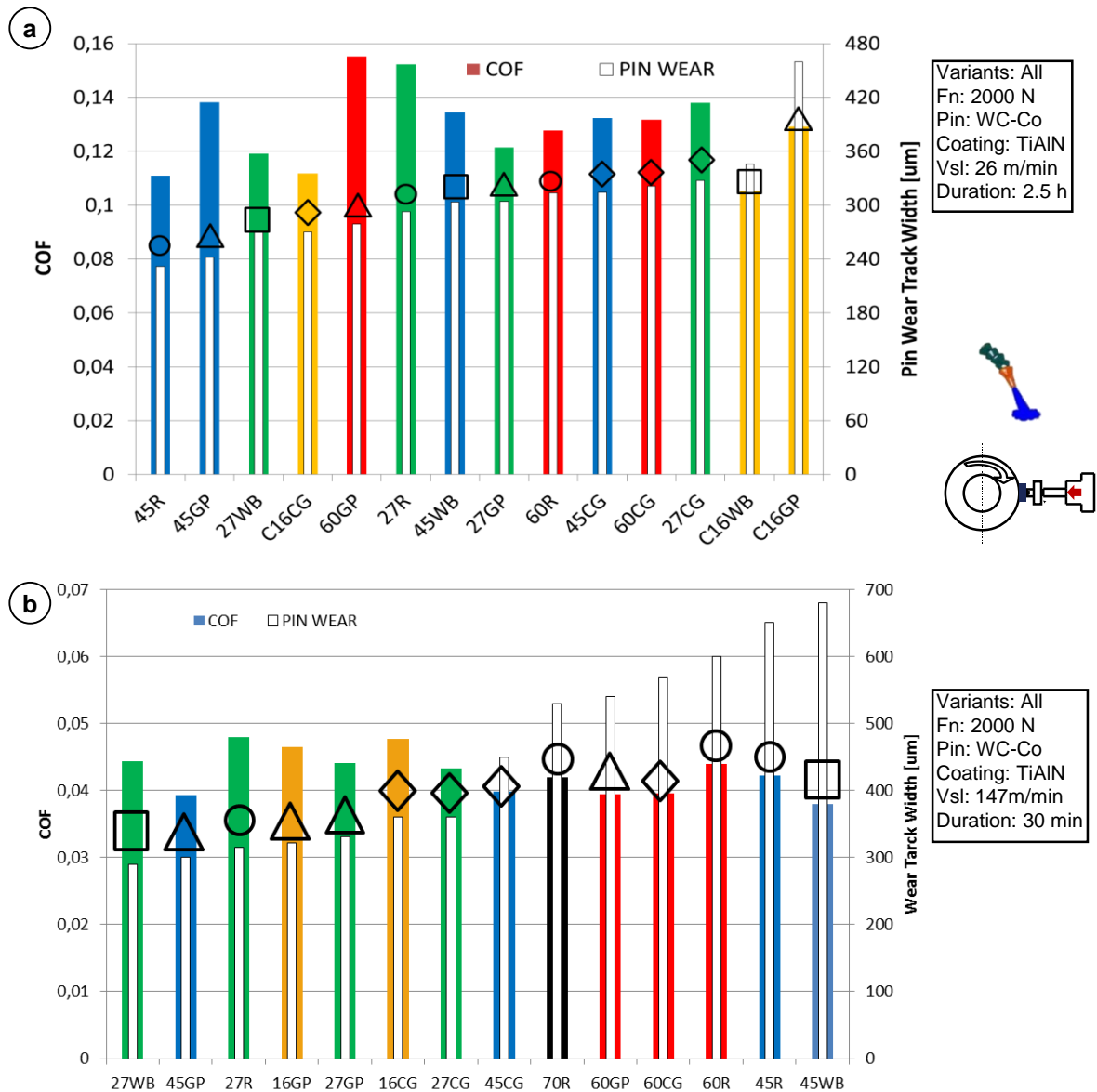
Figure 26: Friction coefficients and wear track widths measured at a) 26 m/min and b) 147 m/min under MQL conditions

b) Broaching oriented tests with straight oil

Note (4): A dedicated experimental campaign has been focused finally on the 8 variants selected in deliverable D1 instead of the 3 expected ones. A single sliding velocity corresponding to the cutting speed exhibiting the highest differences between the variants in dry broaching (2 m/min) have been selected and tested with the 2 tool systems.

Again, the clear effect of the coating was observed in Figure 27 but most important, was the drastic friction reduction resulting from the application of the lubricant. Friction coefficients reached values between 0.12 and 0.14 for every variant and whatever the pin material. This showed the high contribution of the lubricant compared to the microstructural properties of the variants. Nevertheless, this does not direct the results in terms of wear under lubricated conditions as, if some type of wear can be significantly reduced (adhesive wear), abrasive wear will not be affected and thus will still occur.
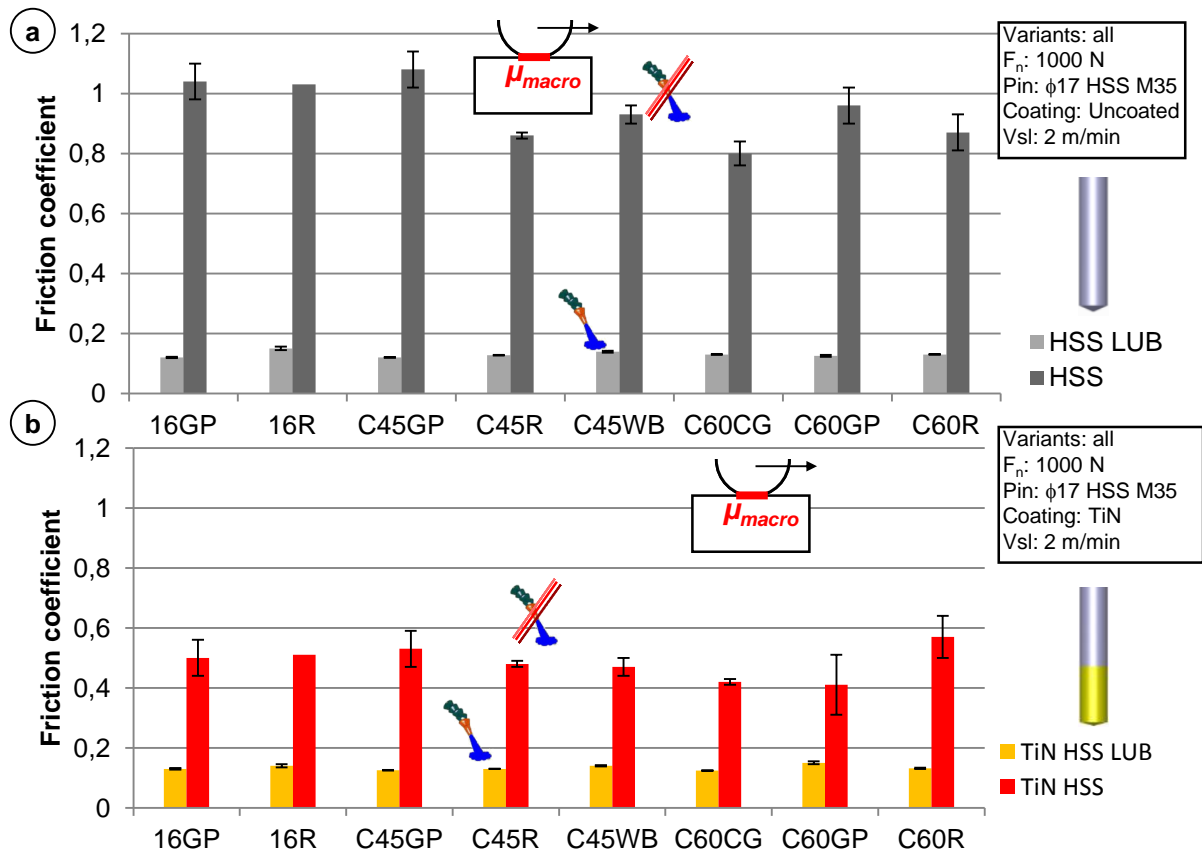
Figure 27: Influence of the lubricant (straight oil) on the friction coefficient compared to dry conditions with the a) uncoated HSS M35 pins and b) TiN coated HSS M35 pins.

CONCLUSION

From a practical point of view, the following conclusions can be extracted for each of the investigated processes:

1. **Turning** – TiN coated WC-Co pins
   a. Sliding velocity is an important parameter which drastically affects the tribological behavior of the different variants;
   b. Differences in terms of friction coefficient were mostly found at low sliding velocities;
   c. Using a globular pearlite tended to increase the friction coefficient but limits wear of the friction pin;
   d. Using a coarse pearlite grain tended to reduce the friction coefficient and leads to higher wear for some variants;
   e. Adhesion and wear tendency are mainly governed by the ferrite-pearlite ratio.
   f. A friction model depending on the sliding velocity and ferrite content has been proposed with a correction factor to include CG and GP effects;
   g. A heat partition model depending only on the sliding velocity has been proposed.

2. **Broaching** – uncoated and TiN coated HSS pins
   a. The sliding velocity had a more limited effect on the tribological behaviour;
   b. The frictional behavior was highly unstable when using uncoated HSS pins;
   c. The TiN significantly improved the tribological behavior by reducing friction and making it more stable;
   d. Differences in terms of friction coefficient were mostly found at the lowest sliding velocity of 2 m/min;
   e. Using a globular pearlite microstructure tended to increase the friction coefficient;
   f. The trend was not obvious as coarse grain and banded structures were concerned;
   g. The use of a lubricant drastically reduced the friction level and completely erased the differences between the variants;

h. A friction model depending on the sliding velocity and ferrite content has been proposed for uncoated HSS pins with a correction factor to include CG and GP effects (limited use between 2 and 20 m/min);

3. **Drilling** – TiAlN coated WC-Co pins
   a. Friction coefficient was drastically reduced as soon as the lubricant was applied;
   b. Friction decreased even more when increasing the sliding velocity;
   c. At higher velocities 147m/min, higher pin wear was detected for steel with higher C content;
   d. No clear tendency was observed depending on the microstructure type;
   e. Lubricating with MQL was able to limit the occurrence of material transfer to the tool.

Only three significant deviations from the work plan occurred: (i) the impossibility for CRF to perform the tests under dry conditions, (ii) the limited effect of the normal load observed by ENISE and (iii) the lack of sensitivity and damage of the heat flux measurement system. Extension of the experimental campaigns to additional variants and/or contact conditions and/or tool systems were selected as alternatives and resulted in valuable results.

Important aspects such as local wear and material transfer phenomena would have deserved more time than what was possible but it emphasized several promising perspectives.

2.2.4 WP4: Steel manufacturing - testing devices - experimental design N°2

Task	Title	Initial plan	Actual plan	Note
Task 4.3	Steel variants selection	It is planned to study 6 steel variants	8 steel variants were studied	(1)

TASK 4.1 Production process analysis

With information given by the production line of FCA, the manufacturing line were analyzed in term of machining operations, parameters, cutting tools and lubricant, in order to define the laboratory tests in WP5, WP6, WP7 and WP8. The cutting conditions are representative to the type of component described in the Figure 28.
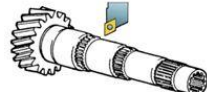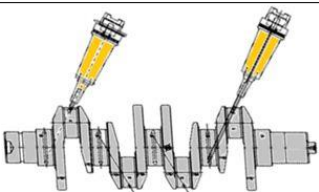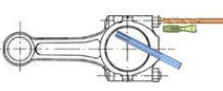
Grades	Structures	Automotive Components	Machining operation types	Machining operation zone
16MnCr5	Ferrite	**Gears** . helical gears . gearshaft	. Gear hobbing . Turning/facing . Internal broaching	
27MnCr5	Ferrite+perlite	**Gears** . helical gears . gearshaft	. Gear hobbing/facing . Turning	
C45	Ferrite+perlite	**Crankshaft**	. Deep drilling for engine oil passage in the crankpin . Tapping on the flywheel	
C70	Perlite	**Connecting rod**	. Big eye boring . Piston pin hole deep drilling and tapping	

Figure 28: industrial component associated with steel grades and machining operations

TASK 4.2 Selection of tools and cutting conditions

The ferrite-pearlite design modelling approach will take into account both low and high cutting speed operations. Based on the information collected by CRF, lubricant conditions such as tools have been defined by all the partners for each machining operation planned in the project. A brief summary of these conditions is presented in the Table 10 below, and the detail information is specified in the different machining tasks.

Cutting operation	Tool*	Lubricant conditions*	Task concerned	Leader
Turning	Coated cemented carbide	Dry	5.2	SIDENOR
			5.3	MGEP
Drilling	Coated cemented carbide	Emulsion 10%	6.2	WZL
Broaching	Coated and uncoated HSS	Dry and Oil	7.2	ENISE

Table 10 : selection of tools and cutting conditions

(*) specification of tooling and lubrication are indicated in the WPs concerned

TASK 4.3 Steel variant selection for experimental design N°2

WP2 (rheology) and WP3 (tribology) propose to identify the impact of ferrite-pearlite microstructures on friction laws and material constitutive models to provide accurate results with cutting models. Thermal properties of all the variants are also proposed by WP1 to be used in the machining modelling tasks. Taking into account all these results, steel variants that lead to interesting mechanisms, compared to Reference variants, are proposed to be studied in the machining WP (WP5, WP6, WP7 and WP8).

Note 1 : in the proposal, it was planned to study 6 steels variants for this second experimental design. During the first half of the project, we selected 3 Reference variants (27R, 45R and 60R) in advance so as to cause no delay in the project planning. In view of the previous work (WP1, WP2 and WP3), we decided to select 5 interesting added variants instead of 3: 16R, 16GP, 45WB, 45GP and 60CG.

Reasons for the decision:
- The 3 damaged microstructure variants manufactured from 27MnCr5 shown no significant changes in behaviour, consequently they were not selected for the continuation of the project.
- The variant 16GP (16MnCr5 with Globular Pearlite) can be distinguished at low speed from tribology tests (near broaching application), and is of special interest for industrial partners (ASCO, GERDAU) and end-user (CRF). This variant has to be compared with the Reference 16R. On its part, 16R could be compared with others Reference grades 27R, 45R and 60R in order to integrate the impact of ferrite/pearlite ratio in the models.
- Regarding Reference 60R, the variant 60CG demonstrated a different behaviour in tribology at medium speed (near drilling application) and in rheology at high strain rate (near drilling and turning). It's the variant with the greatest grain size.
- The variant 45WB was particularly well done on a metallurgical aspect compared to 45R; moreover, this microstructure shown significant impact on tribological tests at low and high speed (from broaching to turning).
- The choice of variant 45GP was motivated by its impact in rheology at high strain rate probably due to its very high level of globalization compared to 16GP. It is therefore a technically interesting choice in an industrial and a modelling point of view.

The Table 11 and Table 12 below summarize the selection of variants and the microstructural impacts studied:

STEEL GRADES	STRUCTURE STATUS			
	Standard	Coarse pearlite grain	Globular pearlite	With more bands
16MnCr5	16R	X	16GP	X
27MnCr5	27R	X	X	X
C45	45R	X	45GP	45WB
C60	60R	60CG	X	X

Table 11 : selected steel variants for experimental design N°2

Microstructures	Impacts	Machining operation to observe close up
16R – 45R – 60R	Ferrite/pearlite ratio	All
16R – 16GP	Pearlite in a way of globulization	Broaching
45R – 45GP	High globalization of pearlite	Drilling and turning
45R – 45WB	Bands	All
60R – 60CG	Pearlitic grain size	Drilling
16GP – 45GP	Level of pearlite globulized	All

Table 12 : microstructure impacts

Task 4.4 Steel variants manufacturing and heat treatment for experimental design N°2

For each steel variant selected, it was necessary to treat additional bars from the heats produced in the quantity required for each specific machining characterisation.

Task 4.5 Material supply

Initially, it was planned to study 6 steel variants for experimental design N°2. As we decided to select 2 added variants, the delivery of these steel variants has been delayed.

2.2.5 WP5: Turning operation

Task	Title	Initial plan	Actual plan	Note
Task 5.3	Fundamental study	Analyse the influence of variants on cutting and feed forces, tool side temperature, chip thickness and tool chip contact length. High speed filming to analyse microstructure deformation	Analyse the influence of variants on cutting and feed forces, tool side temperature, chip thickness and tool chip contact length.	(1)
Task 5.1 Task 5.4	Modelling	2D FE modelling 3D FE modelling	2D FE modelling	(2)

The main stages of the WP are listed below:

- Machinability determination of ferritic-pearlitic steels in turning tests:
  - Materials machinability testing in turning process in 3D machining (nose turning tests V20).
  - Microstructure level investigation of cutting phenomenon that occurs during turning (chip formation, tool wear mechanisms…).
  - 2D fundamental study of chip formation process: high speed filming, infrared measurements to analyse the influence of microstructure ferrite-perlite.

- Development and validation FE models for turning ferritic-pearlitic steels
  - 2D modelling investigations (ferrite-pearlite microstructure influence for turning)
  - 3D modelling investigations (ferrite-pearlite microstructure influence for turning)

- Optimization and prediction strategy for ferrite-pearlite microstructure design derived from cutting process experiments and simulations with respect to higher machinability performance.

Task 5.1 2D finite element modelling considering microstructure

In this section, the main attributes of the developed ALE model are specified in the following manner: (1) general description, (2) boundary conditions and predefined fields, (3) tool-workpiece interface contact definition, (4) mesh discretization and (5) tool and workpiece material properties.

General description of the model

Conceptually, the idea of the model is to visualize the workpiece as a fluid flowing through a deformable "pipe" that interacts with a solid part (tool). The entry of material is associated with the deformable workpiece, and the exits correspond to the flow of the chip and the finished workpiece. The quantity of material that is evacuated from each of the exits is not predefined.

The corresponding part of the tool was modelled as a rigid body fixed in space, assuming that deformations in the tool are negligible compared to those of the workpiece. Geometrically, the rake face, the flank face and the rounded cutting edge can be differentiated (appendix 7.3.1). The rake angle 6°, the clearance angle 6° and the cutting edge radius 40µm were identical to those of the orthogonal cutting experiments.

Concerning the initial pre-shape of the part that corresponds to the workpiece, two main sections were differentiated: the workpiece itself and the chip. The geometry was delimited by a certain number of surfaces which are illustrated in appendix 7.3.1:

- Free surface (AB). Lagrangian free surface of the outer part of the workpiece (not machined surface).
- Exit chip (BC). Eulerian surface to simulate the material flowing through the chip.
- Workpiece contact (CD). Lagrangian surface that makes contact with the surfaces of the tool.
- Exit material (DE). Eulerian surface to simulate the exiting material flow.
- Bottom part (EF). Lagrangian surface on the bottom of the workpiece which is fixed in space and constrains the movement of the workpiece.
- Entry material (FA). Eulerian surface to recreate the material flowing against the tool at a velocity equal to the cutting speed.

The dimensions of the model were fixed so that the limits of the boundaries did not affect the different areas of analysis. The length and height of the model were large enough so as to not have stress and thermal concentrations in the limits, and the tool was sufficiently wide that the boundaries did not interfere with the heat flow.

Boundary conditions and predefined fields

Boundary conditions are classified in mechanical and thermal boundaries, which are specified in appendix 7.3.2. Thermal conduction, convection and radiation in the outer surfaces of the model were disregarded. Only conduction was enabled in the contact between tool and workpiece once the gap between the two bodies was less than 10^{-4} mm. The workpiece was fixed at the bottom, where displacements were constrained in both directions. Concerning the Eulerian boundaries, in the entry and exit material surfaces the displacement was constrained in U1 direction, while the surface assigned for the chip outflow was $U_2=0$. The degrees of freedom of the tool were constrained U_1, U_2, $R_3=0$.

With regards to the predefined fields, both tool and workpiece were set at 20°C, and from the beginning of the simulations in the Entry surface (surface F-A) a material flow of $dU_1/dt=Vc$ was defined.

Contact model in the tool-workpiece interface

The mechanical contact was modelled by the Coulomb law with a sliding velocity dependent friction coefficient, µ. This model is certified in the literature to accurately represent the contact behaviour in the interface between tool and workpiece. The characterization is described in WP3.

Mesh discretization

The mesh of the numerical model was formed by coupled temperature-displacement elements of the type CPE4RT. These are of reduced integration quadrilateral elements under plane strain condition.

The topology of the workpiece was divided into diverse sections to enable meshing with refined elements in the regions of interest (appendix 7.3.3). These are mostly the three shear zones (PSZ, SSZ, and TSZ), including the vicinities of the cutting edge. The tool was also refined up to a radii longer than the contact with the workpiece. The dimensions of the elements oscillate between 4 µm and 100 µm. The elements with the smallest size were near the cutting edge. The workpiece was modelled with 15600 elements and the tool with 9300 elements.

The whole workpiece was defined under the Adaptive Meshing domain based on the Arbitrary Lagrangian Eulerian formulation. The main feature of this formulation is that the material can

behave under Lagrangian or Eulerian formulation depending on the absence or presence of the domain and type of the outer surfaces of the model.

In the region under Eulerian domain the mesh is allowed to move independently of the material, but without altering the topology of the mesh. The limits of the model can be set with adaptive Lagrangian or Eulerian contours. When a Lagrangian surface is selected, this deforms together with the material. In contrast, if the surface selected is that of Eulerian type, it permits the material flow through the borders. As shown in appendix 7.3.1, the Entry material, Exit material and Exit chip surface were modelled as Eulerian, allowing the material flow through them. The surfaces named Free surface and Part contact were modelled with adaptive Lagrangian surfaces. No constraints were fixed in these surfaces so as to permit adaptation while the chip is forming.

Material properties

In coupled thermo-mechanical analyses the thermal and mechanical properties of the workpiece are mandatory. These were defined in function of the temperature, as the simulation was considered as adiabatic, and the variation that temperature causes in material properties were known to be significant.

The required input data has already been characterized throughout the framework of this research. The flow stress data is modelled based on the homogenization of ferritic and pearlitic phase behaviour with an IsoWork assumption (WP2). The thermal properties for both tool and workpiece materials were characterized in the WP1.

The main outputs to validate the numerical model are those measured experimentally in Task 5.3. Specifically, these are the cutting and feed forces, tool temperature, chip thickness and tool-chip contact length. These are discussed in the following lines for the specific case of the cutting condition of 300 m/min cutting speed and 0.2 mm feed. Simulations were only carried out for the steels selected in WP4.

The higher is the C content the lower the chip thickness in both numerical and simulated results. Although numerical absolute values were not accurate (20-30% of difference), the trends among the steels was considered good and consistent except for the 45WB variant (Figure 29).

In general, the predicted contact length in the simulations was about 40% lower than that occurred in the orthogonal empirical trials. This result was found to be one of the major drawbacks of the numerical model. However, experimentally the measured contact length corresponds to that of the maximum length, in which the full contact and the stick-slip of the chip are considered. As in the FE model this stick-slip effect does not occur, it is reasonable to have such differences between the two frameworks. Despite these differences in the quantitative results, the main trends occurred in the experiments were accurately followed by the numerical model concerning the change the grades and variants (Figure 30).
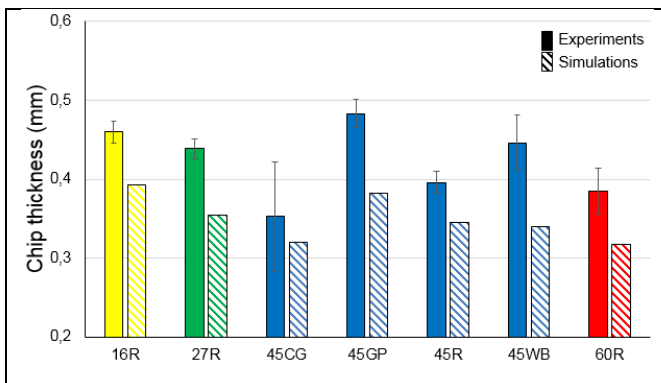
Figure 29: Comparison of chip thickness between experimental and simulation results	Figure 30: Comparison of contact length between experimental and simulation results
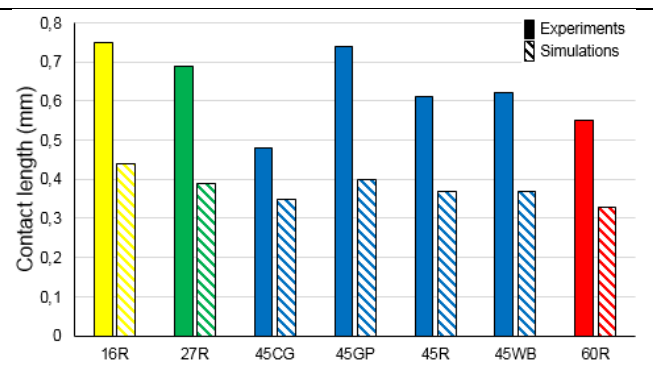
Tool contact temperature trends were not exactly accurate, but simulated and calculated contact temperature values were in similar range (Figure 31). It is worth noting that contact temperatures were calculated based on tool side temperatures and applying the analytical theories of heating. These theories are based on the work developed by Soler et al. [38] and the calculation of heat due to shearing effects proposed by Merchant [39].

Predicted cutting forces are about 10% lower than in experiments. In both experimental and numerical frameworks no clear trend among steels was observed (Figure 32). Simulated results were consistent with the empirical results.

Figure 31: Comparison of tool contact temperature between experimental and simulation results

Figure 32: Comparison of cutting forces between experimental and simulation results
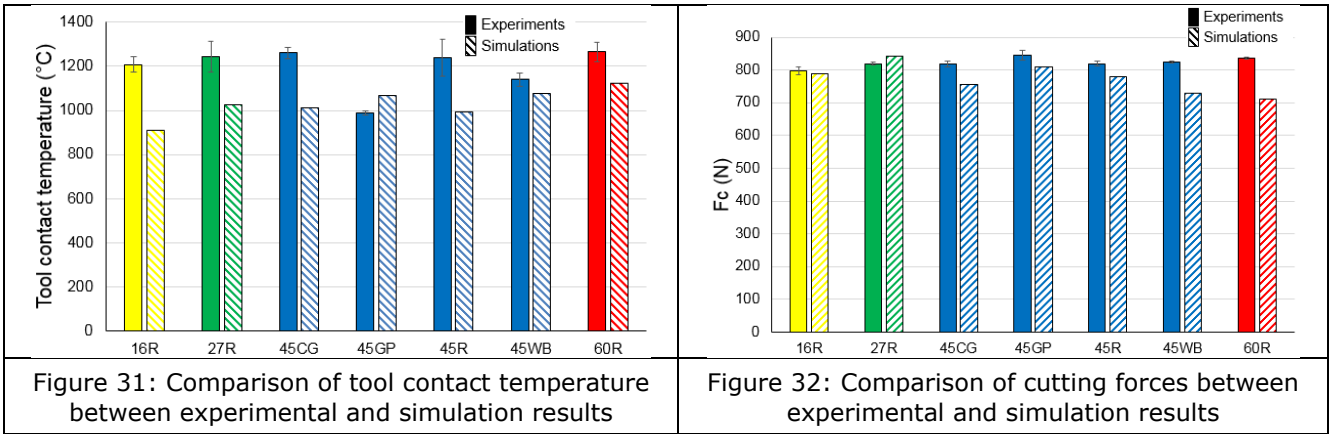
Predicted and experimental feed forces differ by an average 30%. Considering that the prediction of the contact length was lower than that obtained experimentally, and the feed forces are almost related to the shearing effects in the rake face, these lower predicted feed forces were in line with other simulated results. Although in general, in the experimental framework a lowering of the feed forces was observed with increasing ferrite content, in the specific case of Vc=300 m/min and f=0.2 mm no clear trend was found between all the studied variants. Only when the standard (R) variants were analysed, a slight lowering of the feed forces occurred with increasing pearlite content, although the 27R presented a higher Ff than that of 16R. Same occurred in the numerical results, in which no clear trend was observed between all variants, but the trend found in the R variants was found to be similar to that of the orthogonal tests (Figure 33).
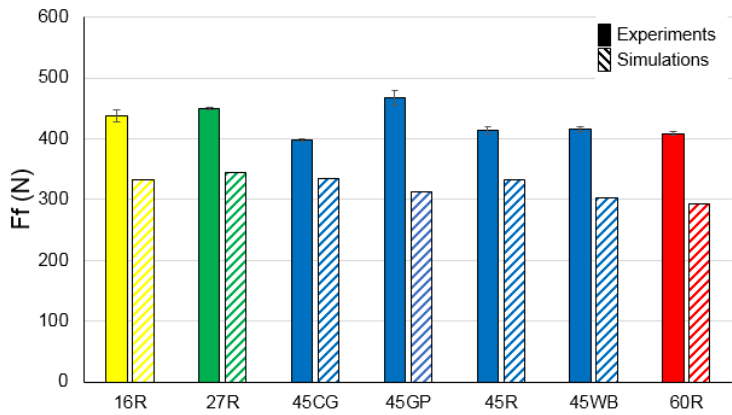
Figure 33: Comparison of feed forces between experimental and simulation results

The major drawback concerning the outputs obtained from the numerical FE models was mainly the prediction of contact length. This influenced significantly the predictions of feed forces. Other analysed variables such as cutting forces, temperatures and chip thickness were considered accurate. In addition, as is presented in the following Task 5.6, other outputs such as contact pressure or sliding velocity were also extracted from the numerical models to predict machinability and gave accurate results when evaluated in the prediction of machinability index.

Task 5.2 Machinability tests in turning

The main goal of these tests is to assess the machinability of the different steel variants chosen in WP4 in order to quantify the impact of microstructural parameters (%pearlite, globulization, grain size and banding level) on turning performance at high cutting speed. All the experiments were conducted following the indications of the standard ISO 3685 using a hard metal tool with a TiCN+Al2O3 coating. Although, the cutting conditions employed were depth of cut, ap =1 mm and feed, f = 0.2 mm/rev. Some experiments were also carried out using ap = 2 mm and f = 0.3 mm/rev in order to determine that the trends observed were not influenced by the cutting conditions. As shown Figure 34, in both cases the trends were similar, but with the more severe conditions, globular pearlite and coarse grain effect are more noticeable. The rest of the tests were conducted with ap = 1 mm and f = 0,2 mm/rev.
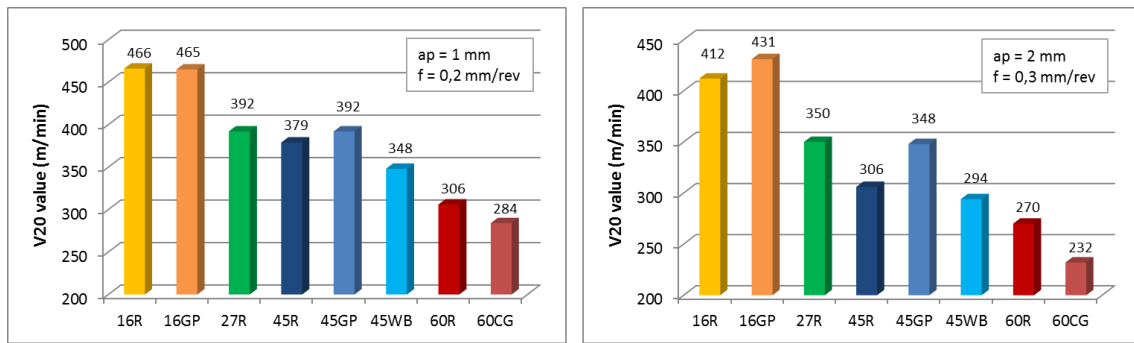
Figure 34: V20 tests at (left) ap=1 mm and f=0.2mm/rev and (right) ap=2 mm and f=0.3mm/rev

The four reference variants (obtained after an isothermal annealing) were tested to determine the influence of the ferrite-pearlite ratio (linked to the C content) on the steel machinability. The obtained Taylor curves and V20 values showed that the higher the C content, the worse the steel performance during turning Figure 35 left. This trend was expected given that it is well known the negative influence of the hardness on the steel machinability.

Two steel grades (16MnCr5 and C45) were chosen to determine the influence of the pearlite globulization on the steel machinability. It's important to remember that the level of globulization is different for these 2 variants (75% broken pearlite for 16GP and 100% globulized pearlite for 45GP). The GP variants were compared with the reference (R) ones. In an industrial point of view, for high cutting speeds around 300-400 m/min, the machinability of GP variants and their respective R variants can be considered as similar (Figure 35 right). For cutting speed higher than 400 m/min, machinability of 45GP is better regarding 45R due to his very high level of globulized pearlite.
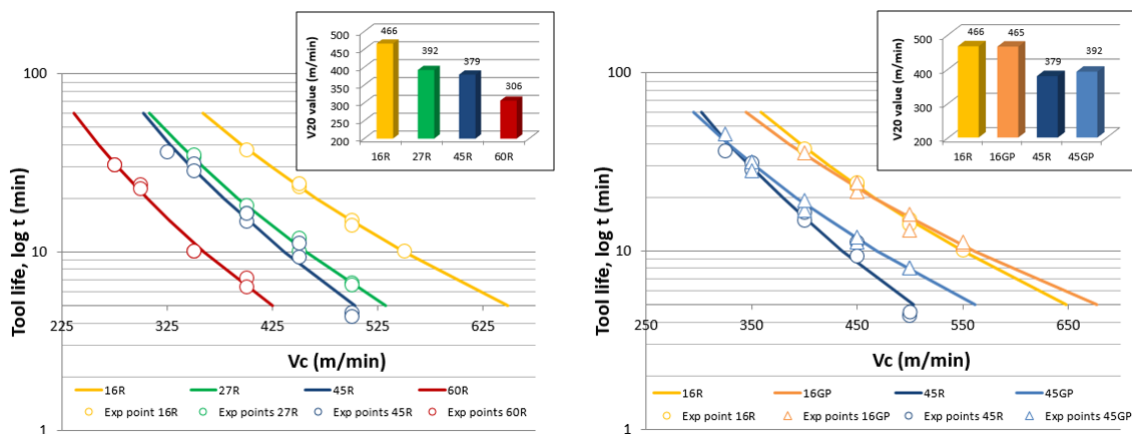
Figure 35: V20 tests of standard variants obtained by isothermal annealing (left) and to determine the influence of the pearlite globulization (right)

The C45 grade was chosen to study the influence of the banding level on the steel machinability at high industrial cutting speed (300 – 400 m/min). The V20 values of the considered variants, 45R and 45WB, shown that the machinability of the 45WB was a little bit worse (Figure 36 left).

In order to determine the influence of the pearlitic grain size on the steel machinability 60R and 60CG variants were selected. It was observed, for the whole cutting speeds range, that the steel machinability worsened when the pearlitic grain size was increased (Figure 36 right). In this case, the significant difference of hardness between the 2 variants plays an important role.
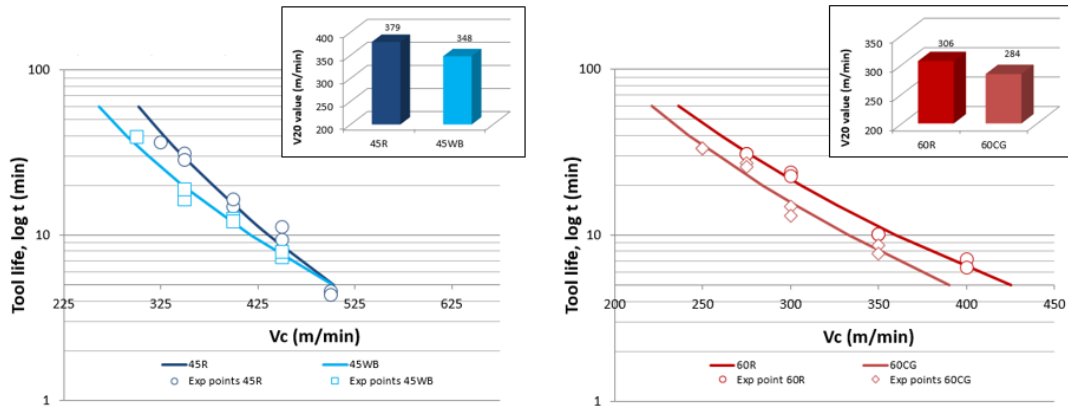
Figure 36: V20 tests to determine the influence of the banding level (left) and the influence of grain size (right)

The machinability classification obtained in this turning test demonstrated that the dominating wear mechanism is abrasion due to steel variants hardness.

Task 5.3 Fundamental study of chip formation process

The task was divided into two subsections, the first one focused on the measurement of fundamental variables during orthogonal cutting, and the second on high speed filming of the cutting process to measure the strains and strain rates.

Fundamental variable measurement

For fundamental variable measurement, an orthogonal cutting set-up was mounted on a CNC vertical milling machine as shown on appendix 7.3.4. The tool and tool holder were clamped on a dynamometer (Kistler 9121) to measure cutting and feed forces. These and the infrared (IR) camera (FLIR Titanium 550M) were fixed on the moving table of the machine-tool. The orthogonal cutting specimen in form of tube was held on the spindle, giving the rotation movement and the vertical feed. A ground surface was machined on the insert to generate a perpendicular surface for IR measurements, making possible to capture the thermal field on a side view of the tool.
Tests were developed in four different cutting conditions (two cutting speed: **S150 and S300** m/min, and two feed: **F0.1 and F0.2** mm/rev), over 15 of the 16 selected steel variants (70R variant was not possible to test due to its short bar diameter). The employed cutting insert was a coated carbide Sandvik TPUN160308 – 3215.

A summary of the results is presented in the following lines.

- The contact length has been found to be related with the ratio of ferrite (Figure 37 left). The increase on ferrite content generates an increase on contact length. Between variants, higher differences are found on C45 and C60 grades. No clear differences between low %C content variants (16MnCr5 and 27MnCr5).
- Chip thickness, in the same manner as contact length, increases together with the ferrite content of the steel. In contrast to the contact length, the differences in lower %C steels are a little bit more noticeable (Figure 37 right).
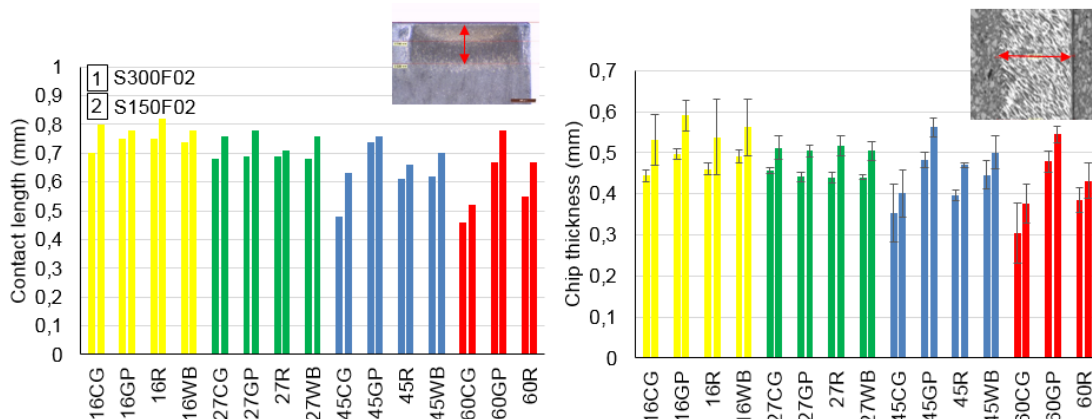
Figure 37: Contact length (left) and chip thickness measurements (right)

55

- Cutting forces do not present differences between the tested variants, in spite of the differences in mechanical properties (Figure 38 left). Cutting forces is function of normal pressure and contact length. The severe variations found on contact length could have generated these forces results. In order to make possible a comparison, cutting forces have to be switched to normal pressure values.

- As for cutting forces, feed forces showed slight differences between variants, with a maximum difference of a 27% comparing the maximum and minimum obtained forces. When focusing on the tested grades, the biggest differences between variants are found on C45 and C60 grades. 16MnCr5 and 27MnCr5 variants present similar values. Again, a slight relation has been found with the ferrite content, obtaining an increase on feed forces with the increase of ferrite content, results that are more noticeable with the lowest cutting speed and highest feed (Figure 38 right). This could be linked to the longer contact lengths generated with the increase of ferrite ratio.
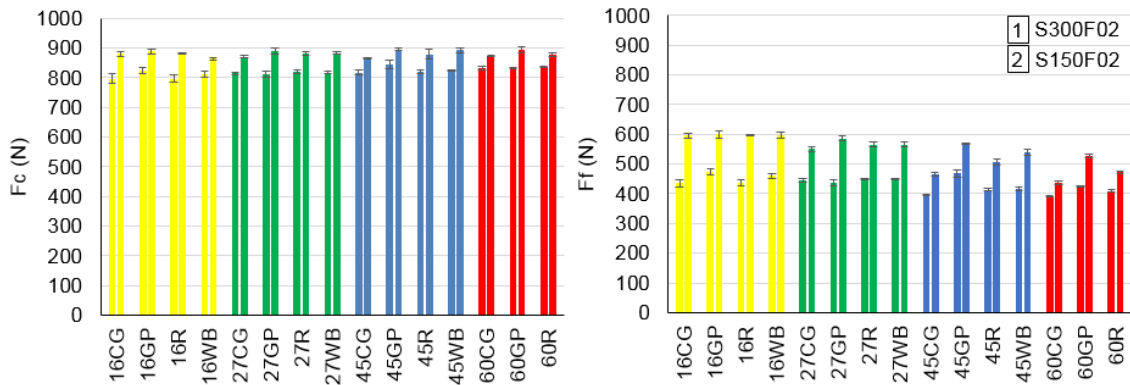
Figure 38: Forces measurements

- When cutting forces are transferred to normal pressure data (CP-CPRESS), a stretch relation is found with the ferrite content or %C. The contact pressure was higher in high C content steels grades, that's when tool chip contact length and ferrite content decreases. This is more noticeable at high cutting speeds. Between reference and damaged structure variants, higher differences are found on C45 and C60 grades (Figure 39 left).
- No clear trend was observed when switching the feed forces to contact shear stresses (CS-CSHEAR). Only in the case of C60 grade when compared to that of C45, depending on the variant, a higher shear stress was observed. This was more significant in the case of CG structure (Figure 39 right).

$$CP = \frac{Fc}{Lc \cdot Wc}$$

$$CS = \frac{Ff}{Lc \cdot Wc}$$
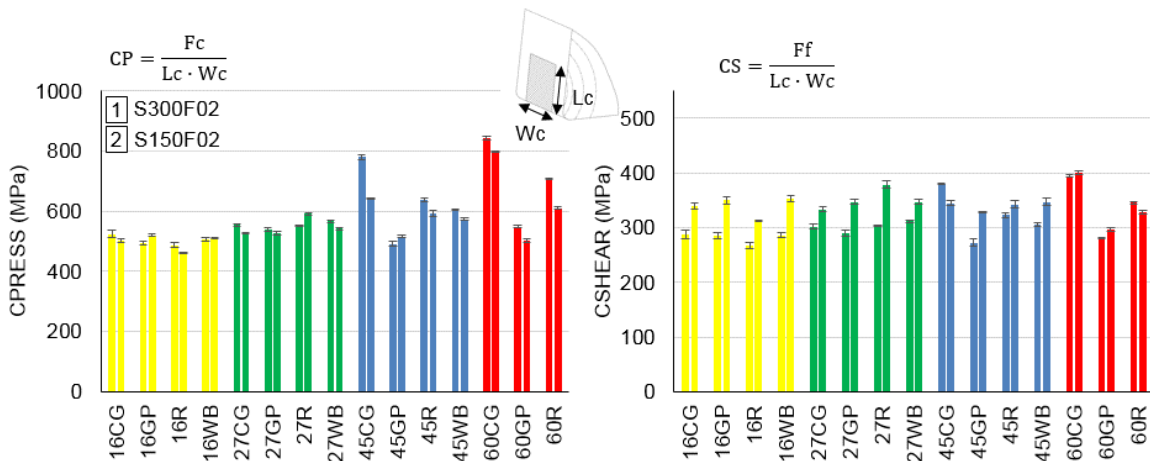
Figure 39 : normal pressure (left) and shear stress (right)

- Concerning temperature measurements, experimentally, only tool side temperatures are possible to be measured in a ground surface of the insert. In order to be comparable to finite element results, these measured temperatures should be extrapolated to the mid-plane of the tool-chip contact region, for example, based on analytical equations of heating theory. Obtained results present an increase on tool side temperature with the increase of ferrite content. This is more relevant at S300F02 and lower the effect is with the less harder cutting conditions. Between reference and damaged structure variants, only at high cutting speed (higher temperatures) can be observed that CG and GP have bigger differences. R and WB variants presented similar temperatures (Figure 40).
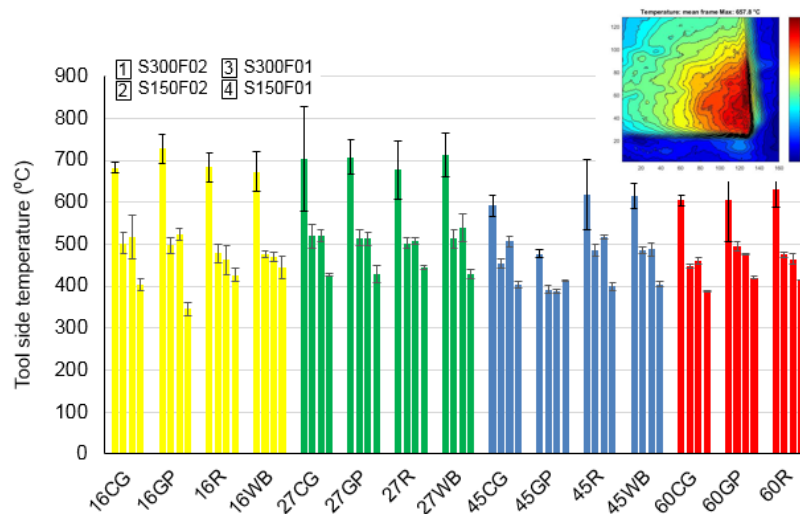
Figure 40: Tool side temperature measurements

Above all the analysis, the effect of cutting conditions was consistent among all the studied variants. Increased cutting speed caused a reduction of the contact length, chip thickness, cutting and feed forces, and the tool side temperature to increase. The effect of increasing the feed provoked an increase in all the analyzed fundamental variables.

Strain and strain rate tests – device and measuring methodology

Note 1: an experimental set-up using high speed filming was developed to measure simultaneously the forces and the strain and strain rates during the chip forming of the orthogonal cutting process.

In the very first attempts, it was not possible to measure any strain nor strain rate. Although the obtained images were of high quality, some problems were faced that avoided making any good measurement. Firstly, the system could be more rigid as in the first tool-workpiece contact the tool went back and after beginning the cutting came back to its original position. The use of the EDM as marking method seemed to be useless as when the cutting started some points changed its brightness or simply disappeared. Besides, the outflow movement of the chip did not allow making any measurement in the deformation zones. Finally, the twisting of the work piece made confusing the study of the chip forming and left a rough surface (appendix 7.3.5).

In the last essays there were solved some of the previous problems such as the rigidity, changing the workpiece clamping system and setting the tool directly in the spindle. These changes also solved the twisting problems faced in the preliminary campaign. On the other hand, the employed marking method was also different, employing airbrush painting. This way the DIC software tracked better the points allowing certain measurements (appendix 7.3.5). Nevertheless, there was no chance to stop the outflow of the chip, so although the improvement of the image quality was high there still continued occurring measurement problems on the primary shear zone (PSZ).

For the future essays, the use of lens that could provide higher depth of field (Z axis) or the use of two cameras might solve the blurred images problems. Finally, although the use of coaxial light is not necessary, undoubtedly would improve the quality of the images.

Task 5.4 3D Finite Element Modelling of a longitudinal turning operation

Note 2: the development of this 3D FEM model, as described in the mid-term report, had to be stopped as the limitations of the methodology were faced. The main drawback of such approach is that the chip formation is not computed, and its geometry must be known to create the mesh. There is thus a highly time-consuming work to done on CAD models preparation as well as meshing the resulting chip geometries. Moreover, the results obtained in Task 5.2 and 5.5 in longitudinal turning showed that it was really difficult to extract a clear difference between 3 standard variants (Task 5.2) and that the wear modes were not completely the expected ones (Task 5.5).

Therefore, considering (i) the time it would have required to collect the chips, scan them, built the 3D geometry and mesh it, (ii) the discussion going on during the last year of the project regarding the rheological data and preliminary not satisfactory results obtained in WP5-6-7 and (iii) the fact that it was not sure in the end to extract useful and reliable data from this model that could be compared to the experimental ones, this development, already begun, has been stopped not to increase the delay of the project.

Task 5.5 Tool wear and tool chip contact zone studies

The tool-chip contact length on the rake face side of cutting tools was obtained by orthogonal face turning tests. The motivation of the work was to provide further understanding of the material dependent chip curl of the steels included in the project. Starting with a workpiece bar three flanges 2 mm thick were machined by grooving. Upon cleansing cuts the three flanges were machined in a sequence using a triangular cutting tool without chip breaker, Coromant TPUN 160308 GC3225, the grade designation means that the tool is coated by CVD TiCN+Al2O3.

In the full matrix of tests the cutting data that used were: cutting speed Vc=225 m/min, feed f=0.25 mm/rev. The depth of cut was (apparently) equal to the flange width of ap=t=2 mm. Dry machining was used.

NOTE: The unstable stick-slip contact zone width showed relatively clear differences, see Figure 41. However, at this stage most attention is given the summed contact length numbers. The corresponding top views of tool rake contact zones of the C45 steels is given in Figure 42.
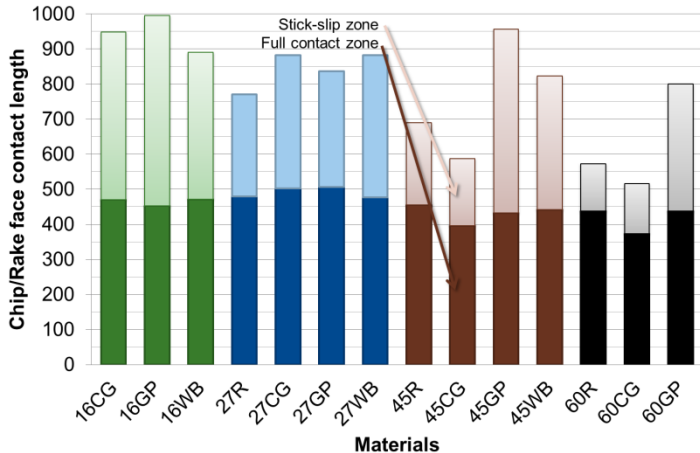
Figure 41: Tool-chip contact length of the steels tested.

At first glance the tool-chip contact numbers are linked to the steel hardness. That can be explained by the belief that the tool-chip contact zone reflects the chip curl, which in turn relies partly on the chip temperature. The more heat that is generated in the secondary shear zone of the tool-chip contact chip the more curls the chip gets, due to the thermal expansion of the underside, as compared to the not sheared upper side of the chip.
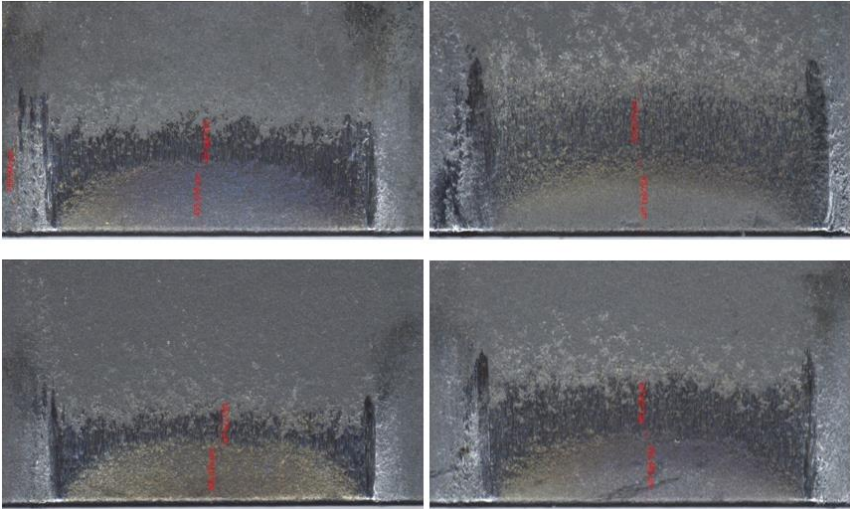
Figure 42: Overviews of tool-chip contact lengths of (a) 45R, (b) 45GP, (c) 45CG and (d) 45WB. (LOM)

Task 5.6 Identification of parameters driving machinability in turning

Prior to the analysis of the microstructure parameters that most affect machinability in turning, the machinability of steels is classified by means of weighted point evaluation, in the same way that is proposed in the other cutting operations studied in the project. This method is an objective comparison tool that uses several evaluation criteria (*EC*) of predetermined importance (weighting factor) which are ranged in values between 1 and 8 (utility value, UV), to then evaluate in this specific case the machinability index ($I_{machinability}$). The general equation (15) to describe this evaluation is the following:

$$I_{machinability,\,j} = TUV_j = \sum_{i=1}^{n} W_i \cdot UV_{j,i} \qquad (15)$$

$$UV_{i,min} = 1 \text{ (worst)}$$

$$UV_{i,max} = 8 \text{ (best)}$$

For the case of increasing EC improves machinability, the UV is calculated with the equation (16):

$$UV_{j,i} = \frac{UV_{i,max} - UV_{i,min}}{EC_{i,max} - EC_{i,min}} \cdot \left(EC_{j,i} - EC_{i,min} \right) + UV_{i,min} \qquad (16)$$

In the opposite case in which increasing EC worsens machinability, the UV is calculated with the following equation (17):

$$UV_{j,i} = \frac{UV_{i,min} - UV_{i,max}}{EC_{i,max} - EC_{i,min}} \cdot \left(EC_{j,i} - EC_{i,min} \right) + UV_{i,max} \qquad (17)$$

The different evaluation criteria (EC) were identified according to the widely employed wear rate equation of Usui et al. [40]. This equation (18) links the rate of wear to parameters such as the normal pressure, the sliding velocity and tool temperature.

$$\frac{dW}{dt} = C_1 \cdot \sigma_n \cdot V_s \cdot e^{-C_2/T} \qquad (18)$$

For the experimental framework, tool temperature corresponded to that measured on the tool side, contact pressure was calculated as the average pressure when dividing the cutting force by the contact area, and the sliding velocity of the chip was estimated to be linked to the chip thickness, following the shear plane model developed by Merchant (1944). Flank wear results (V20 value) were also included when estimating the empirical machinability index ($I_{machinability}$). For the case of the numerical estimation of the machinability ranking, all these variables were extracted directly from the outputs of the model. In both frameworks, the shear stresses were also included, as is the opinion of the researchers involved in this task that shear stresses are also relevant for machinability prediction.

The utility value calculation for the experiments is depicted in the Table 13.

Evaluation criteria	Weighting factor	16R	27R	45R	45CG	45GP	45WB	60R
Tool contact temperature	10	2.5	1.6	1.1	8	1.7	4.2	1
Avg. contact pressure (Fc / lc)	10	8	5.8	4.3	1	7.3	5.3	1.8
Avg. Shear stress (Ff / lc)	10	8	4.7	4.7	1	7.6	6.1	2.5
Chip thickness	10	6.6	5.2	3.2	1	8	5.1	2.3
Flank wear (V20)	10	8	4.9	2.8	1*	4.8	2.2	1
Total utility value (TUV)	$I_{machinability}$	331	222	161	120	294	229	86
Ranking of machinability		1	4	5	6	2	3	7

Steel with the highest machinability

*Estimated from other V20 test results

Table 13: Estimation of empirical $I_{machinability}$ and machinability ranking of steels

For the case of the numerical model, the calculation carried out is shown in Table 14.

Evaluation criteria	Weighting factor	16R	27R	45R	45CG	45GP	45WB	60R
Tool max. temperature	10	8	4.1	5.2	4.6	2.9	2.5	1
Contact pressure (CPRESS)	10	8	4	4.5	1	5	2.5	3
Shear stress (CSHEAR)	10	4.3	3.1	8	1	7.3	4	6.1
Sliding velocity	10	8	4.4	3.5	1.2	7	3.1	1
Total utility value (TUV)	$I_{machinability}$	282	155	212	78	221	121	111
Ranking of machinability		1	4	3	7	2	5	6

Steel with the highest machinability

Table 14: Estimation of numerical $I_{machinability}$ and machinability ranking of steels

When compared the predictions between the two frameworks and the V20 wear tests, the following ranking of machinability was assessed (Table 15):

*Estimated from other V20 test results

Test	16R	27R	45R	45CG	45GP	45WB	60R
Ranking of machinability (V20 turning tests)	1	3	4	7*	2	5	7
Ranking of machinability (Orthogonal turning tests)	1	4	5	6	2	3	7
Ranking of machinability (simulations)	1	4	3	7	2	5	6

Steels with the highest machinability   Steels with the lowest machinability

Table 15: Comparison of V20 wear results with empirical and numerical machinability ranking of steels

In all the cases, the steel with better machinability ranking was the 16R followed by the 45GP. Those steels with the poorest machinability were the 45CG and 60R. From the results in task 5.3, and the machinability classification presented in Table 15 a qualitative evaluation of the influence of microstructure parameters on the machinability concerning turning operation is shown in Table 16. The main selected microstructure parameters were the pearlite and ferrite fraction, pearlite grain size and interlamellar spacing of pearlite.

From a macroscopic point view, the analysis was also set out depending on the microstructure variant, in which results of Table 16 are compared to that of the standard variant.

Table 16: Qualitative analysis of the influence of microstructure parameters on the machinability in turning process

60

CONCLUSION

The microstructure parameter that clearly most affected turning performance was the pearlite fraction (opposite to ferrite fraction), which was directly linked to the C content and the hardness of the steel variants. The higher the C content or the higher the fraction of pearlite, the worse the steel machinability. The increase observed in turning V20 tests could be attributed to the lowering of the contact area that drove an increase of contact pressures. Additionally, the reduction of the chip thickness could have also caused the chip to slide faster in the tool-chip interface, also provoking the wear to rise. This confirms that the predominant wear mechanism in high speed turning is abrasion.

Regarding impact of "damaged microstructure", from the macroscopic point of view, the most relevant results were obtained mainly when analyzing the C45 and C60 variants. From these, it was concluded that coarse grains caused a greater degree of wear than standard grades, while the effect of a high level of globulization improved a little bit the machinability in terms of tool wear. In general, the increase or reduction of wear was linked to the variation of contact area, which directly affected the contact pressures.

The prediction of the machinability ranking based on the weighted point evaluation gave accurate identification of the best/worst machinability of steels from both empirical and numerical frameworks when compared to V20 wear tests.

The proposed numerical model was able to predict the main trends observed in the empirical orthogonal tests. However, there were still large gaps in the quantitative prediction of variables such as contact length and feed forces. Despite this drawback, the prediction of non-measurable variables such as contact pressures and shear stresses were identified to be accurate when evaluated with the weighted point method and when compared to experimental evaluations.

2.2.6 WP6: drilling operation

Task	Title	Initial plan	Actual plan
Task 6.5	Modelling at the micro range	Development and validation of a drilling model (d = 1 mm, homogeneous and heterogeneous microstructure)	Development and validation of a homogeneous drilling model for d = 1 mm: done The heterogeneous model was not successful due to the out of control of the remeshing process in the new version of Deform3D

The main objective of WP6 is the development and validation of a microstructure based computation tool capable to predict and optimize the machinability of ferritic-pearlitic steels by drilling operations including:
- Development and validation of 3D FE models for twist drilling ferritic-pearlitic steels
- Determination and classification of the machinability of ferritic-pearlitic steels in drilling tests
- Determination of a correlation between the microstructure and machinability
- Optimisation criteria for ferrite-pearlite microstructure design derived from cutting simulation.

Task 6.1 Modelling investigation at the macro range

In the framework of task 6.1, a 3D FE computation model is developed for macro twist drilling using the Lagrangian formulation with the implicit FE code DEFORM-3D^{TM}. The drilling process is characterised by forming, cutting, and friction processes. By drilling is the cutting edge of the tool curved, the rake and clearance faces are not planar, and cutting speed vary along the cutting edge. Furthermore, the chip removal and chip transport are very difficult. Due to the above mentioned high complexity of drilling process, the inputs and the boundary conditions for FE simulation, as summarised in Figure 43 have to be carefully defined in order to obtain an accurate prediction of the drilling process reactions. The drills, used within the framework of this research task, are selected from the project partner CRF FCA. The selected 8 mm drills are double-edged solid carbide twist drills of type RT100U_5510 from the tool manufacturer Gühring. The drills are coated and internally cooled, see Figure 43. Since the geometry of the tool influences strongly the drilling process, the design of the selected twist drills has to be accurate. Only then, the FEM-model is able to reflect real process behaviour during cutting.

The CAD model of the used drill is provided from the Gühring as STEP format and with sharp cutting edges. After measuring the cutting edge rounding of the supplied carbide drills (cutting adge radius $r_ß$ = 30 μm), the micro geometry of the CAD drill model is adjusted by means of the CAD program SolidWorks. For more efficient computing, the volume of the modelled tool and workpiece was selected as small as possible. The CAD models have been transferred in Deform 3D[TM] as STL format and meshed using 3D tetrahedron elements.

Boundary conditions adjustment

- Twist drill: Rigid with mesh d = 8 mm and $r_ß$ = 30 μm
- Workpiece: Visco-plastic D x H = 12 x 4 mm with heat dissipation 100,000 3D-Tetrahedron
- Contact: friction, heat transfer (Conduction & Convection)

Twist drill CAD model

RT100U_5510
d = 8 mm
$r_ß$ = 30 μm
Gühring KG

Twist drill

Workpiece

Cutting parameters definition

- Workpiece material: 16R, 27R, 45R, 45CG, 45GP, 60R
- Tool material: HW
- Cutting speed: 120 m/min
- Feed rate: 0.25 mm/rev

Constitutive material laws

- Material law: ASCO
- Friction law: ENISE
- Thermal properties: MGEP

Figure 43: 3D FE computation model for macro drilling (d = 8 mm, homogeneous microstructure)

In the FE computation, a gradient continuous auto-remeshing is used for generating the mesh of the workpiece. To minimize the interpolation error and to improve the convergence of the solution, the mesh density in areas with high gradients of plastic strain has to be increased. Because of the extensive computation time by continuous remeshing, the FE computation has been started by the full contact of the cutting edge of the drill and the adjusted workpiece (Figure 43). The drills are modelled as rigid. They have a constant mesh, which is finer at the cutting part of the tool to calculate the temperature distribution within the tool. The cutting process in drilling is modelled as forming operation and the chip formation is simulated by continuous remeshing, so that no material fracture criteria are needed. The movement of the drill (rigid body with mesh) is specified by its translation and angular velocities in z-direction, while the workpiece (deformable) was constrained on the bottom and the round surfaces in the x, y, and z directions. Friction at the objects interfaces, tool-workpiece and chip-workpiece is governed by the friction law developed in WP3. For the thermal boundary conditions, conduction and convection of the generated heat are applied. The gap conductance and the thermal convection coefficient between two contacting surfaces are assumed to be 10^7 W/m^{2}K and 20 W/m^{2}K, respectively. The thermal properties of the investigated steel variants are used in the drilling model. The workpiece and tool temperatures are initially set at room temperature (20°C). In order to adapt the energy balance in the modelled workpiece to the experiment, the nodes temperature at the bottom and the round surfaces is kept constant at a value of 20°C. The implicit 3D simulation of the drilling process requires an enormous amount of CPU time. Therefore, parallel computing (2 x 3.2 GHz) is necessary to solve such a complicated problem. The thermo-mechanical material flow behavior in the simulation is described by means of the constitutive material law developed in WP2. The developed 3D FE computation macro model for the drilling process is validated using the experimental results of the present investigations. Under the same cutting conditions of the performed twist drilling tests (d = 8 mm, $r_ß$ = 30 μm, v_c = 120 m/min, and f = 0.25 mm), twist drilling in the grades 16R, 27R, 45R, 45CG, 45GP and 60R is simulated dry. Figure 44 shows some results of the FE drilling simulation (feed force, cutting torque, chip compression ratio, max. normal pressure and max. drill temperature). The predicted values of the feed force and torque are in good agreement with the measured results (feed force: max. deviation < 20%, cutting torque: max. deviation < 17%).

Feed force / kN — (grades: 60R, 45GP, 45CG, 45R, 27R, 16R; Simulation, Experiment)

Torque / Nm — (grades: 60R, 45GP, 45CG, 45R, 27R, 16R; Simulation, Experiment)

Drill diameter d: 8 mm, cutting speed: 120 m/min, feed rate: 0.25 mm/rev, tool material: HW

Chip compression ratio h_{chip}/h

$$h = f/2 \sin(\kappa)$$

h_{chip} computed at the middle of the main cutting edge

Max. normal pressure / MPa

Computed values at the corner

Max. temperature / °C

Figure 44: Results and validation of the developed 3D FE computation model (dry cut)

The computed chip compression ratio and the maximal normal pressure as well as the maximal temperature are representative for the predicted chip form and wear respectively. They are utilized to characterize and classify the computed machinability of the investigated grades.

Task 6.2 Machinability of ferritic-pearlitic steels in twist drilling tests

In order to examine the machinability of the investigated grades in drilling, tool life tests were carried out on 8 mm coated carbide drills from Gühring (Type 5510, Fire-coat: TiAlN/TiN multilayer coating). The drilling tests were conducted with a cutting speed of $v_c = 120$ m/min, a feed of $f = 0.25$ mm/rev, a drilling depth of $t = 3xd = 24$ mm and the application of coolant (10% Emulsion Ecocool TNA 2525 HP, pressure 25 bar). Figure 45 shows the drilling test setup.
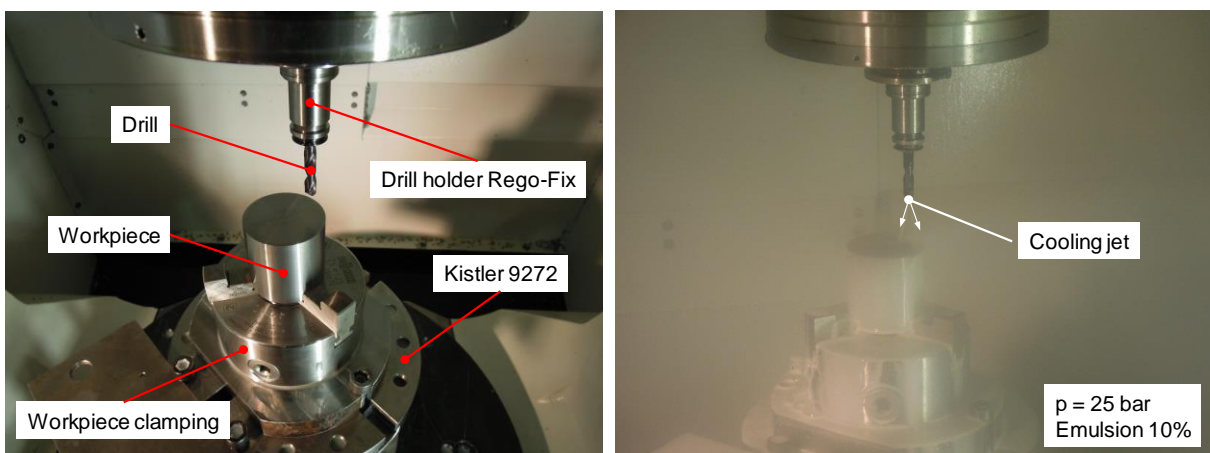
Figure 45: Drilling test setup: Machine, workpiece and tool

The evaluation parameters of the drilling test results are feed force, cutting torque, tool flank wear (VB) and the quality of the machined holes. Figure 46 shows exemplary the measured torque and chip form during drilling tests. The reference grades 16R, 27R, 45R and 60R scale in a nice manner regarding the carbon content (the fraction of pearlite) of the machined grades, as illustrated in Figure 46. The grades with globular pearlite (GP) show the highest values of feed force and torque due to the dominant material adhesion on the tool cutting edge during drilling. Additionally, the cutting torque increases with the number of the drilled holes due to the progressive wear of the used drill. Regarding the chip form, independent of the drilled grade, short chips are detected, as seen in Figure 46. A closer look on the machined chips reveals that the chip size decreases with the fraction of pearlite (from 27R, through 45R to 60R).
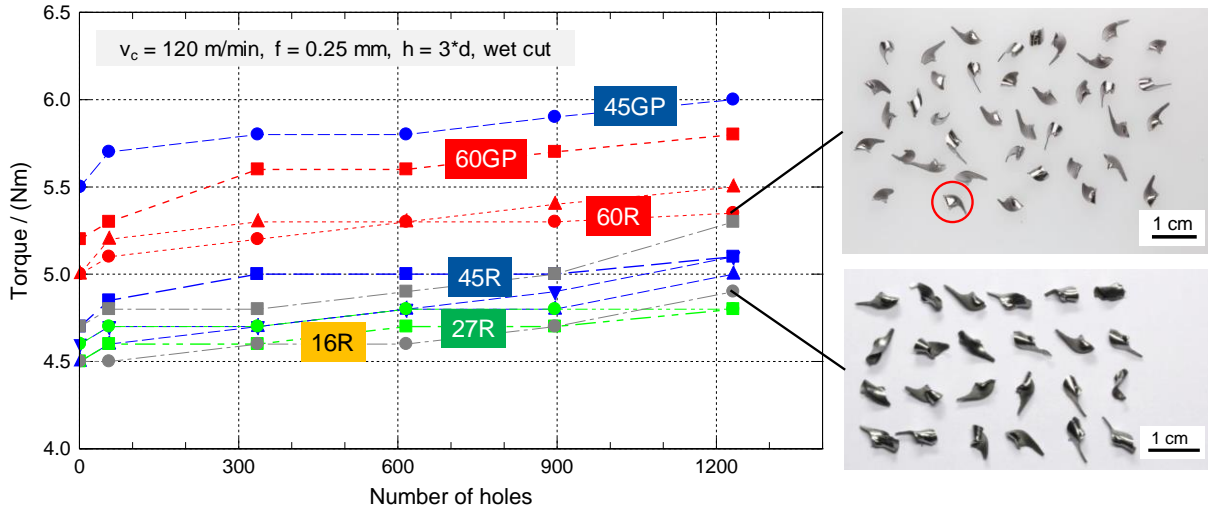
Figure 46: Measured cutting torque and chip form during the drilling tests

The development of the measured tool flank wear (VB) over the number of the machined holes is plotted in Figure 47. The tool flank wear increases continuously with the number of the drilled holes and reaches values depending on the acting mechanical load. Thus, the tool flank wear of the used drills correlates well with the measured torque and is more pronounced in the case of the more ductile grades 45GP, 60GP and 16R due to the formation of material adhesion, consult the SEM pictures in Figure 47. The wear behavior of the cutting edges is controlled by the wear mechanism abrasion when drilling the reference grades 27R, 45R and 60R, as seen in Figure 47. This abrasive wear has led to coat spalling on the cutting edge. In the case of the grades 45GP, 60GP and 16R, the dominating wear mechanism is, as expected, adhesion.
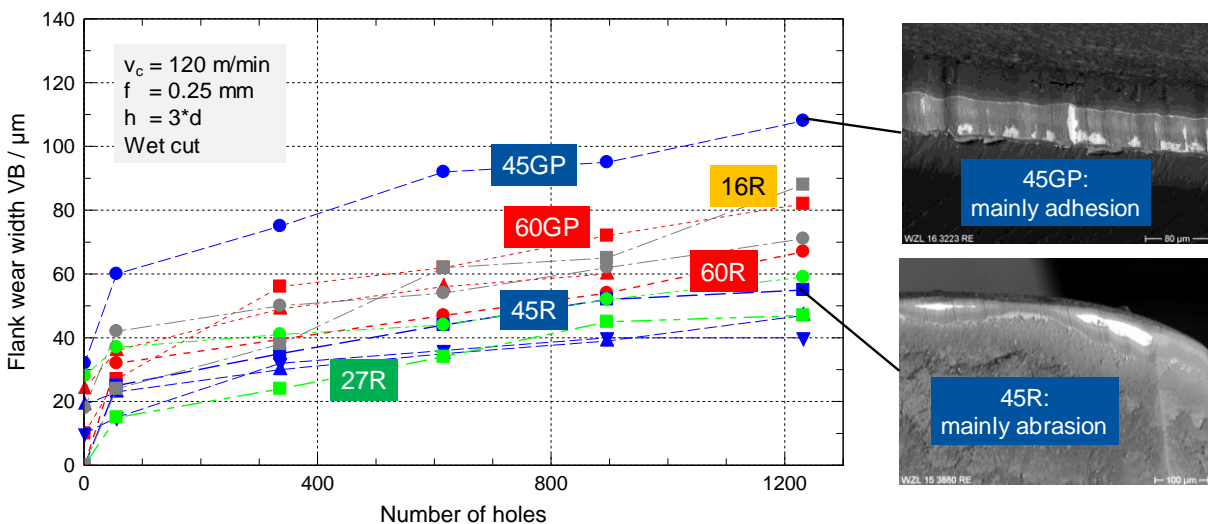
Figure 47: Tool flank wear development the controlling wear mechanism during the drilling tests

To compare the quality of the machined holes in the different grades, the surface roughness (R_a, R_z), the radial burr formation and the hole cylindrical form are measured after drilling 1232 holes. The best hole quality has been achieved by the reference grades, especially by the grade with the higher content of carbon (60R), see Figure 48. In contrast, the grades 16R, 45CG and particularly 45GP show poor hole quality. This result also correlates with the measured tool wear behaviour when drilling the investigated grades, compare with Figure 46 and Figure 47.
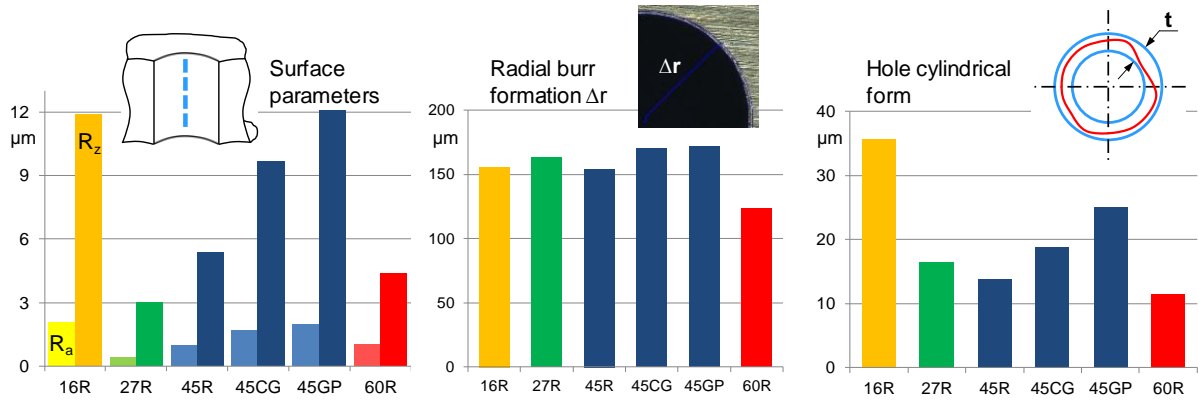
Figure 48: The hole quality after drilling 1232 holes (v_c = 120 m/min, f = 0.25 mm, h = 3*d, wet)

Within the framework of WP6, the machinability of eleven grades 16MnCr5 (16R, 16GP), 27MnCr5 (27R, 27GP), C45 (45R, 45WB, 45CG, 45 GP), C60 (60R, 60CG, 60GP) is determined and classified. Due to the limited number of pages for each WP, the complete result should be represented in the appendices of WP6. It should be stressed here that additional dry drilling tests (no tool life tests) without wear occurrence on the drill cutting edges were performed for the validation of the simulation results.

Task 6.3 Machinability classification

The classification of the machinability when drilling of the investigated grades is performed by means of the weighted point evaluation method considering the selected number 1232 of drilled holes. This method is an objective comparison tool that uses several key criteria of predetermined importance to evaluate competing products, services or characteristics and arrive at a numerical score (index), which is then used as the basis for product selection (ranking). In our case, the classification quantity is the machinability of each steel variant and the evaluation criteria are feed force, torque, chip form, tool flank wear, the surface roughness (R_a and R_z), the radial burr formation **Δr** and the hole cylindrical form t, as shown in Table 17. The evaluation method results in the following machinability ranking: 45R, 27R, 45CG, 60R, 16R, 45GP. The 45R with the "moderate" pearlite content shows the best machinability. The 45GP with high globalization of pearlite shows significantly the worst machinability.

Evaluation criterion	Weighting factor	16R	27R	45R	45CG	45GP	60R
Feed force	10	7.00	8.00	7.00	7.00	1.00	3.00
Torque	10	7.00	8.00	7.00	7.00	1.00	2.00
Chip form	10	1.00	2.40	8.00	5.20	3.80	8.00
Tool flank wear	10	5.25	8.00	7.08	8.00	1.00	5.70
Surface parameter R_z	5	1.15	8.00	6.16	2.86	1.00	6.92
Radial burr formation Δr	5	3.29	2.29	3.57	1.29	1.00	8.00
Hole cylindrical form t	5	1.00	6.55	7.33	5.86	4.07	8.00
Total utility value (TUV)	I_machinability	230	348	376	322	98	302
Ranking of the machinability		5	2	1	3	6	4

Legend: **Steel grade with the higher machinability**
C_j, j = 1 - 3:   Investigated cases (cutting conditions)
Weighting factor (W_i):   1 (less important) to 10 (very important)
Utility value (UV_{ji}):   1 (worst case) to 8 (best case)

$$TUV_j = \sum_{i=1}^{7} W_i \cdot UV_{ji}$$

Table 17: Machinability classification by means of the weighted point evaluation method for a predefined number 1232 of drilled holes (v_c = 120 m/min, f = 0.25 mm, h = 3*d, wet)

Task 6.4 Correlation between the microstructure and the machinability

Based on the machinability classification (Task 6.3) and the results performed in WP1, a qualitative evaluation of the influence of the microstructure parameters (Pearlite fraction, pearlitic grain size, pearlite interlamellar spacing and globular pearlite volume fraction) on the machinability of the investigated grades is shown in Table 18. An increase of the pearlite fraction leads to higher cutting force, shorter chip form, higher tool wear and higher hole quality. This behaviour characterizes the machinability of pearlite (low deformability and greater hardness: significant abrasive wear, high cutting forces, less burr formation, favourable chip forms, improved surface quality). The microstructure parameters pearlitic grain size, pearlite interlamellar spacing and globular pearlite show similar impact on the machinability. So with them the cutting force and tool wear increase and the hole quality decreases due to the dominating material adhesion mechanism. However, these microstructure parameters have a minor influence on chip form, see Table 18.

Legend: ↑: Increase ↓: Decrease →: Minor impact		Machinability			
		Cutting force	Chip length (form)	Tool wear	Hole quality
Microstructure	Pearlite fraction ↑	↑	↓	↑	↑
	Pearlitic grain size ↑	↑	→	↑	↓
	Pearlite interlamellar spacing ↑	↑	→	↑	↓
	Globular pearlite volume fraction ↑	↑	→	↑	↓

Table 18 : The influence of the microstructure parameters on the machinability

Task 6.5 Modelling investigation at the micro range

To check the quality of the developed material and friction laws when drilling at the micro level, a modelling concept has been developed for the simulation of twist drilling process at the micro range using the 3D Finite-Element-Technique, see Figure 49. The used FE mesh is isotropic and without any heterogeneity regarding the material properties. The material and friction behaviours in the simulation are described by means of the constitutive laws developed in WP2 and WP3 respectively.

Boundary conditions adjustment

- Twist drill: Rigid with mesh d = 1 mm and $r_ß$ = 15 µm
- Workpiece: Visco-plastic D x H = 1.4 x 0.470 mm with heat dissipation 100,000 3D-Tetrahedron
- Contact: friction, heat transfer (conduction & convection)

Twist drill CAD model

Gühring KG 6400

d = 1 mm
$r_ß$ = 15 µm

Cutting parameters definition

- Workpiece material: 16R, 27R, 45R, 45CG, 45GP, 60R
- Tool material: HW
- Cutting speed: 40 m/min
- Feed rate: 0.03 mm/rev

Constitutive material law (WZL)

- Material law: ASCO
- Friction law: ENISE
- Thermal properties: MGEP

Figure 49: 3D FE computation model for micro drilling (d = 1 mm, homogeneous microstructure)

The developed FE micro drilling model is validated for drilling in the investigated grades with a drill diameter d = 1 mm, cutting speed v_c = 40 m/min and feed rate f = 0.03 mm, see Figure 50. The comparison between the predicted and measured feed force and cutting torque shows a maximum deviation less than 10% for the grades 16R, 27R, 45R, 45CG, 60R and of 28% for the grade 45GP. The higher deviation in the case of the grade 45GP is due to the significant material adhesion on the drill cutting edge during the real drilling process. This phenomenon could not be taken into

account in the drilling simulation. In addition, the simulation reproduces the influence of the microstructure on the drilling process reaction. In this regard, the behaviour of the computed and measured feed force and cutting torque is similar regarding the machined grades (compare with the results in Task 6.2).
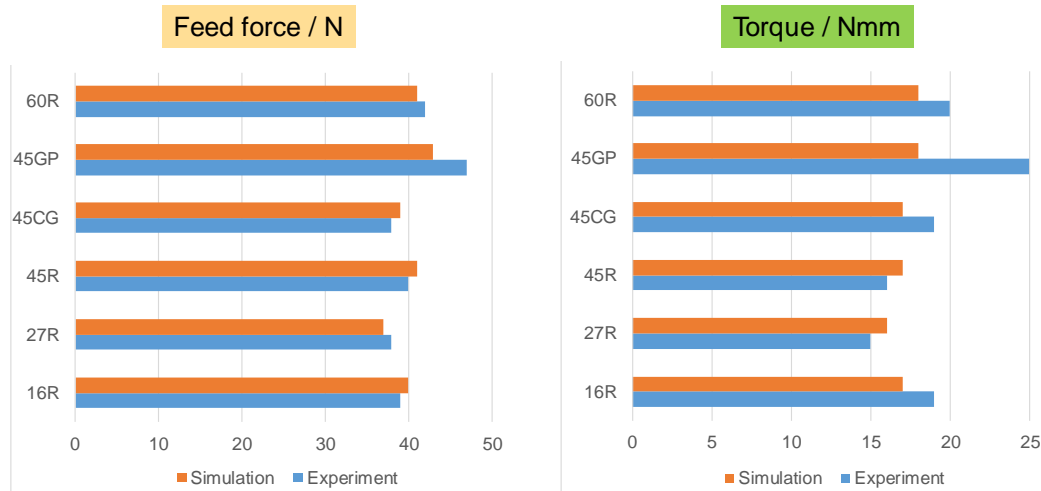
Drill diameter d: 1 mm, cutting speed: 40 m/min, feed rate: 0.03 mm/rev, tool material: HW

Figure 50: FE model validation by drilling at the micro range (d = 1 mm, dry cut)

Task 6.6 Microstructure parameters driving the machinability in drilling

Based on the experimental and simulative investigations in WP6 and the correlation obtained between the microstructure and the machinability in Task 6.4, the microstructural parameters driving the machinability performance in drilling are the pearlite volume fraction f_p, the pearlite grain size d_p, the pearlite interlamellar spacing S_p and the globular pearlite volume fraction f_{gp}. These microstructure parameters characterise the morphology and the content of pearlite of the investigated grades. To mathematically describe the deduced correlation between the microstructure parameters and the machinability of the machined grades, an empirical formulation for the relative machinability index I_r (in %) is developed and summarised in equation (19) as follows:

$$I_r = 100 \cdot \frac{\left[1 - 3 \cdot \left(f_p - 0.9\right)^2\right]}{e^{\left[0.2 \cdot \frac{d_p}{d_{p,max}} + \frac{S_p}{S_{p,max}} + \frac{f_{gp}}{f_{gp,max}}\right]}} \tag{19}$$

The relative machinability index I_r is calculated based on equation (19) and the measured microstructure parameters listed in Table 19. The classification of the machinability by means of the relative machinability index is similar to the results obtained in Task 6.3, as represented in Figure 51. Thereby, the grade 45R shows the best machinability and the grade 45GP, in contrast, the worst.

Steel grade	f_p	d_p / µm $d_{p\,max} = 89$ µm	S_p / nm $S_{p,max} = 635$ nm	f_{gp} $f_{gp,max} = 0.90$	I_r	Ranking
16R	0.42	11	190	0.05	21.1	5
27R	0.60	15	285	0.06	42.1	3
45R	0.75	22	293	0.19	45.2	1
45CG	0.85	89	366	0.04	43.6	2
45GP	0.90	0	632	0.90	13.5	6
60R	0.86	62	372	0.21	38.1	4

Table 19: Machinability classification by means of the empirical equation (19)
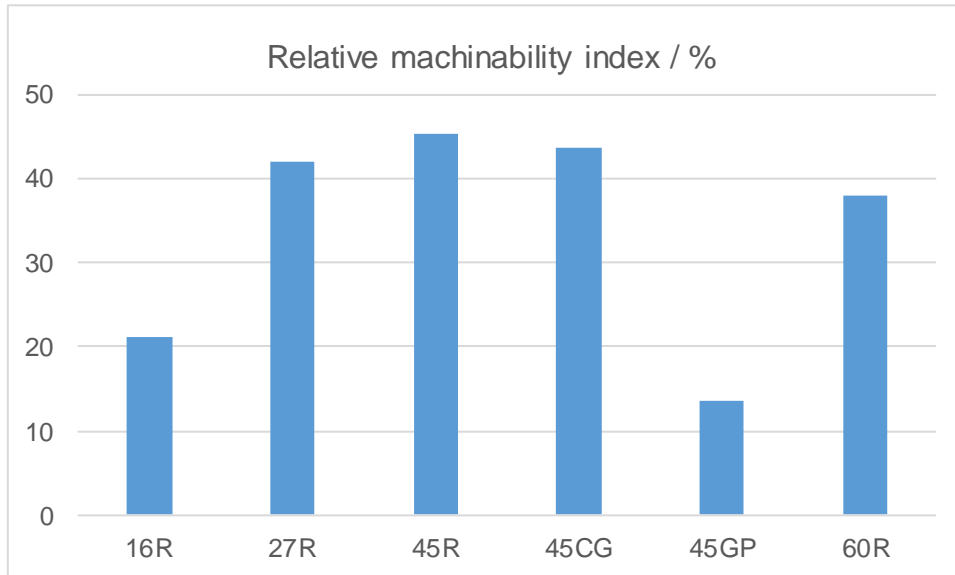
Figure 51: The calculated relative machinability index I_r for the investigated grades

In order to compare the predicted and measured machinability, a machinability index is defined with help of the weighted point evaluation method (used in Task 6.3) and considering the machinability criteria (feed force, cutting torque, tool wear, chip form and surface quality), as shown in Figure 52.

$$I_{Machinability, j} = TUV_j = \sum_{i=1}^{n} W_i \cdot UV_{ji} \qquad UV_{ji} = 8 - 7 \cdot \frac{(EC_{j,i} - EC_{min})}{(EC_{max} - EC_{min})}$$

Higher values of $I_{Machinability}$ → Higher machinability

UV_{ji}: *Utility Value*
W_i: *Weighting factor*
TUV_j: *Total Utility Value*
EC: *Evaluation Criterion*

Figure 52: Definition of the machinability index based on the weighted point evaluation method

The evaluation criteria used to calculate the machinability index based on the experiment and simulation results are listed in Table 20. The computed chip compression ratio is representative for chip form and the computed maximal temperature as well as pressure on the cutting edge are representative for tool wear. The hole quality will be better with increasing the pearlite volume fraction (consult Task 6.3 and Task 6.4). So, to take the hole quality in the evaluation based on the simulation results, the ration $(100/f_P)$ is defined as additional evaluation criterion.

	Evaluation criteria EC						
Experiment	Feed force	Cutting torque	Chip form	Tool flank wear VB	Surface roughness R_z	Radial burr formation	Hole cylindrical form
Simulation	Feed force	Cutting torque	Chip compression ratio	Max. temperature on the cutting edge		Max. pressure on the cutting edge	100/fp (in%) (hole quality)

Table 20: The evaluation criteria for the calculation of the machinability index

It should be noted that the pearlite volume fraction f_P is one input parameter for the FE drilling model describing the material flow behaviour of the workpiece material, as shown in Figure 53. Higher hole quality corresponds to lower values of the ratio $(100/f_P)$. Furthermore, there is no variation of the cutting conditions (cutting parameters, tool material, tool geometry, coating, etc.) to provide adequate comparability of the determined machinability. At this point, it is pointed that all FE simulations were performed with the implicit FE code DEFORM-3D[TM]. The used FE drilling model is optimised regarding the remeshing procedure (weighting factors controlled autoremeshing) and the boundary conditions.
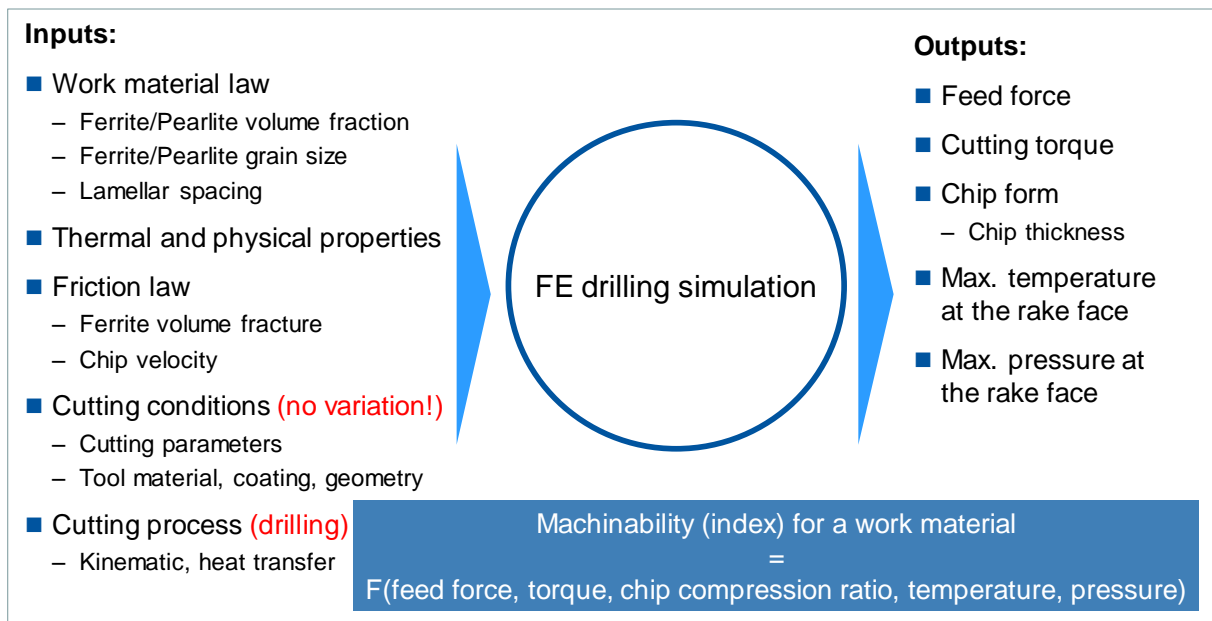
Figure 53: The inputs and outputs parameters for the FE drilling simulation

Figure 54 shows the comparison of the machinability classification by means of the above defined machinability index calculated based on experiment (tool life drilling tests), FE drilling simulation and the empirical model described in Task 6.6. It is obvious that both the FE drilling simulation and the empirical model predict adequately the machinability of the investigated steel variants.
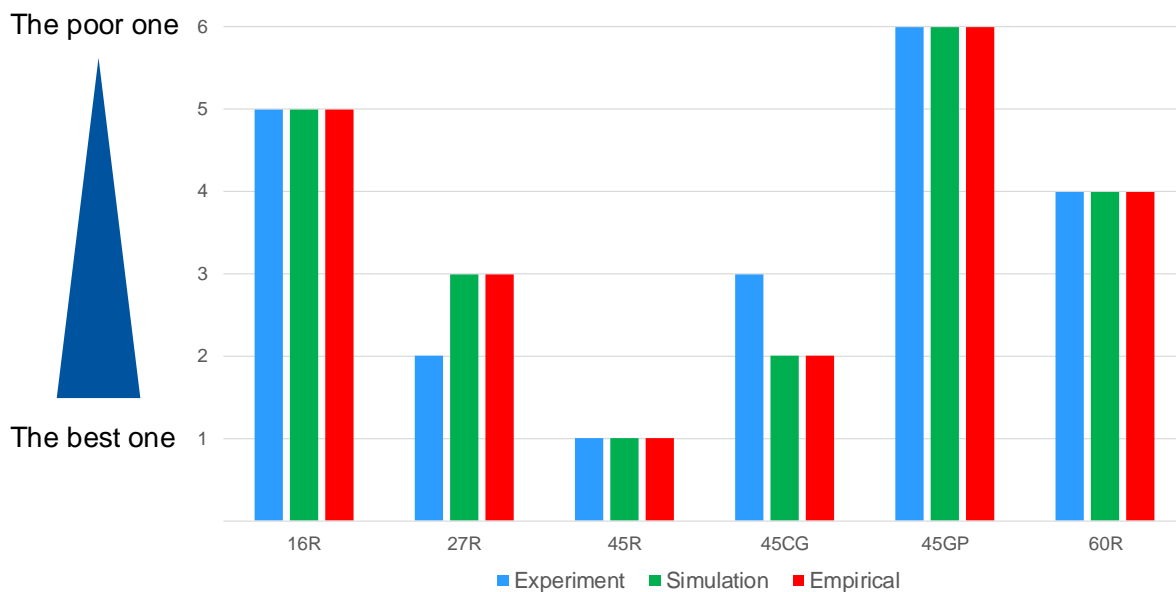
Figure 54: Machinability classification based on experiment, simulation and empiric

CONCLUSION

The experimental tool life tests have demonstrated that :
- The pearlite volume fraction controls in a nice manner the cutting forces when drilling the reference grades 16R, 27R, 45R and 60R.
- The grades with globular pearlite (GP) show the highest values of feed force and torque due to the dominant material adhesion on the tool cutting edge during drilling.
- Regarding the chip form, independent of the drilled grade, short chips are detected and the chip size decreases with the volume fraction of pearlite.
- The tool flank wear of the used drills correlates well with the measured torque and is more pronounced in the case of the more ductile grades 45GP and 16R due to the formation of material adhesion.
- The wear behavior of the cutting edges is controlled by the wear mechanism abrasion when drilling the reference grades 27R, 45R, 45CG and 60R.

The classification of the machinability was performed by means of the weighted point evaluation method and it results in the following machinability ranking:
- 45R, 27R, 45CG and 60R : classify by their abrasion impact on cutting tool
- Following by 16R, 45GP : classify by their adhesion impact on cutting tool

Based on the machinability classification and the results performed in WP1, a qualitative correlation between microstructure and machinability could be deduced.

The machinability of the steel variants selected could be empirically and numerically predicted and compared with the experimental measured machinability:
- The microstructural parameters driving the machinability performance in drilling are the pearlite volume fraction f_p, the pearlite grain size d_p, the pearlite interlamellar spacing S_p and the globular pearlite volume fraction f_{gp}.
- A machinability index could be defined with help of the weighted point evaluation method.
- An empirical formulation for the machinability has been developed based on the microstructure.
- A 3D FE computation model has been developed to predict the drilling process values feed force, cutting torque, chip compression ratio, max. normal pressure and temperature (on the rake face), which was used to compute the machinability.
- Both the FE drilling simulation and the empirical model predict adequately the machinability ranking of the investigated grades.

2.2.7 WP7: broaching operation

Task	Title	Initial plan	Actual plan	Note
Task 7.1	2D/3D modelling	Lagrangian based model to predict the full chip formation	ALE approach to predict the physics around the tool edge radius	(1)
		Multi-cutting edge 2D model including data from WP2 and WP3	Single-cutting edge 2D model including data from WP2 and WP3	(2)
		3D model to investigate edge effects		
Task 7.2	Experimental broaching device	4 teeth simplified broaching tool	1 tooth simplified broaching tool	(3)
		Upgrade of the preliminary set-up including high speed imaging	Development of a new set-up with a different broaching configuration	(4)
Task 7.3	Influence of microstructural parameters	Analysis of machining forces, heat flux, chip characteristics on the 6 steel variants selected in WP4	Analysis of machining forces and surface roughness on the 16 variants	(5)
			Tests with 3 tool systems under dry conditions and 9 cutting conditions + lubricated conditions	(6)
Task 7.4	Cutting mechanisms	Analysis of local temperature and strain distributions using imaging as well as collected chips	Analysis of the collected chips only	(4-7)

Task 7.1 2D/3D Modelling

Note (1): The initially developed Lagrangian approach faced some difficulties in terms of mesh distortion when data from WP3 were implemented. This was expected but to a lower extent as the friction coefficients obtained under dry conditions were significantly larger than planned. Moreover, it suffered also from a bad capability of modelling properly the feed force due to the deletion of an element layer (inherent of the modelling approach). If cutting force and chip curvature were

thought to be the most important components at the beginning of the project, discarding the feed force and the local phenomena close to the cutting edge was in fact a mistake.

Therefore, a new model has been developed based on the ALE approach (Figure 55) with the following advantages:

- It enables a more physical material separation around the tool cutting edge without using a damage criteria which would be impossible to properly identify during this project (different approach);
- Friction data can be consistently implemented without excessive mesh distortion and numerical tricks;
- The same approach is used in WP5 by MGEP allowing a joint work on the modelling part and leading to an interesting comparison between results from WP5 and WP7. In these two, the same numerical approach, FE code, same input data are employed which makes the comparison between the two different machining configurations even more relevant.
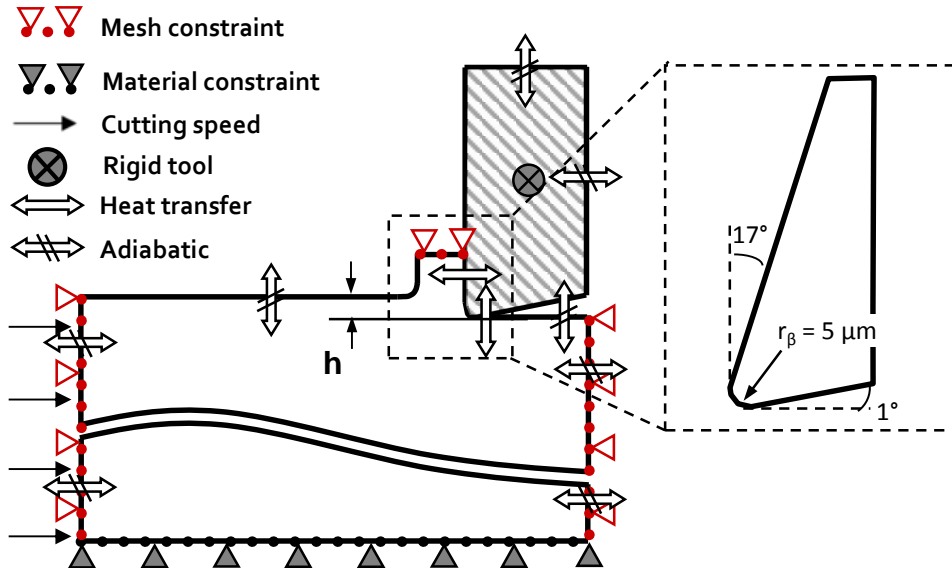
Figure 55: Boundary conditions of the developed 2D ALE broaching model.

As the development of the numerical model was conducted in parallel of the experimental campaign Task 7.2, the interaction between both emphasised that some changes were needed compared to the initial work plan.

Note (2): Some preliminary tests revealed that broaching tests with several teeth was not possible due to a lack of stiffness that will be detailed in the next section. Moreover, when analyzing the chips, the expected larger chip width compared to the initial width of cut did not occur showing that the material lateral flow was not dominant on these materials (contrary to stainless steel or nickel based-alloys). Therefore, developing a 3D model did not appear to be a priority.

Data from the tribological campaign WP3 were implemented in this numerical model. Concerning the rheological model developed in WP2, only one modification had to be done on the temperature dependency. The range of temperatures in WP2 was relatively large and investigated temperatures were ambient, then 300 °C and beyond. The broaching process, especially under low cutting speed and lubricated conditions, does not lead to a high heat generation and therefore resulting temperatures in the cutting zone are definitely below 300°C.

After some preliminary simulations once the model was developed, large discrepancies were reported which questioned the applicability of the constitutive model to this cutting configuration. Disabling the temperature dependency of the proposed model led to more consistent results (as described in the next sections) and confirmed the fact that the identified temperature dependency on the selected range was overestimated as far as "low temperature" processes were concerned. An additional rheological campaign would have been needed to focus more on the range 20-150°C. The consistency of the results observed when disabling the temperature dependency tends to show that it is not a predominant factor in broaching.

Task 7.2 Experimental broaching device

Broaching is a complex process and can only be investigated via a "simplified" experimental set-up that can be easily instrumented. Conducting fundamental broaching tests was necessary to properly emphasize the effect of each variant/microstructure on the targeted outputs. The objective of the project was first to upgrade a dedicated experimental set-up fitted on a PCI METEOR 3+1 axis machine able to run tests up to 60 m/min. The principle of the first broaching configuration is shown in Figure 56.

Note (3): After an extensive preliminary experimental campaign, the main limitation was, compared to what was initially planned, that broaching with several teeth was not possible with the defined specimen geometry. Even if the distance between the tool and the specimen was reduced to the maximum, it appeared that the spindle and corresponding slidings were not stiff enough to avoid a slight bending of the workmaterial specimen. The latter then, compared to the scale at which the material is removed, induced a fluctuating depth of cut, unstable cutting phenomena and a high deviation on the results. It has been decided to perform only single tooth broaching operation. A second configuration has been developed and will be discussed in WP8.
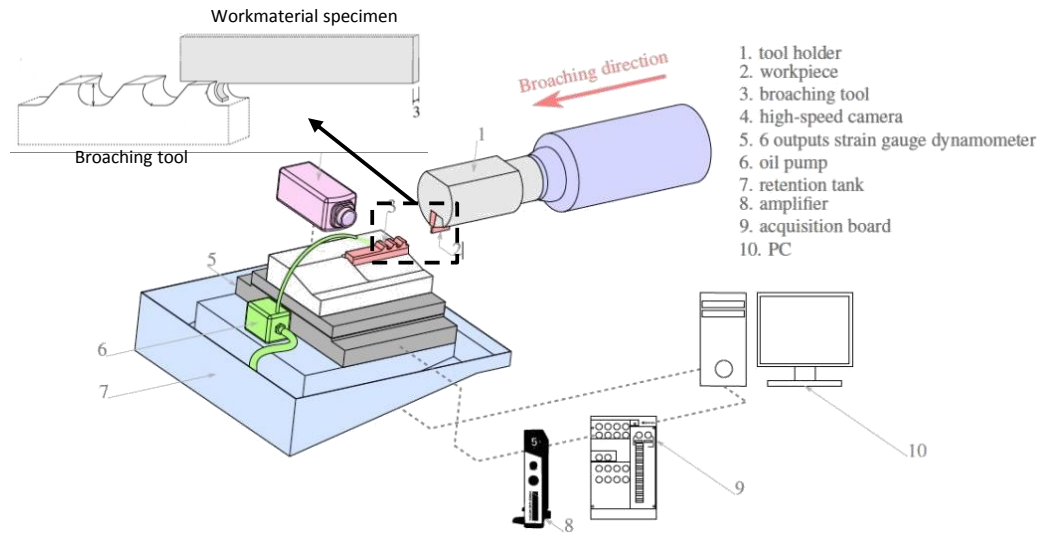
Figure 56: Principle of the developed broaching setup.

Moreover, a holding system was developed to set a microscope or more advanced camera (high speed or infrared) in front of the cutting tool. More details are given in Appendix 7.5.1. The Figure 57 shows an example of what can be observed when an infrared camera is employed.

Operation: Broaching
Materials:
27R-45R-60R
Tool : HSS M35
Coating : TiN-flank
Edge : $r\beta = 5$ µm
$\gamma_n = 15° \lambda_s = 0° \alpha_n = 5°$
$a_p = 3$ mm
Vc = 40 m/min
h = 40 µm
Lubricated/Dry
1000 FPS
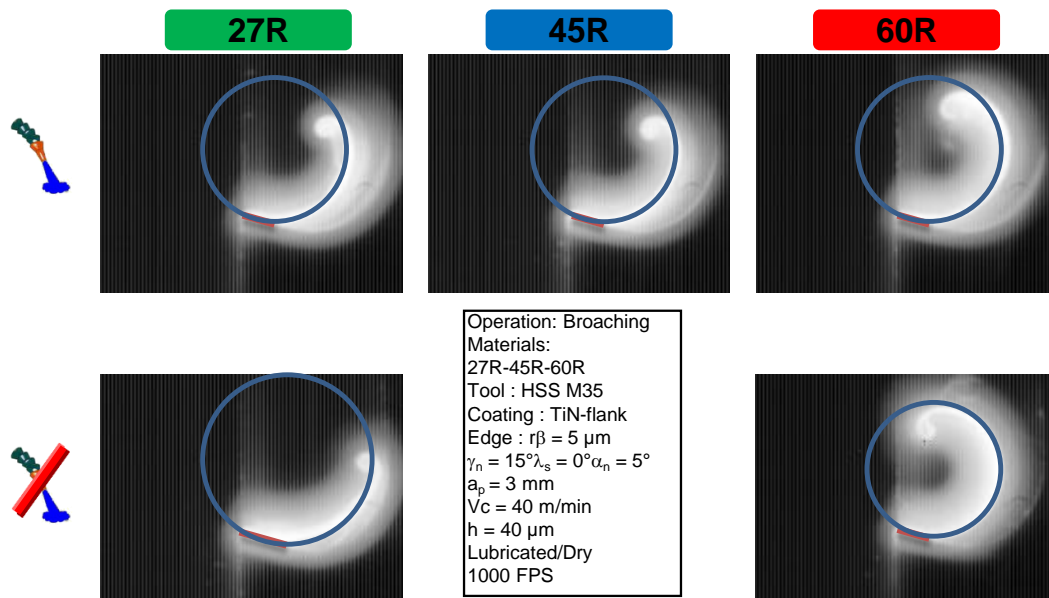
Figure 57 : Gray level images obtained with the IR camera to investigate chip curvature.

Note (4): Using imaging in this set-up was proposed to in-situ capture the chip formation process and observe chip curvature and tool-chip contact length. As broaching is not an intense dissipative process, getting clear gray level maps was difficult as temperature of the environment was relatively close to the temperature within the chip. It was noticed that contact length was pretty unstable and greatly affected by small scales vibrations generated by the broaching configuration itself. According to the time required to record and post-treat these data, using imaging has been left apart.

Task 7.3 Influence of microstructure parameters

The first actual campaign aimed at highlighting the general behaviour of all the variants under the most severe broaching conditions and over a wide range of cutting conditions. Therefore, the 16 variants were investigated over 3 cutting speeds, 3 rises per tooth under dry conditions with an uncoated broaching tool. 5 repetitions were performed leading to a total of 720 runs.

Note (5): According to the limitations faced with the high speed imaging, cutting forces and roughness on the last cut were recorded. Results in terms of cutting force are shown in Figure 58.
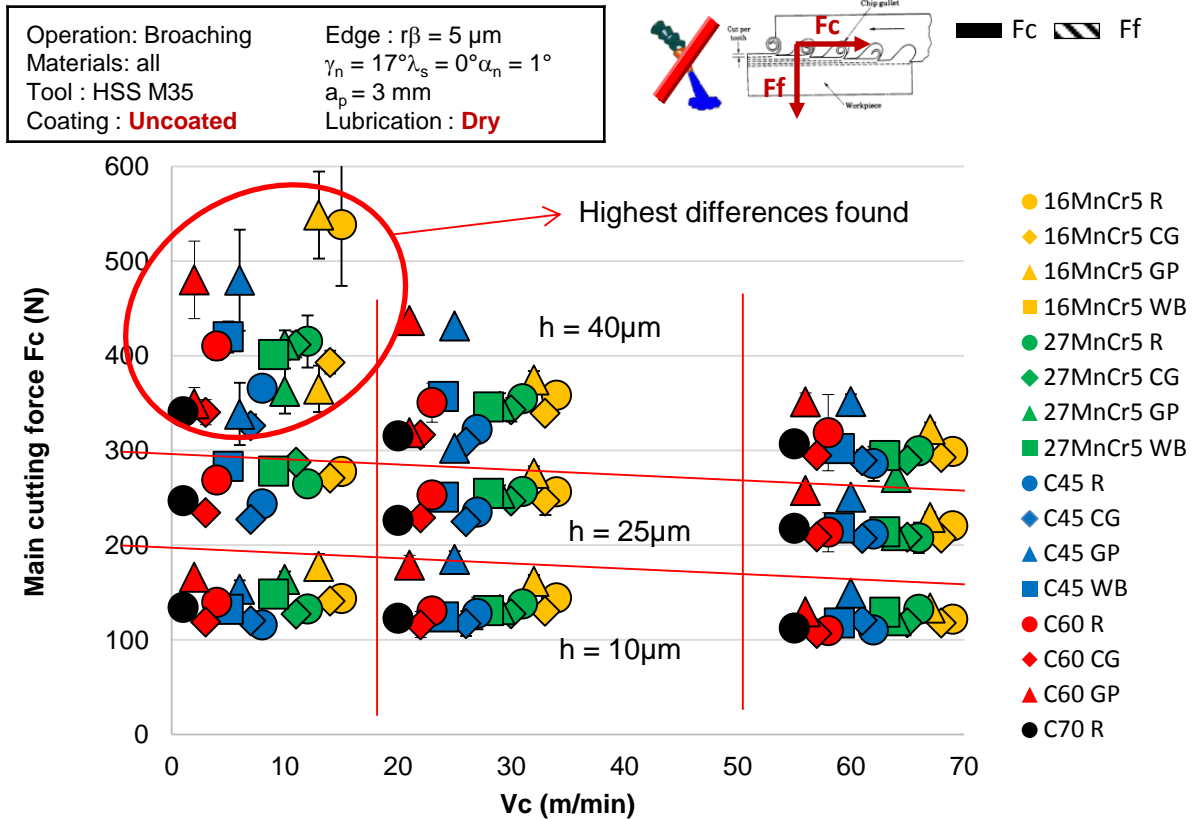
Figure 58: Main cutting force recorded in broaching during the first campaign for all the variants depending on the cutting speed and rise per tooth (h) under dry conditions.

Differences between the variants in terms of roughness and machining forces were found to decrease as cutting speed increases and rise per tooth decreases. The GP variants always exhibited a different behaviour with higher forces and roughness Ra, except 16GP with perlite in a way of globulization (75% of broken pearlite).

Plotting the results versus the macro-hardness (Figure 59) revealed an unexpected phenomena: machining forces decreased when increasing the hardness of the steel. Analysing this in terms of microstructure showed that the ferrite content was the most sensitive microstructural parameter. Increasing the ferrite content led to an increase of the machining forces. This effect was amplified when reducing the cutting speed and increasing the rise per tooth (Figure 60). In WP3, increasing the ferrite content was proved to increase friction and adhesion at the tool-chip interface. Thus a strong correlation started to appear between cutting and tribological behaviours.
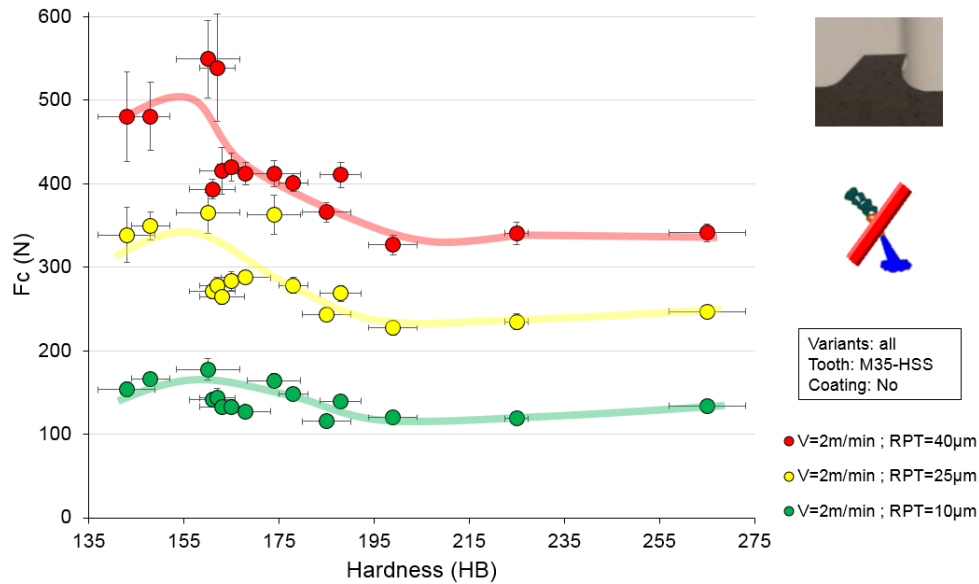
Figure 59: Main cutting force recorded in broaching for all the variants depending on the rise per tooth under dry conditions versus the macro hardness
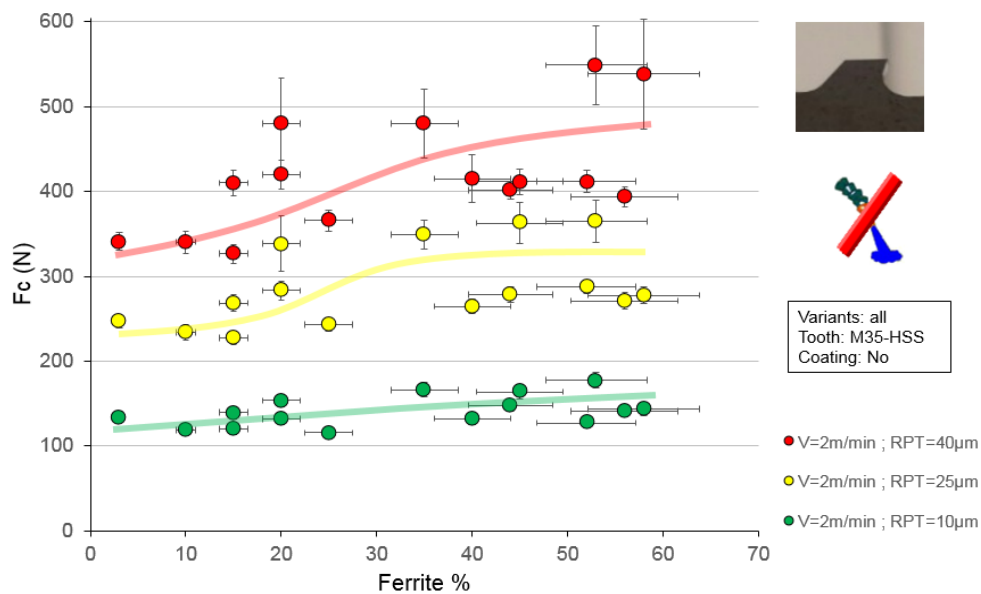
Figure 60: Main cutting force recorded in broaching for all the variants depending on the rise per tooth under dry conditions versus the ferrite content

This extensive campaign demonstrated that the largest differences could be seen at le lowest cutting speed of 2 m/min and rise per tooth of 40 µm. The variants selected in D1 were thus studied (16R, 16GP, 27R, 45GP, 45R, 45WB, 60R, 60CG and 60GP) based on those cutting conditions.

Note (6): Contrary to the initial plan, it was decided to investigate different tool systems. Indeed, broaching tools are usually uncoated on the rake face but coated on the flank face. This plays an important role in the tribological interaction between the tool and the workpiece. In order to exact assess the contribution of the coating as well as the lubricant, i.e. different tribological conditions, experiments were carried out under dry and lubricated conditions using 3 tool configurations:
- An uncoated broaching tool ;
- A fully TiN coated tool ;
- A broaching tool uncoated on the rake face but TiN coated on the flank mimiking an industrial broaching tool.
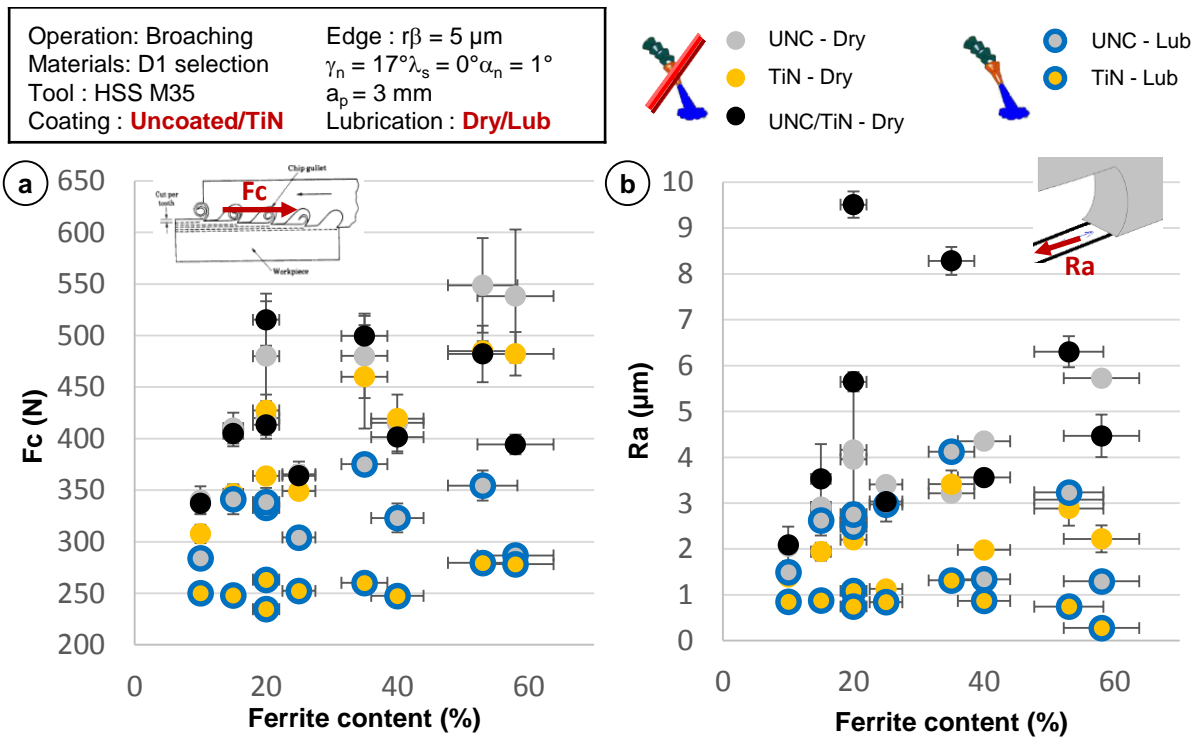
Figure 61: Main cutting force FC (a) and Ra surface roughness (b) measured during the second campaign focusing on the D1 selected variants.

The Figure 61 presents the results in terms of cutting force Fc (Figure 61a) and Ra roughness (Figure 61b) for all these configurations. Surprisingly, forces and roughness were found to increase as the ferrite content increases for each tool system. This proved the larger contribution of the tribological phenomena against the plastic behaviour of the workmaterial in broaching.

This was confirmed by the fact that, as the lubricant was applied, both forces and roughness drastically decreased. However, if the effect of the coating was relatively weak under dry conditions, the combination of fully coating and lubricant have a major effect leading to the lowest cutting force and Ra. Using a partially coated tool (industrial one) led to similar forces than the other two configurations but slightly larger Ra compared to the fully coated one. This showed that the contribution of the coating on the rake face cannot be neglected.

It has been noted that GP variants exhibited the highest Ra and cutting force especially with the industrial tool.

Task 7.4 Cutting mechanisms

Note (7): According to the limitations faced in Task 7.2 regarding the high-speed/IR imaging, as well as those in Task 5.3 (digital image correlation), extracting strain and temperature fields was unfortunately impossible. Instead, chips were carefully collected during the previous experiments, embedded in resin, polished, etched and thoroughly analysed. The objective was to observe the deformed microstructure and measure the average chip thickness.

The microstructure was found to be highly deformed with, even under lubricated conditions, an intense shear occurring at the tool-chip interface (Figure 62a). If a pseudo serration could be observed on the standard R and coarse grain CG variants, a more pronounced one was visible on the globular pearlite GP ones. This serration could be related to the amplified sticking behaviour characterising these type of microstructure as seen in WP3. An innovative finding was that GP variants behave almost as a purely ferritic material as the ferritic matrix is deformed whereas the pearlite globules only move within this matrix.
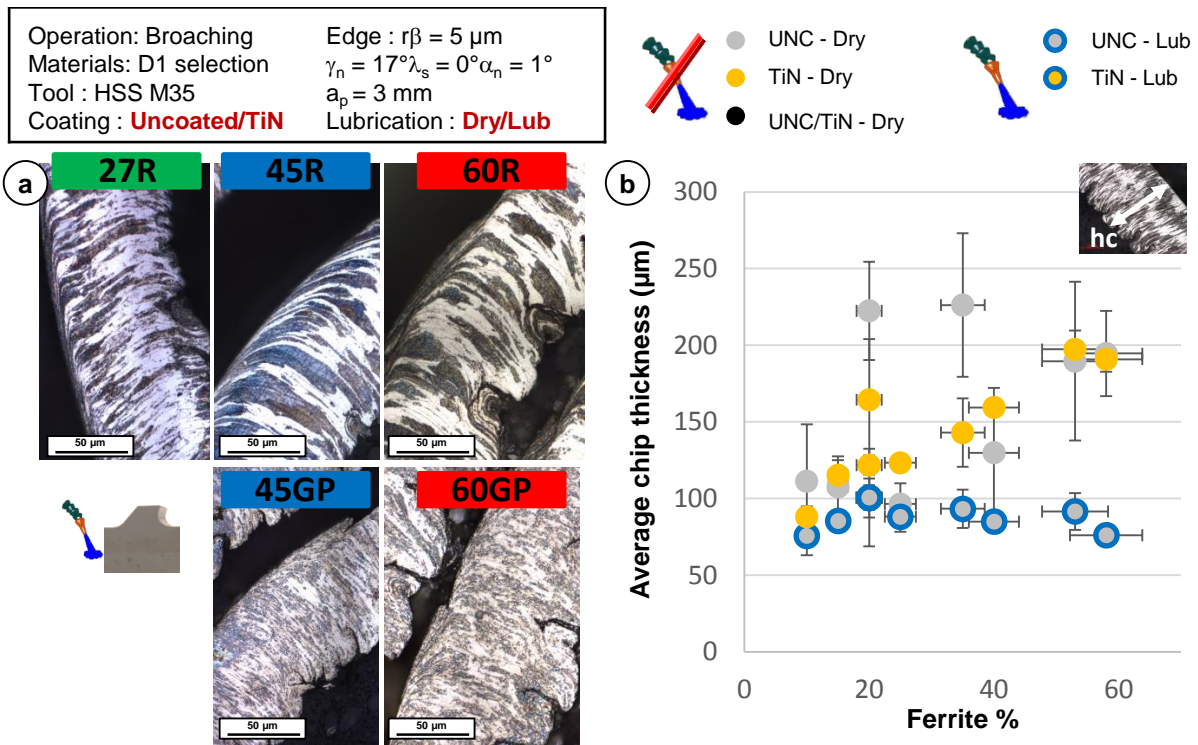
Figure 62 : Examples of chip micrographs showing the deformed microstructure (a) and (b) correlation between the average chip thickness and the ferrite content.

Average chip thickness is an interesting output parameter providing an image of the average chip sliding speed over the tool (mass flow conservation): thicker chips correspond to a slower chip meaning that larger friction can be expected. On the contrary, thinner ones are generated when the chip can easily slide over the tool meaning lower friction at the tool-chip interface.

Thus, increasing the ferrite content increased the chip thickness under dry conditions whatever the tool configuration (Figure 62b). The two runs exhibiting a thicker chip between 20 and 40% of ferrite correspond to the 45 and 60 GP variants. This was in good correlation with the findings from WP3 showing that friction during the tribotests increased with the ferrite content and when changing to the GP variants.
Using a lubricant reduced the chip thickness which became constant around 100µm whatever the ferrite content. This was again in good agreement with the data from WP3 as the friction coefficient under lubricated conditions was close to 0.12 for all the investigated variants.

Interesting trends were also found regarding the pearlite grain size (Appendix 7.5.3) which induces a chip thickness reduction beyond 25µm.

Task 7.5 Microstructure parameters driving machinability in broaching

The previous experimental campaigns highlighted the contribution of the microstructure and the fact that ferrite content was the predominant microstructural parameter affecting the broaching performances. Changing from a normalised to a globular structure reduced these performances whereas a coarse pearlite grain tended to improve them.

The objective of this task was thus to check the capability of the simulation to take these effects into account. The weighted point evaluation method proposed in Task 6.3 was applied to assess the agreement level between the simulation and the experiments on the selected variants, a single cutting condition, an uncoated tool and without lubrication.
The first step of this method is to define the criteria to be compared. In broaching, machining forces, roughness of the generated surface but also chip characteristics were considered as the most important ones. A larger weight was given to the chip properties and surface roughness as shown in Figure 63.

Edge : rβ = 5 μm
$\gamma_n = 17°$ $\lambda_s = 0°$ $\alpha_n = 1°$
a_p = 3 mm
Vc = 2 m/min
RPT = 40 μm
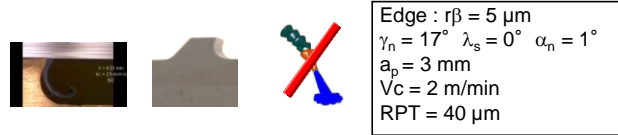
Evaluation criteria	Weighting factor	16R	27R	45R	45CG	45GP	60R
Fc	5	1,0	5,1	6,7	8,0	2,9	5,2
Ff	5	1,0	6,0	6,3	8,0	2,4	6,7
Chip thickness	10	6,7	3,9	1,1	-	8,0	1,0
Chip diameter	10	1,2	5,8	8,0	-	1,0	7,9
Ra roughness	10	1,0	3,5	3,5	8,0	4,2	6,1
Total utility value (TUV)	$I_{machinability}$	2,5	4,7	4,8	8,0	4,0	5,2
Ranking of machinability		6	4	3	1	5	2

Figure 63 : Experimental machinability classification by means of the weighted point evaluation method (vc = 2 m/min, RPT = 40 μm, dry, uncoated)

According to the Figure 63, the C45CG presented the highest machinability index. The worst performances were obtained with the 16R, C45GP and 27R, basically the variants with high ferrite content or the GP variant with a similar highly ductile behaviour.
If focusing especially on the C45 grade, improving the broaching performance can be done by using a coarse grain structure and broaching a globular C45 will affect the broaching quality.

The same methodology was applied on the numerical simulations. However, the consistency of the numerical results had to be checked before applying the ranking method. Cutting and feed forces as well as average chip thickness were the only outputs directly comparable and have thus been considered. Figure 64a shows an example of plastic strain and location where the numerical chip thickness was extracted.

The Figure 64b reports the comparison between the numerically predicted outputs and the experimental ones. If large discrepancies were observed regarding the 16R and to a lower extent regarding the C45GP, the simulation was in good agreement as far as other variants were concerned. Despite the large underestimations on the C45GP, the model was able to predict the main trends when changing from a R to CG and R to GP microstructure.

Operation: Broaching
Materials:
Selected from D4
Tool : HSS M35
Coating : **Uncoated**
Lubrication : **Dry**

Edge : rβ = 5 μm
$\gamma_n = 17°\lambda_s = 0°\alpha_n = 1°$
a_p = 3 mm
Vc = **2 m/min**
RPT = **40 μm**

Evaluation criteria	16R	27R	45R	45CG	45GP	60R
Fc	-46%	-6%	-2%	15%	-20%	-25%
Ff	-75%	-16%	-24%	-23%	-46%	-61%
Chip thickness	-41%	-5%	32%		-37%	15%
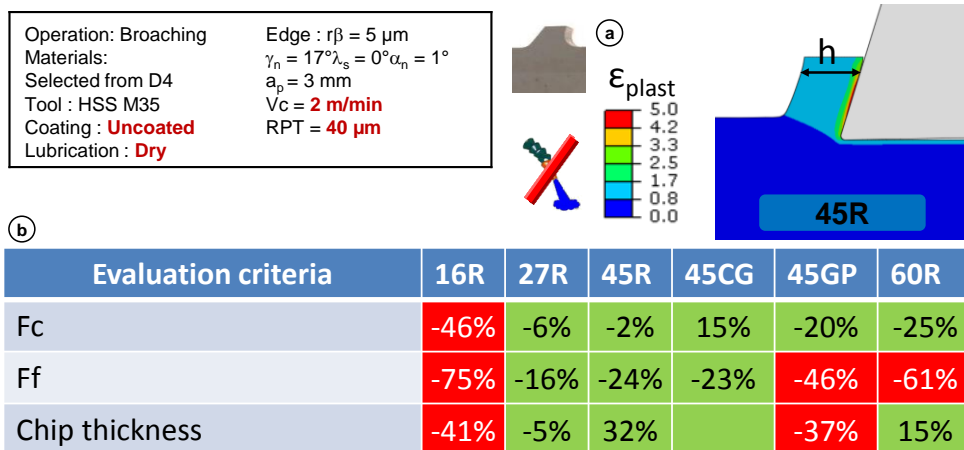
Figure 64: a) Example of plastic strain distribution on the C45 and extraction of chip thickness; b) Deviation reported on the numerical results compared to the experimental ones for the finally selected variant.

Applying the weighted point evaluation method on the numerical simulations resulted in the machinability given in Figure 65. As deviations were extremely large regarding the 16R, it has been discarded from this method in order to avoid any misleading conclusions (black column).

Edge : $r\beta$ = 5 µm
γ_n = 17° λ_s = 0° α_n = 1°
a_p = 3 mm
Vc = 2 m/min
RPT = 40 µm
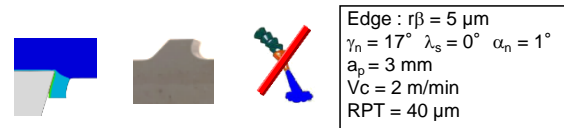
Evaluation criteria	Weighting factor	16R	27R	45R	45CG	45GP	60R
Fc	5	8,0	1,0	3,3	1,9	1,4	6,8
Ff	5	7,7	1,0	2,5	4,4	2,5	8,0
Chip thickness	10	2,0	8,0	5,4	5,7	7,5	1,0
Contact length	10	7,6	1,0	1,3	1,0	1,0	8,0
Subsurface plastic def.	10	6,6	4,1	5,4	6,0	1,0	8,0
Total utility value (TUV)	I$_{machinability}$	6,0	3,5	3,7	4,0	2,9	6,1
Ranking of machinability		-	4	3	2	5	1

Figure 65 : Numerical machinability classification by means of the weighted point evaluation method (vc = 2 m/min, RPT = 40 µm, dry, uncoated)

The machinability ranking is similar to the experimental one (Figure 63) but most important is the capability of the numerical simulation to take into account the effect of a different microstructure on the C45 grade. Numerical broaching performances are reduced when changing from R to GP variant but can be improved when a CG variant is used.

CONCLUSION

Experimental campaign
- Largest differences between the microstructures have been observed at the lower cutting speed and largest rise per tooth;
- Combining a fully coated tool to a lubricant led to the most interesting performance in terms of forces and roughness;
- Under dry conditions, the benefit from the coating can be only visible with the material presenting the largest ferrite content;
- Experimental chip thickness evolution is in good agreement with the tribological results;
- Increasing the ferrite content, using GP variants or dry conditions increase the chip thickness, i.e. the friction at the tool chip interface.
- Broaching steels with a higher hardness improves the performances by reducing forces

2D Modelling
- A new ALE model has been developed;
- Friction coefficients from WP3 have been successfully implanted;
- Rheological model from WP2 have been implemented but without the temperature dependency that was certainly overestimated;
- Relevant qualitative data can be numerically predicted;
- The ranking method showed that the model was able to take into account some main effect of a change in the microstructure;
- The model did not provide consistent outputs on the variants with a high ductility (16R and C45GP), in which the main contact mechanism is adhesion.

As a summary, major achievements of WP7 are:
- An extensive experimental campaign with more than 700 experiments covering a wide range of broaching conditions and configurations;
- A finite element 2D model providing acceptable quantitative data and relevant qualitative ones;
- A capability to numerically predict the effect of a change in the microstructure on the macroscopic outputs;
- From a more scientific point of view, it improved the fundamental understanding of broaching such steels and especially emphasized that tribology, i.e. the tool material interaction, plays a major role in this process. Tribological experiments can thus be used as a fundamental test to anticipate the difficulties that could occur in broaching.

2.2.8 WP8: demonstrator

Task	Title	Initial plan	Actual plan
Task 8.5	Component oriented machining tests	Define the machining performances of the optimized microstructure steel variants	Define the machining performances of the optimized microstructure steel variants and of two additional "damaged microstructure" steel variants

Main objectives:
- Dissemination : establish an appropriate communication of the project results
- Machining tests: perform industrial tests on an optimized FP microstructure steel variant and on damaged FP microstructure variants
- Validation of the numerical approach: compare the machinability classification obtained with industrial tests, with the machinability classification obtained with the numerical simulations.

Task 8.1 Dissemination

One of the objectives of WP8 was to establish an appropriate and effective communication of the project works, developments and results to potential users and interested parties. The dissemination of the project results were undertaken by all consortium partners.
The goal of the dissemination was to create a series of actions able to share IMMAC challenge, approach and results during the project and beyond to appropriate stakeholders.
Publications in scientific journals and the project site, presentations at international and national scientific conferences, congress, seminars and the final Workshop in CRF at the end of the project represented effective tools to disseminate.
NB: the details of the work done in this task are in the section 2.4 "exploitation and impact of the research results".

IMMAC website
In order to prepare the real dissemination effort of the project, during the first mid-term period a particular attention to the first issue is focused: from CRF ICT Services an extranet area was created and offered to the partners in order to contain and share all the documents related to each WP step.

The access to the area was allowed and limited to the consortium partner. The area, called **https://collaboration.fiatgroup.com/sites/IMMACproject**, was structured in simple folders and sub – folders.

The main folders contained administrative documents (contractual documents, annual reports, …), technical documents (meeting presentations, call conference minutes, technical pictures and charts…), and also a folder regarding the work specifically related to the second level of dissemination (papers, fairs or conference or seminars contributions).
In particular, a folder called *Meetings* was divided in some sub-folders where it is possible to organize the activities from different point of view (see picture below):
- from a *time based* point of view, the presentations shared during each six - month meeting are grouped
- from a *WP's goal based* point of view, the work carried out from specific group (i.e. Tribology, or Simulation,…) is addressed
- the simple progressions and choices discussed during several phone conferences are grouped in Minutes

For each partner a personal UserID is created. To guarantee the safety of this extranet area the FCA policy are applied and the access credentials are to be renewed each three months. The extranet area contained also a calendar where all the common events were registered.
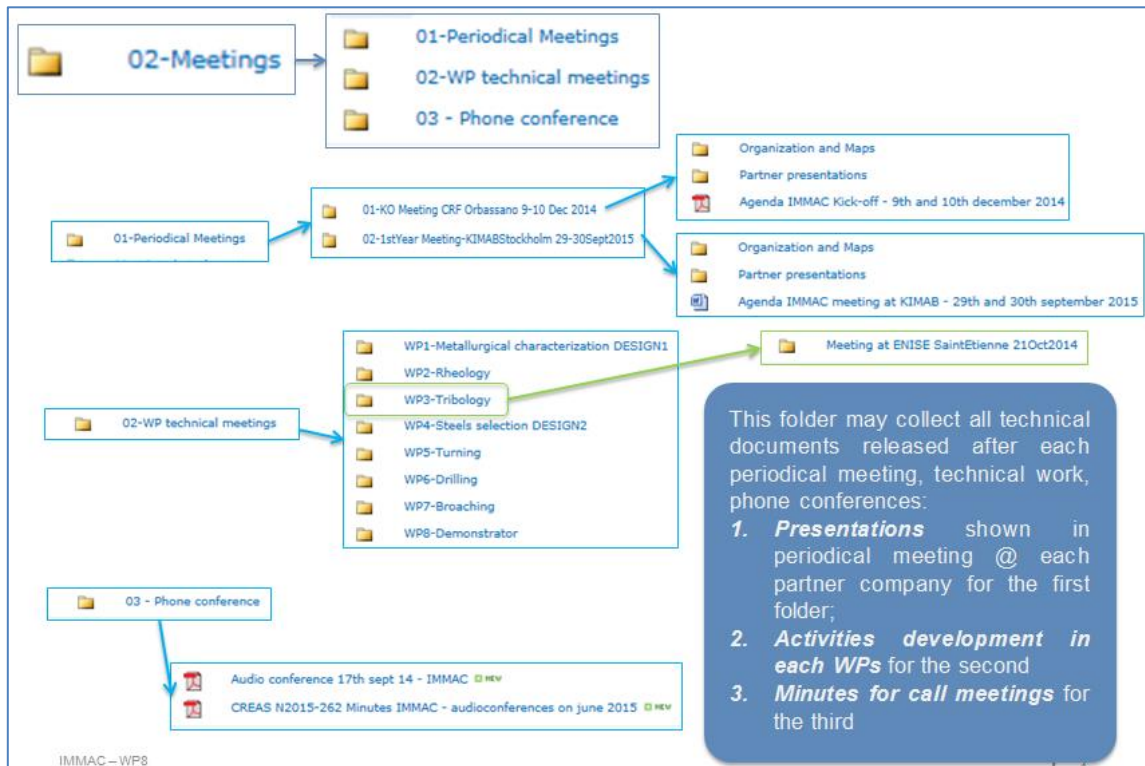
Task 8.2 Choice of an optimized FP grade to validate the numerical approach

Based on the results obtained in the previous WP, the microstructure of the variant 45R was seen as an optimized steel solution for the component oriented machining tests (task 8.5). The machining performances (turning, drilling and broaching) of this reference were compared with those of variants 45WB, 45CG and 45GP in order to make a classification with an industrial point of view.

Task 8.3 Rheology and tribology

Models from WP2 and WP3 were used.

Task 8.4 Numerical simulation

FE simulations and empirical models from WP5, WP6 and WP7 were used.

Task 8.5 Component oriented machining tests

Turning and drilling operations were tested in semi-industrial components, which were simulated by workpieces with similar dimension or shape. In particular, the crankshaft has been identified as the most appropriate automotive component because includes in the manufacturing cycle both operations and the actual reference material of end-user partner (FCA) comprises a medium-high carbon content, similarly to the chosen steel for the IMMAC tests.
For the component oriented broaching test, the steering rack was identified.

Turning and drilling operations were performed through specific tests at CRF Advanced Machining Laboratory, equipped with machines comparable to industrial machines. In both cases insert tool life was observed, cutting forces, insert wear and piece roughness according to the industrial drawing specifications were measured. In the industrial crankshaft the main bearing journal and the crankpin bearing journal are turned. The internal ducts for the oil passages are manufactured through deep drilling. The bars were turned and drilled in transversal direction, as in crankshaft, using specific operation cycle parameters.

Turning tests

The automotive crankshaft manufacturing process presents different turning operations starting from roughening of the forged component to the finishing; in order to represent one of the turning step, the **finishing operation OP150** has been chosen. In this operation the crank cheeks near the journal are **faced for 12 mm** (Figure 66a). In this operation two crank cheek together per time with two inserts are turned in a transversal direction; to reproduce and simulate the OP150 in laboratory a stroke of 12 mm and the use of triangular insert TCMX 11 03 08-WM 4315 from Sandvik Coromant as in the industrial process were considered (Figure 66b).

| (a) OP150 in the crankshaft | (b) Faced turning operation on bars |
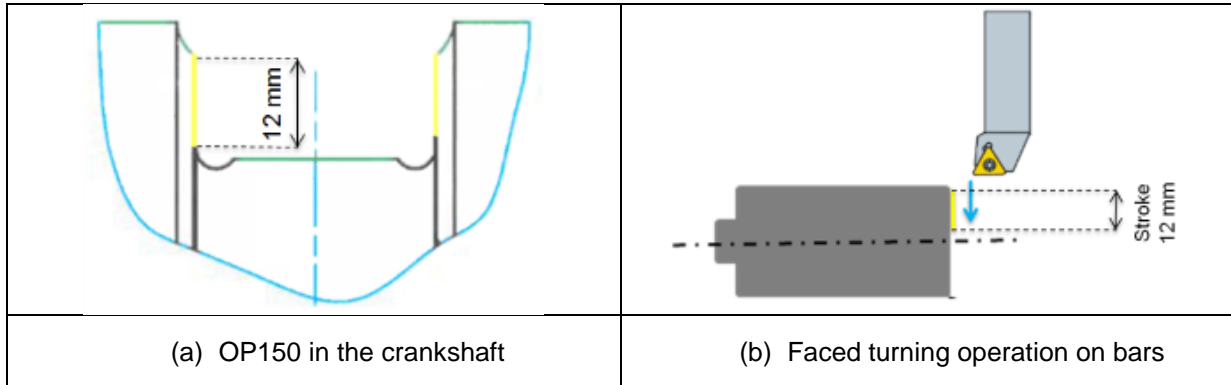
Figure 66: component turning operation studied

The adopted industrial cutting parameters were:
- Depth of cut, a_p = 0,25
- Cutting speed, V_c = 220m/min
- Feed, f = 0,25 mm/rev.

Important point: compared to turning tests carried out in the WP5, **the depth of cut (ap) chosen was significantly lower (finishing operation).** In WP5, ap was 1 or 2 mm. In the production line, the tool change frequency is made each 125 turned crankshaft (representing 4500 mm machined). The turning tests were performed using this limit.

After 4500 mm machined, the tool wear generated in the tools was difficult to estimate and seemed very low, difficult to quantify (Figure 67). Thus, the evolution of roughness was chosen as the parameter that distinguished the steel variants best (Figure 68). With this criterion, the microstructures of 45R and 45CG show the best machinability for turning. This result can be attributed to a suitable tool-chip contact (little or no adhesive phenomenon).
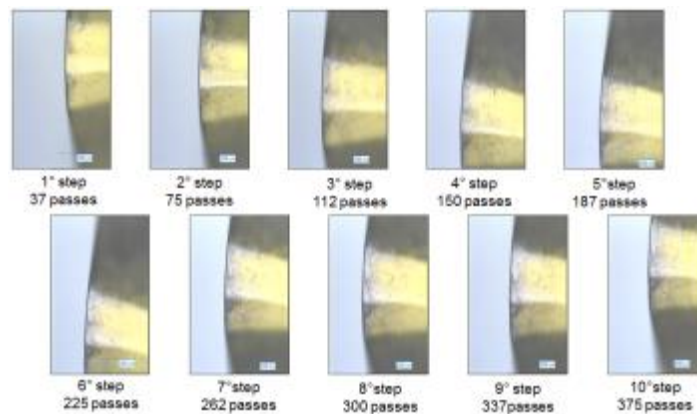
Figure 67: Flank of the insert behaviour
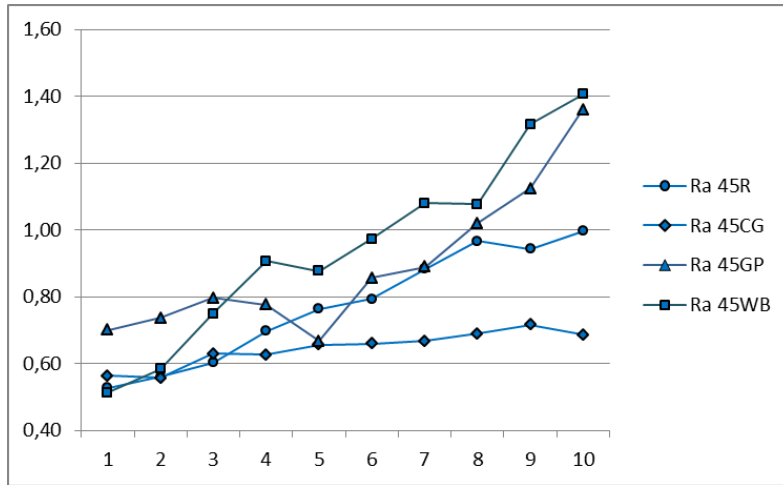
Figure 68: Roughness measurements on the billet turned surface

Following the cutting forces (Figure 69 below), the ranking is: **45R**=45WB=45GP>45CG.
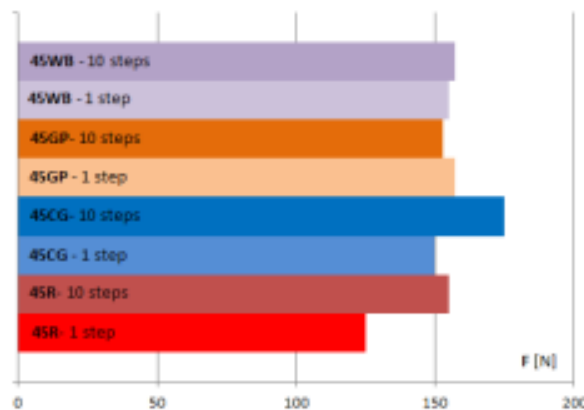
Figure 69 : turning cutting forces

For this specific finishing turning operation and the associated quality requirements, the microstructure 45R and 45CG was considered as good candidates.

Drilling tests

In the crankshaft the internal passages/ducts for the oil are manufactured through deep drilling (Figure 70a). The IMMAC bars were deep drilled in transversal direction (Figure 70b), as in crankshaft, using specific automotive operation cycle parameters and the cutting forces were recovered using Kistler rotating dynamometer.

| (a) OP70 deep drilling of internal passages/ducts for the oil | (b) Deep drilling operation on bars |
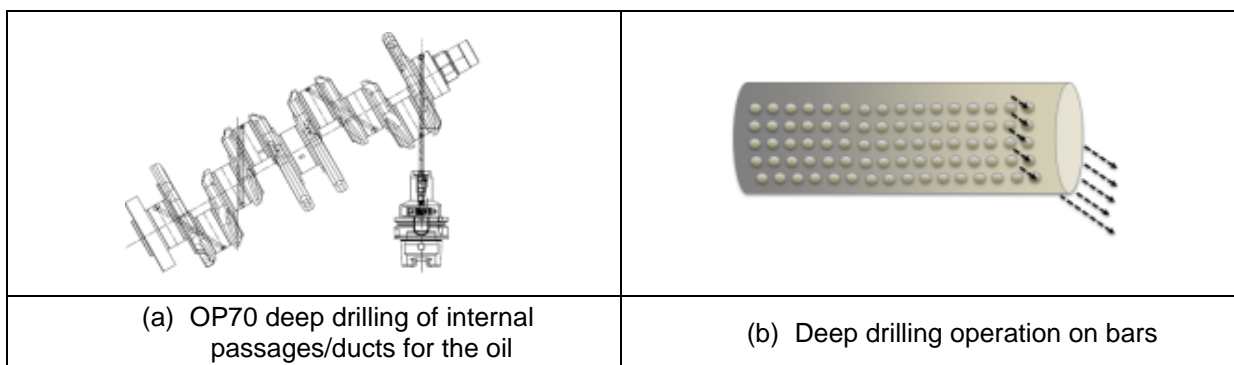
Figure 70 : component deep drilling operation studied

The tool was a deep carbide drill with coating. The cutting speed and the feed are similar to those used in the WP6 (Vc= 90 m/min and f = 0.2 mm/rev), but **the cutting length and the lubricating mode are different: MQL instead of emulsion.** To set up the test two different drill diameters were used, Ø5mm and Ø8mm, due to an average crossing length through the bar diameter.

Considering the drills with Ø8mm, feed force and torque acquisition during the tests were carried out (Figure 71). The feed force is a little higher for 45CG and similar for the other C45 variants (around 1050 – 1080 N). The torque of 45GP (globular perlite) is 10 to 15% higher compared to other variants (adhesive effect); same trend was observed in WP6 work (short drilling with emulsion).

(a) Forces Fz (N) for hole n.216	(b) Torque Mz (N.m) for hole n.216
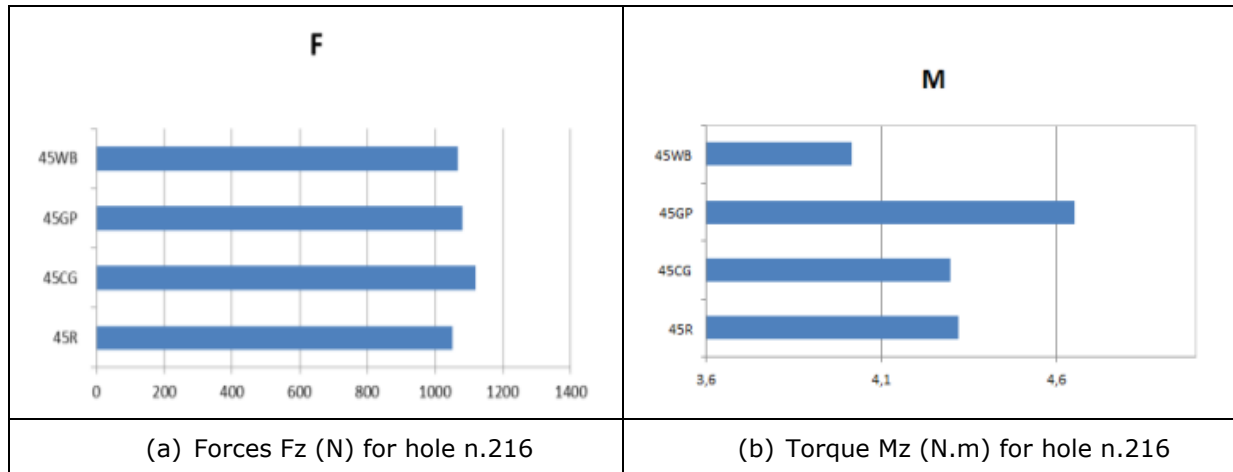
Figure 71: axial force and torque measurement

Considering the drills with Ø5mm, tool life tests were performed in order to analyse the flank wear of drill. It was decided to perform the test until a cutting life of 60 meters drilled (usual industrial cutting life for carbide drill). Following the flank wear behaviour during the test for each C45 variants, the results highlighted that:

- The microstructures of 45R and 45WB (with a good pearlite ratio lamellar pearlite/globulized pearlite) have the better and similar deep drilling performances with industrial conditions applied in FCA production line (around 57 m drilled).

- For 45GP, the test was stopped at 17 meter drilled due to the material gluing along the chip evacuation channels (adhesive mechanism observed also in WP6 machining tests).

- For 45CG (coarse perlite grain), **the tool life was very short** (< 2 m drilled) due probably to the significant abrasive effect generated by the higher percentage of lamellar perlite (80%). This effect was not noticeable on tool life with the WP6 drilling conditions (short drill – emulsion); only the roughness of hole was significantly different between 45R and 45CG. **The friction aspect between MQL and emulsion merits further study.**

Broaching tests

As the development of the 3D model in WP5 (Task 5.4) had to be stopped due to a lack of time and guaranty that it would bring relevant data, it was decided instead to use the Task 8.5 not only to perform the component oriented tests but to extend it to a wear test campaign to assess wear tendency.

This generated extra-time has been used to develop a second setup to ensure a higher stiffness. Broaching was thus performed vertically with the tool mounted into a specific holder clamped in the spindle whereas the material specimen was clamped vertically on the machine table. The new set-up can be seen in Figure 72.
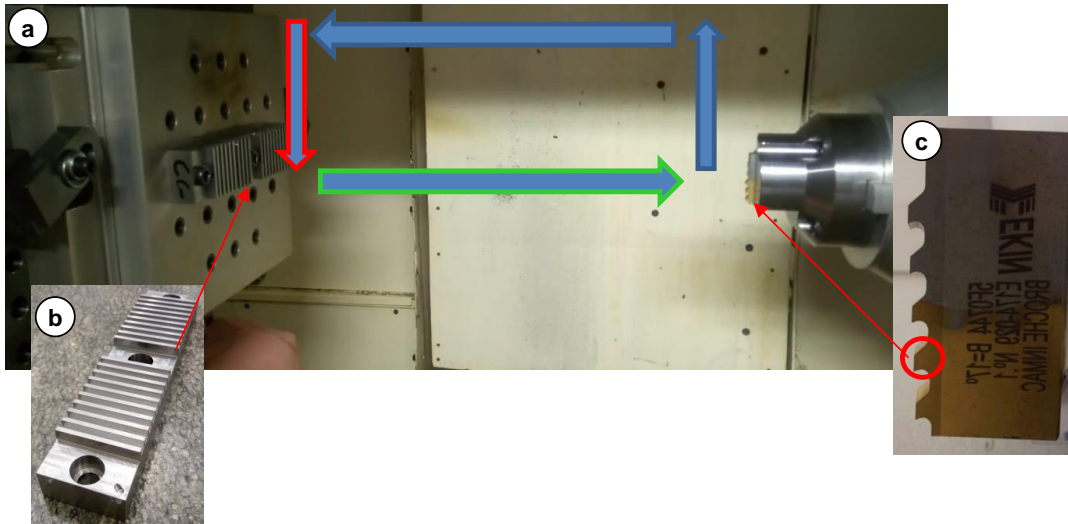
Figure 72: Improvement of the broaching set-up to perform the component oriented tests and wear campaign: a) overview of the set-up, b) material specimen and c) broaching tool.

The selected specimens were prepared to mimic the broaching of a steering rack and were pre-machined to limit the time necessary to cut it with a single tooth. Industrial tools, i.e. uncoated on the rake face and TiN coated on the flank face, were selected as the most relevant configuration. A single cutting condition of Vc = 20m/min and RPT = 40µm without lubrication was applied with a new broaching tool for each variant. Machining forces and surface roughness were periodically recorded.

A broached distance of 30 meters was selected as a reference, corresponding to 600 cuts. The Figure 73 presents the evolution of both machining forces versus the broached distance. The main trends appeared consistent with the previous campaigns, i.e. higher forces with the C45GP than C45R and C45CG, and minor variations were observed after the first 5 meters machined. The machining forces surprisingly dropped from the first cut to the next few ones when cutting the C45GP. After checking the 3D topography of the corresponding tool, it was shown that the cutting edge radius was not well prepared, especially with a burr on the flank face due to the grinding of the rake face after coating.

Extended tests were carried out with the C45CG which was expected to be the most abrasive variant compared to the other two. Tests were run until 75 meters but no specific variations were observed, neither in terms of forces (Figure 73) nor surface roughness (Figure 74). About the latter, broaching the CG variant led to better longitudinal roughness whereas the other two variants exhibited a very similar behaviour (Figure 74a). No specific degradation of the surface finish was observed, tending to indicate that tool wear did not occur.
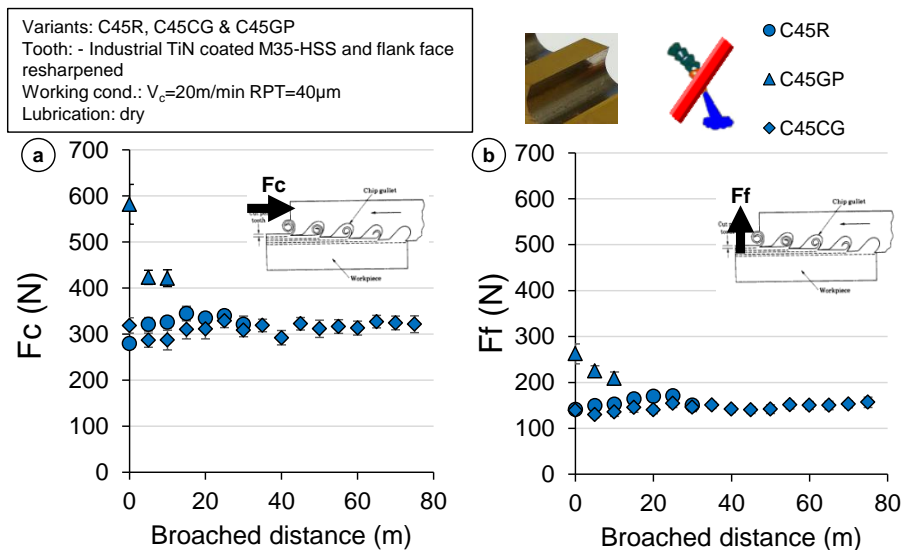
Figure 73 : Evolution of a) the main cutting force Fc and b) feed force Ff versus the broached distance for the three C45 variants.
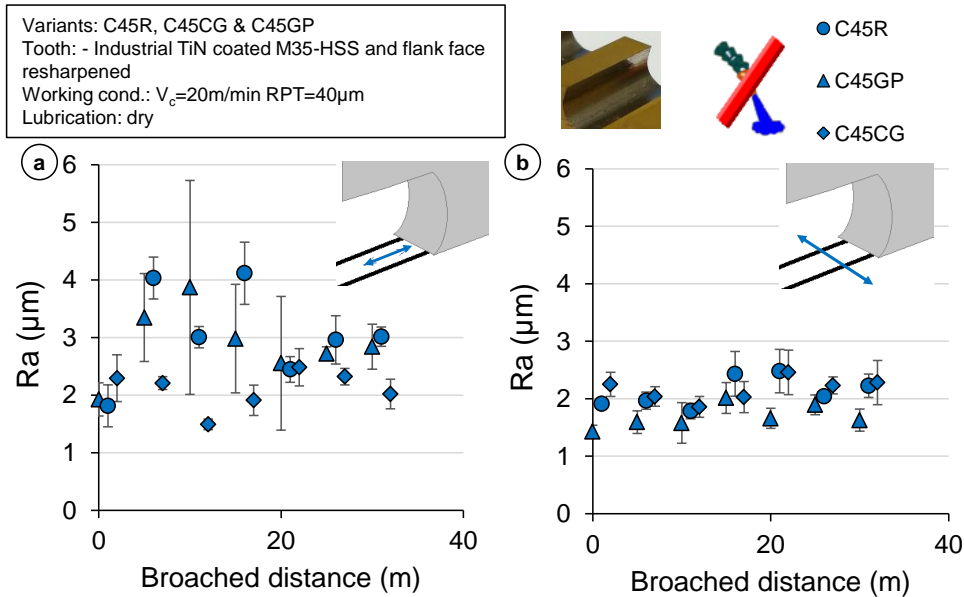
Figure 74 : Evolution of a) Ra roughness in the longitudinal and b) transversal direction versus the broached distance for the three C45 variants.

Each broaching tool was scanned with a confocal microscope (Alicona Infinite Focus) and flank face as well as cutting edge were analysed. No specific phenomena were reported depending on the variants unless a significantly more pronounced material transfer as far as the C45GP was concerned. Even after 75 meters machined, no clearly measurable flank wear could be extracted (Figure 75).
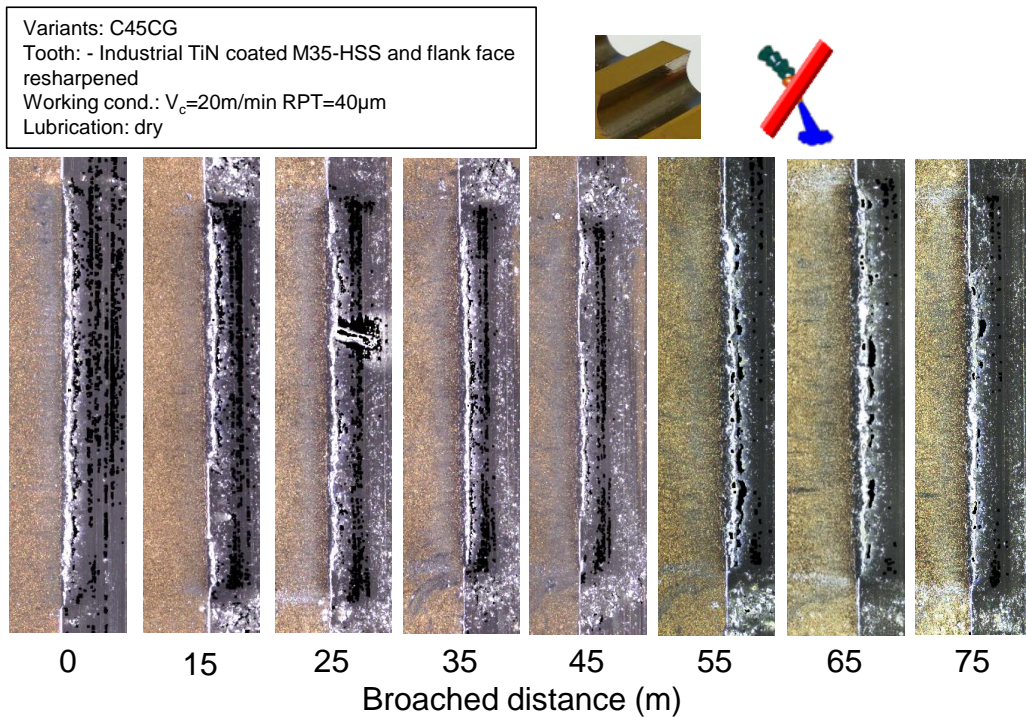
Figure 75 : Scans of the flank and rake face of the industrial broaching tools when cutting the C45CG variants at different broached distances.

This component oriented experimental campaign unfortunately reported similar wear behaviours for the 3 selected variants and only confirmed the previously observed trends on the machining forces.

Task 8.6 Validation of the numerical approach

Regarding the different C45 steel variants studied, the models developed in the project for the three cutting technologies clearly target the reference 45R as the microstructure involving the greater chance to obtain the better "global" machining performances. The Table 21 below recalls the classification of the C45 variants studied, the cutting conditions on which the models were built, and those applied for oriented component tests. We also underline the predominant tool-chip contact or tool-material contact mechanism concerned for each case.

Cutting technology	End-use application	Cutting conditions	Classifications	Contact mechanism (main behaviour involved)
High speed Dry Turning	Crankshatf	ap : 1 to 2 mm (10m machined)	Simulation : 45GP > **45R** > 45CG	Abrasion (Tribology)
		ap : 0.25 mm (OP150) (4.5m machined)	Industrial tests : 45CG > **45R** > 45GP (but incomplete results regard with tool wear)	Abrasion-adhesion (rheology and tribology)
Medium speed Lubricated Drilling		Short drilling Emulsion 10% 30m drilled	Simulation : **45R** > 45CG >> 45GP	Abrasion-adhesion (rheology and tribology)
		Deep drilling MQL (OP70) Target: 70m drilled	Industrial tests : **45R** > 45GP >>> 45CG	
Low speed Dry Broaching	Steering rack	V : 2 m/min RPT : 40 µm (forces, chip thickness)	Simulation : 45CG>**45R**>>45GP	Adhesion (rheology++ and tribology)
		V : 20 m/min RPT : 40 µm 75m machined	Industrial tests : Same trends the simulation regarding forces. Incomplete results regarding wear.	Abrasion-adhesion (rheology and tribology)

Table 21 : Comparison of C45 steel variants classification (simulation versus industrial tests)

The component oriented turning tests (OP150) shown that the globular microstructure (45GP) demonstrates the worst results, contrary to his positioning with simulation. This result can be explained by the criteria used for classifying the C45 variants: the roughness after 4,5 meters machined, with tools slightly worn (due to very low depth of cut). The current turning model has integrated data acquired through more severe operating conditions and without any link with roughness of the steel variant machined. To validate this model, the cutting life of the tools should be extended.

Nevertheless, within the context of the **choice of one optimized microstructure for crankshaft application** (turning and deep drilling operation are concerned), the component oriented tests have shown that deep drilling tools are highly sensitive to microstructure variations. Globular pearlite and more critically coarse pearlite grain present important risks of worsening performance of the drill. The drilling model proposed in WP6 reflects well this risk, and for this end-use application, is predominant than turning model for the definition of the most appropriate ferrite-pearlite microstructure: the homogeneous FP microstructure here represented by variant 45R.

We are unfortunately not able to validate the classification propose by the broaching model. Additional tests are needed with higher cutting speed.

2.3 Conclusions

For many years, one of the solutions to compensate the potential negative impact of FP microstructure is the addition of sulfur content or metallic inclusion like lead. Nowadays, it seems to be no longer the norm, for environmental and health reasons, and because automotive industries need higher fatigue properties. **Thus, for the future, the quality of microstructure becomes dominant compared to inclusion.** This fact was confirmed in the RFCS PROMACH project, few years ago (2011), in which were involved the same partners as those participating in IMMAC (except ENISE and University of Lorraine); it was demonstrated that to reach acceptable machinability performances in different cutting technologies, different percentage of sulfur is needed for a ferrite-pearlite steel.

Knowing that is not possible now to obtain different sulfur density in a same part, the question the partners proposed to assess in this project is **"how could the microstructure fit well a given machining process?"**.

During more than three years of work, IMMAC project aimed to answer this question by improving the prediction of the machinability performances of FP steel using numerical cutting models in which the main input data required for computation are the ferrite-pearlite microstructure parameters. For that, a better understanding of thermal stress-strain behaviors (rheology), contact mechanisms (tribology) and thermal properties of FP microstructures and material cutting tool have been achieved.

Concerning rheology, new models have been developed in this project based on work of Bouaziz and Allain. Following a large amount of compression tests, covering a wide range of strain rates and temperatures, we have incorporated in the initial models further mechanisms and improvements:
- An extended empirical description of work-hardening in both phases to cover the interesting range of strains
- An empirical hardening contribution of dynamic strain aging (DSA) to reproduce the flow stress peaks observed in certain temperature/strain rate ranges
- The behavior of globular pearlite as a new phase in the composite microstructure.

We also extended the validity of the previous models to other working conditions, for instance:
- Physically-based description of the strain rate sensitivity which has been applied to pearlite and to strain rates higher than 1000 s^{-1}.
- Microstructure-based models for lamellar components at high temperatures.

The rheological model developed shows good results and is successful to capture the main tendencies of the experimental data taking into account the microstructure of the steel grades.

Nevertheless, the influence of the strain rate on the flow stress could potentially be improved. And to be able to accurately describe the influence of temperature, softening should be taken into account including a deeper analysis of the microstructure during and after compression tests.

With regard to tribological work, the major achievements are:
- An extensive experimental campaign with more than 500 experiments covering a wide range of contact conditions;
- Two friction models and one heat partition (between tool and chip) model extended the capability of the proposed approach including the influence of microstructural features of ferritic-pearlitic steel.

For the three cutting technologies studied (turning, drilling and broaching), the experimental classification of the machinability was done by means of a weighted point evaluation method. Based on the machinability classification and the metallurgical characterizations, a qualitative evaluation of the influence of the microstructure parameters (pearlite fraction, pearlitic grain size, pearlite interlamellar spacing and globular pearlite volume fraction) on the machinability could be deduced.

The main parameters of FP microstructure driving the machinability performances were identified for each cutting operation:
- Turning: hardness (linked to pearlite volume fraction, globular pearlite volume fraction and pearlite grain size)
- Drilling: pearlite volume fraction, pearlite grain size, pearlite interlamellar spacing and globular pearlite volume fraction.
- Broaching: ferrite volume fraction and the globular pearlite volume fraction.

Related to these FP parameters, the main wear mechanisms were identified for each cutting operation:
- Turning : abrasion
- Drilling : Abrasion and adhesion
- Broaching : adhesion

Taking this into account, a 2D FE model was developed for turning and broaching, and a 3D FE computation model was developed for twist drilling, in which:
- Inputs are :
  - The FP parameters of steel variants defined in WP1
  - The thermal properties of steel variants defined in WP1
  - The work material law developed in WP2
  - The friction laws developed in WP3

- Outputs (or evaluation criteria) are :
  - Turning: tool max temperature, contact pressure, shear stress, sliding velocity
  - Drilling: cutting forces, chip compression ratio, max temperature on the cutting edge, max pression on the rake face
  - Broaching: cutting forces, chip thickness, contact length, subsurface plastic déformation

For each cutting technology studied, these output data were used to compute the machinability in order to define a qualitative "machinability index". Compared with the industrial component oriented machining tests carried out by the end-user partner (FCA), the FE simulations predicted adequately the machinability ranking of the investigated FP steel variants. Moreover, an interesting empirical formulation, only for drilling, has been developed based on the microstructure parameters.

These numerical methods can be used to design an optimized FP steel microstructure for a dedicated industrial component.

For future works, the tribological effect of lubricant processes (Minimum quantity lubricant, emulsion) remains area of improvement, as well as the numerical modelling of the tribological behaviour of steels leading to a predominant contribution of adhesion, seen in the work focused on broaching, and on drilling.

2.4 Exploitation and impact of the research results

The results obtained in the IMMAC project are in line with the main orientations of the 2013 Strategic Research Agenda edited by the **European Steel Technology Platform** as the development of tools for the **Factory of the Future** has been explicitly considered as a strategic R&D theme.

The simulation chain developed in the project belongs to the wide family of ICME tools. **Integrated computational materials engineering (ICME)** is the integration of materials information, captured in computational tools, with engineering product performance analysis and manufacturing-process simulation according to the National Research Council of U.S. [41]. ICME models have been developed to manage scientific issues over the past 20 years in the academic world but have been rarely put into practice to address industrial issues. This situation is considered in innovation science as the "Valley of Death". Many reasons have recently been identified by a European expert group (ICMEg) [42]. IMMAC project is the proof that it is now possible to fulfill industrial needs with such integrated and seamless models between material and process.

2.4.1 Technical and economic potential for the use of the results

From the model developed in WP2 (rheology), stress vs. strain curves of each grade and variant were taken as input for the behavior law of the material in the cutting finite elements simulations. This allows considering the impact of the microstructure (translated in the behavior) on the results of the simulation and comparing it with the experimental machining tests. A simple change in the microstructural behavior gives a new behavior law whose impact can be visualized through the simulation results.

These microstructure-based behavior laws developed during the project for machining applications show a very high potential for the micromechanical simulations of other manufacturing process with similar extreme loading conditions. This is the case for instance of cold-rolling (high strain rate but limited temperature), or SPD (Severe Plastic Deformation) process as ECAE (Equal Channel Angular Extrusion) or HPT (High Pressure Torsion) (large strain, high strain rate).

From a scientific point of view, the project has permitted to deepen our knowledge about the behavior of ferrite-pearlite steels. The main microstructure parameters controlling the final properties of the steels have been identified and their respective effects well quantified thanks to our calibration procedure. The model for ferrite-pearlite microstructure will also be surely a basis for development of models for more complex microstructures, such bainitic or tempered martensitic microstructures, which are now commonly used in the automotive industry and driveline parts.

From the tribological point of view, the project provided significantly valuable data and models that can be implemented in any numerical simulation involving ferritic-pearlitic steels. Taking into account microstructural parameters and morphologies is fundamental in order to introduce more physics in manufacturing process simulations. From a more practical point of view, the tribological tests improved the understanding regarding the effect of these microstructures on their tribological properties, which had not really been investigated until now. This is thus an important finding for the scientific community that will be certainly seen as a reference study once published. The obtained data will be used as references as soon as FP steels will be involved considering the considerable body of work performed in IMMAC.

For broaching studies, 2D simulations with multiple cutting-edges should be developed to fully take into account the physics of the industrial process and the previously modified material that will be cut by the following edge.

Another important aspect in this specific cutting technology, or for other finishing operation, is to machine a material with such small depth of cut (< 0.05 mm). This can induce drastically different cutting mechanisms compared to those encountered at a macroscopic one. The material removal occurs at the scale of the materials grain size (appendix 7.5.4). Hence, under a certain scale, the assumption of a homogeneous and isotropic material can be definitely questioned as well as the effect of the size and distribution of the microstructure. These scale effects can significantly affect the simulation performance compared to a macroscopic cutting operation such as turning or drilling.

Taking this into account, several questions need to be answered:
- Is the Finite Element Method appropriate to model broaching of heterogeneous materials?
- Can the constitutive model developed in WP2, as well as the tribological models from WP3 be used to model the cutting behaviour at such a small local scale?
- Would it be more relevant to characterise the properties of each phase and develop broaching simulations of heterogeneous materials?

From steelmakers and end-users point of view the development of a numerical model which allows to predict the steel machinability is of great interest since very time-consuming machining tests could be avoided.

Additionally, as mentioned above, steelmakers and end-users define even now larger tolerances on requirements specification on FP steels, which cause variability on microstructure morphology not always perceptible with common metallurgical characterizations. It is probably linked to the fact that the methods to identify the FP parameters (grain size, pearlite globalization, banding level…) are not standardized. The interpretations are made by comparison with standard images. This qualitative approach can be considered subjective. The numerical methodology proposed in IMMAC could be used by end-users and steelmakers as a basis to renew their manufacturing methods define the associated cutting conditions and specify in a clearer and more robust way the material "specifications/requirements" for each functional component. In particular, for the automotive manufacturing process it would help the prediction about the need of material stock at the forging step, eventually minimizing it, the cutting tool life, optimizing the need of inserts and others and their purchasing, finally favouring the components cadence thus their productivity.

Finally, education in metallurgy and in machining will take advantage of the results of this project as professors and assistant-professor from renowned engineering schools and universities have been involved in the project. The obtained results will be presented in conferences, but as well be employed in training courses and Masters and PHD programs in the University. The project has already contributed directly to the high-level education of two PhD Students, who has gained direct and valuable expertise in machining for the European industry.

2.4.2 Publications / conference presentations resulting from the project

Experimentelle und simulative Untersuchungen zur Zerspanbarkeit von ferritisch-perlitischen Stählen eim Bohren

Fritz Klocke, Mustapha Abouridouane, Benjamin Döbbeler

Abstract
This book contribution is dedicated to the experimental evaluation and numerical modeling of machinability characteristics in the drilling of ferritic-perlitic steels. The use and validation of innovative ICME tools enable a realistic virtual prediction and real presetting of the machinability of ferritic-perlitic steels based on their microstructure.

Characterisation and modelling of the machinability of ferritic-pearlitic steels in drilling operations

Mustapha Abouridouane, Fritz Klocke, Benjamin Döbbeler
Laboratory for Machine Tools and Production Engineering (WZL),
Chair of Manufacturing Technology, RWTH Aachen University, Steinbachstrasse 19, Aachen 52074, Germany

Abstract
The machinability of work materials strongly affects the chip formation mechanics, tool wear behaviour and the process performance. Therefore, the characterisation and modelling of the machinability are a very important issues. This paper deals with experimental and simulative investigations on the machinability of ferritic-pearlitic steels with different microstructures by twist drilling. The machinability of the investigated
steels is evaluated and classified by means of the weighted point evaluation method. To predict four aspects of the machinability (thermo-mechanical load, feed force, cutting torque, and chip form), a 3D FE computation model is developed and successfully validated.

Effects of Microstructure on the Dynamic Strain Aging of Pearlitic Steels at High Strain Rates

A. Mardoukhi[1], J. Rämö[1], T. Vuoristo[2], A. Roth[3], M. Hokka[1], V.-T. Kuokkala[1]
[1]Tampere University of Technology, Laboratory of Materials Science, FI-33720 Tampere, Finland
[2]Swerea KIMAB, Isafjordsgatan 28A, SE- 164 40 Kista, Sweden
[3]ASCO Industries CREAS, BP 70045, 57301 Hagondance Cedex, France

Abstract
Mechanical properties of steels are strongly affected by strain rate, temperature, and microstructure of the material. The flow stress of steels is very sensitive to strain rate and temperature, as the response of the material depends on the thermally activated dislocation motion and dislocation drag. Typically, the strength of the material decreases when temperature is increased, but the strength of the material can also increase at elevated temperatures due to dynamic strain aging. This is caused by the diffusion of small solute atoms into the dislocation cores preventing the dislocations from moving freely. The dynamic strain aging requires enough mobile (substitutional) solute atoms and a high enough temperature for their fast diffusional movement. In pearlitic steels the dynamic strain aging is typically caused by carbon, nitrogen, and possibly some other small solute atoms. Therefore, the thermomechanical treatments affect strongly how strong the dynamic strain aging effect is and at what temperature and strain rate regions the maximum effect is observed. In this work, we present results of the high temperature dynamic compression tests carried out for three different pearlitic steels, 16MnCr5, C60, and C70, that were heat treated to produce different microstructure variants of these standard alloys. The microstructures were analyzed using electron microscopy, and the materials were tested with the Split Hopkinson Pressure Bar device at three different strain rates at temperatures ranging from room temperature up to 680 °C to study the effect of the heat treatments and the resulting microstructure on the dynamic behavior of the steels and the dynamic strain aging effect. The overall characterization of the dynamic behavior of the materials is presented in the paper, and detailed attention is paid to the effects of the microstructural features of the steels on the dynamic strain aging observed at the tested strain rates and temperatures.

The mechanics of cutting: In-situ measurement and modelling

15th CIRP Conference on Modelling of Machining Operations
Mustapha Abouridouane, Fritz Klocke, Dieter Lung, Dražen Veselovac
Laboratory for Machine Tools and Production Engineering (WZL)

Abstract
This work presents a new constitutive modelling approach to describe the operating friction mechanisms in material cutting. The modelling approach is based on an advanced experimental set-up with high speed filming and thermography of the orthogonal cutting process as well as the Merchant's circle force diagram. Finite element cutting simulations on carbon steel AISI 1045 with different uncut chip thicknesses were conducted to validate the developed friction modelling approach. A realistic analytical and numerical prediction of chip formation, local thermo-mechanical load and cutting force could be achieved.

Experimentelle und simulative Untersuchungen zur Zerspanbarkeit von ferritisch-perlitischen Stählen beim Bohren

Fritz Klocke, Mustapha Abouridouane, Benjamin Döbbeler

Abstract
This book contribution is dedicated to the experimental evaluation and numerical modeling of machinability characteristics in the drilling of ferritic-perlitic steels. The use and validation of innovative ICME tools enable a realistic virtual prediction and real presetting of the machinability of ferritic-perlitic steels based on their microstructure.

Influence of the ferritic-pearlitic steel microstructure on surface roughness in broaching of automotive steels

Abstract

The aim of this work is to characterize the effect of microstructural parameters on surface roughness in dry broaching with a special emphasis on the ferrite-pearlite (FP) ratio. An experimental approach combining cutting and tribological tests has been developed on three grades 27MnCr5, C45, C60 covering a wide range of FP ratio. Fundamental broaching tests have been performed with a single tooth to analyse the resulting surface quality with uncoated M35 HSS tools. A specially designed open tribometer has been used to characterize the friction coefficient at the tool–chip–workpiece interface under appropriate conditions. Specific phenomena have been observed depending on the FP ratio and an interesting correlation with the tribological tests has been found. This clearly shows that friction has an important contribution in broaching and that phase distribution has to be highly considered when cutting a FP steel at a microscopic scale. This work also provides quantitative data of the friction coefficient depending on the sliding velocity and FP content which can be implemented in any analytical or numerical model of a broaching operation.

Influence of Microstructure on Chip Formation when Broaching Ferritic-Pearlitic Steels

Abstract

Broaching is a specific process characterized by relatively low cutting speeds and uncut chip thicknesses. The latter is in the range of 0.1 to 0.25 mm in the roughing section of the tool but can decrease down to 0.0015 mm in the finishing one. This induces drastically different cutting behaviours compared to macro-scale processes such as turning. The question of the scale effects in such conditions is thus clearly raising and especially the size and distribution of the microstructure. This paper proposes an investigation to assess the importance of the material heterogeneities on chip formation when broaching ferritic-pearlitic steels.

Effet de la microstructure d'un acier ferrito-perlitique sur son comportement tribologique sous conditions extremes

Introduction

Les aciers ferrito-perlitiques peuvent être vus comme des matériaux multi-phasés, constitués d'îlots d'une phase dure (perlite) englobés dans une matrice ferritique. D'une manière générale, augmenter la fraction volumique de perlite tend à augmenter la résistance du matériau tandis que celle ferritique tend à améliorer la ductilité. Maîtriser cette combinaison peut notamment permettre d'atteindre des résistances mécaniques et des taux d'écrouissage plus élevés que pour d'autres aciers présentant des limites élastiques similaires. Ceci se présente comme une voix intéressante pour développer des nuances avec de meilleures propriétés mécaniques mais aussi de meilleures aptitudes à la mise en forme. En revanche, ces combinaisons peuvent fortement affecter leurs propriétés tribologiques qui ne peuvent être négligées dans certaines applications. De nombreuses études se sont intéressées à ces microstructures principalement dans le contexte du contact roue-rail [2-4] mais peu ont mis en évidence la contribution des paramètres propres à la microstructure (ratio ferrite-perlite, taille de grains…) sur le frottement ou leurs tendances à l'adhésion et à l'usure. L'objectif est donc ici de mener une étude fondamentale visant à mettre en évidence l'influence des propriétés de ces structures sur leur comportement tribologique sous de fortes sollicitations de contact (pression de contact > 1 GPa et vitesse de glissement jusqu'à 5 m/s).

Experimental study of machinability in broaching of ferritic-pearlitic steels
Arrieta, C. Courbon, F. Cabanettes, P.-J. Arrazola, J. Rech (2016)
Proceedings of the 13th High Speed Machining Conference (HSM 2016), October 4-5, Metz, France.

Abstract
Case-hardening and carbon steels with Ferrite-Pearlite (FP) microstructure are used in many automotive components especially transmission shafts, gear wheels, pinions or wheel hubs. They appear as a tough material that features a hard and wear-resistant outer skin and an impact-resistant core. Internal cutting operations are usually performed in the latter such as broaching. Even if steels with a FP structure are among the most common materials, they are not at the very least the easiest materials to machine. Their machining performance in low cutting speed processes appears to be highly dependent on metallurgical parameters such as the FP ratio.
The aim of this work is thus to characterize the machinability of such steels in dry broaching with a special emphasis on the FP ratio. An experimental approach combining cutting and tribological tests has been developed on three grades 27MnCr5, C45, C60 covering a wide range of FP ratio. Fundamental broaching tests have been performed with a single tooth to analyse the cutting behaviour, chip formation mechanisms and resulting surface roughness with uncoated M35 HSS tools. A specially designed open tribometer has been used to characterize the friction coefficient at the tool–chip–workpiece interface under appropriate conditions.
This work also provides quantitative data of the friction coefficient depending on the sliding velocity which can be implemented in any analytical or numerical model of a broaching operation.

Tool Wear Prediction in Machining Process Using a Microstructure-Based Finite Element Model.
Sáez- de-Buruaga, M., Poveda, I., & Arrazola, P. J. (2015)
Key Engineering Materials.

Abstract
The microstructure of materials has a significant influence on tool life, however most of the research in modelling to date considers the material as homogeneous. This research aims to develop a microstructure-based Finite Element Model in order to qualitatively analyze the influence of the scale of the microstructure on the generated tool wear. In particular, this paper is focused on the orthogonal cutting process of a ferrite-pearlite dual-phase steel using uncoated carbide tools. Based on individual mechanical properties of these phases, a 3D coupled Eulerian Lagrangian heterogeneous model was developed. An empirical tool wear rate prediction model was implemented by a user subroutine in both models (heterogeneous and homogeneous) to predict wear and wear rate values. A comparison between the microstructure-base model (heterogeneous) and the homogeneous model considering wear and wear rate values was made. The results demonstrate the validity of microstructure-based Finite Element Model for an improved prediction of the wear phenomena.

2.4.3 Other aspects concerning the dissemination of results

Organization of a Workshop

The final Workshop required a lot of time in order to prepare the event through different steps. First, the selection of the interested parties between **Academia, Industrial companies and End Users.** A flyer with the explanation of the project aim and objectives and the workshop agenda was sent during the invitation phase.
The Workshop took place at Centro Ricerche FCA on November 29th, 2017. During the event, the IMMAC project was introduced by the coordinator, and then each WP leader explained the work done during the three years of the project.
For each WP also the posters were prepared in order to give visibility to the specific activities. At the end of the event, there was space for comments and speeches from the different guests as tool supplier (Walter, Sandvik, Guhring), Academia (Ecole Nationale Supérieure des Mines de Nancy), other industries (CIE automotive forging and ZANARDI steel maker) and FCA automotive end user.
After the Workshop a questionnaire was sent by email to each participant due to their expert and specialized support in the technical/scientific field of material, process/treatment, machining and industry: the survey aim was done to understand stakeholder technical involvement and satisfaction and to effectively gauge and give rise to a constructive reflection on the work done in IMMAC during the project period.
The questions done collected specific resonances in order to help the Consortium to solicit locate and define new or different technical point of view.

The questions:
- Congruence between workshop contents and dissemination objectives
- Correspondence between workshop contents and initial expectations
- Correspondence between workshop contents and professional interests
- Applicability of the dealt topics in relation with one's work aim
- How do you evaluate your involvement degree in the discussed topics?

obtained the following ranking (Figure 76) :

1 Not satisfactory	2 Partly satisfactory	3 Satisfactory	4 Very satisfactory

academia, tool maker, Industry

Figure 76: Survay ranking

Some comments regarded the **organization**: "Very interesting Workshop, well organized and managed, the tight rhythm is stimulating''.

Other, about the technical point of view of the **material**: "Could be interesting machine for a part, with optimized microstructure, and have an extensive machining test in order to have as much as possible feedback in terms of tool life, quality machining. Actually and in the next future automotive development, aluminium take a big part of the components. In the aluminium casting production, like a die casting, often happen to find for a ferritic matrix which cause for several breakage in the tool. Further, in this aluminium, there're several difference linked to the temperature''.

Other, about the **machinability**: "Machining processes often don't consider enough how all the material characteristics influence the performance (wear of the tools, residual stress and quality on the surface of the component, etc…). I think that all partners have constantly to keep in touch sharing new experience and way to work. The goal could be staying closed to the component to manufacture it as better as we can, all together: material maker, machine tool maker and tool maker."

And finally some comments from the **forging point of view**: "Could be also interesting to understand effect of different row material condition (cast or forged component). It's possible to simulate the impact of a percentage of bainite in a ferrite-perlite microstructure (lived experience on forged crankshaft) ?''

All the consideration, remarks, doubts were much stimulating because they underlined other aspects not developed in this project.

During the workshop have put in dialogue the different industrial experiences, from the basic research to the application through the material design, the forging and the production experience, encouraged new possibilities about model simulation development for other materials and product machinability improvement for powertrain components in new studies and databases.

The IMMAC approach impressioned thinking to optimize cutting tools and regarding the classification of steel variants.

Figure 77: Final Workshop participants

3. List of figures

4. List of tables

5. List of acronyms and abbreviations

2D	2 dimension
3D	3 dimension
ap	Depth of cut
ALE	Arbitrian Lagrangian Eulerian
ASTM	Method to evaluate grain size
BCC	Body centered cubic
CAD	Computer-Aided Design
CEL	Coupled Eulerian Lagangian
CP	Cutting pressure
CS	Contact shear stress
CG	Coarse Grain
CPU	Central processing Unit
COF	Coefficient of Friction
CRF	Centro Recerche FCA
CVD	Chemical Vapor Deposition
DIC	Digital Image Correlation
DSA	Dynamic Strain Aging
D1 and D2	Deliverable N°1 and Deliverable N°2
EBSD	Electron backscatter diffraction
EDM	Electrical Discharge Machining
EDS	Energy Dispersive Spectroscopy
EDX	Energy Dispersive X-ray Spectroscopy
EC	Evaluation criteria
f	Feed
Ff	Feed force
Fc	Cutting force
FCC	Face centered cubic
FE	Finite Element
FEM	Finite Element Modelling
FP	Ferrite Pearlite
GND	Geometrically necessary dislocation
GP	Globular Pearlite
GS	Grain Size
HB	Brinell Hardness
HW	Non coated cemented carbide
HSS	High Speed Steel
ICME	Integrated computational materials engineering
IR	InfraRed
LP	Lamellar pearlite
LOM	Light optical microscope
MQL	Minimum Quantity Lubricant
MGEP	University of Mondragon
P GS	Pearlite grain size
PSZ	Primary shear zone
R	Reference
Ra	Roughness criteria
RPT	Rise per tooth
SEM	Sanning Electron Microscopy
SHPB	Split Hopkinson Pressure Bar
STL	STereoLithography
UC	Uncoated
UL	Université de Lorraine
UV	Utility value
VB	Flank wear
Vc	Cutting speed
WB	More bands
WC	Tungsten Carbide
WC-Co	Tungstene carbide with cobalt
WP	Work Package

6. Full list of references

[1] F. Klocke. Manufacturing Processes 1: Cutting. Springer; 1st Edition, 2011.

[2] D.V. Doane. Softening high hardenability steels for machining and cold forming. Journal of Heat Treating, 6:97 – 109, 1988.

[3] A. Ebrahimi and M.M. Moshksar. Evaluation of machinability in turning of microalloyed and quenched-tempered steels: Tool wear, statistical analysis, chip morphology. Journal of Materials Processing Technology, 209:910 – 921, 2009.

[4] T. Akasawa, I. Fukuda, K. Nakamura, and T. Tanaka. Effect of microstructure and hardness on the machinability of medium-carbon chrome-molybdenum steel. Journal of Materials Processing Technology, 153 - 154:48 – 53, 2004.

[5] Y. Ozcatalbas and F. Ercan. The effects of heat treatment on the machinability of mild steels. Journal of Materials Processing Technology, 136:227 – 238, 2003

[6] F. Klocke, K. Gerschwiler, and Mustapha Abouridouane. Size effects of micro drilling in steel. Production Engineering, 3:69 – 72, 2009.

[7] A. Mian, N. Driver, and P. Mativenga. A comparative study of material phase effects on micro-machinability of multiphase materials. The International Journal of Advanced Manufacturing Technology, 50:163 – 174, 2010.

[8] I. Chuzhoy, R.E. Devor, S.G. Kapoor, and D.J. Bammann. Microstructure-level modelling of ductile iron machining. Journal of manufacturing science and engineering, 124:162–170, 2002.

[9] M. Nygards and P. Gudmundson. Three-dimensional periodic voronoi grain models and micromechanical fe-simulations of a two-phase steel. Computational Materials Science, 24:513 – 519, 2002.

[10] M. Nygards and P. Gudmundson. Micromechanical modelling of ferritic/pearlitic steels. Materials Science and Engineering: A, 325:435 – 443, 2002.

[11] S. Park, S. G. Kapoor, and R. E. DeVor. Microstructure-level model for the prediction of tool failure in wc-co cutting tool materials. Journal of Manufacturing Science and Engineering, 128(3):739–748, 2006.

[12] L. Chuzhoy, R. E. DeVor, and S. G. Kapoor. Machining simulation of ductile iron and its constituents, part 2: Numerical simulation and experimental validation of machining. Journal of Manufacturing Science and Engineering, 125(2):192 – 201, 2003.

[13] A. Simoneau, E. Ng, and M.A. Elbestawi. The effect of microstructure on chip formation and surface defects in microscale, mesoscale, and macroscale cutting of steel. CIRP Annals - Manufacturing Technology, 55:97 – 102, 2006.

[14] A. Simoneau, E. Ng, and M.A. Elbestawi. Modelling the effects of microstructure in metal cutting. International Journal of Machine Tools & Manufacture, 47:368 – 375, 2007.

[15] M. Abouridouane, F. Klocke, D. Lung, and O. Adams. A new 3d multiphase fe model for micro cutting ferritic-pearlitic carbon steels. CIRP Annals - Manufacturing Technology, 61(0):71 – 74, 2012.

[16] S. Allain and O. Bouaziz. Microstructure based modelling for the mechanical behavior of ferrite-pearlite steels suitable to capture isotropic and kinematic hardening. Materials Science and Engineering: A, 496:329 – 336, 2008.

[17] Courbon C., PhD thesis (2011)

[18] Niechajowicz A., Tobota A., J. Mat. Proc Tech 106 (2000) 123-130

[19] Nemat-Nasser S., Guo W-G., , Mechanics of Materials, 35 (2003) 1023-1047

[20] Bouaziz O., Lecorre C., Mat. Sci. Forum 426–432 (2003) 1399-1404

[21] Allain S., Bouaziz O., Lemoine X., Revue de Métallurgie 106 (2009) 80-89

[22] Uenishi A., Teodosiu C., constitutive modeling of the high strain rate behaviour of interstitial-free steel – International Journal of Plasticity 20 (2004) 915-936

[23] Rauch E.F., HDR report (1993)

[24] Bui-Van A., Allain S., Lemoine X., Bouaziz O., Int J Mater Form 2 (2009) 527-530

[25] Ghosh G., Olson G.B., Acta Mater. 50 (2002) 2655-2675

[26] Wang J., Guo W-G., Gao X., Su J., IJP 65 (2015) 85-107

[27] Allain S., PhD report (2004)

[28]   Estrin Y., Unified Constitutive Laws of Plastic Deformation, Academic Press, San Diego (1996)

[29]   Kocks U.F., Mecking H., Acta Met. 29 (1981) 1865-1875

[30]   Bergström Y., Mat.Sci. Eng. A 5 (1969) 193-200

[31]   Bouaziz O., Aouafi A., Allain S., Mat. Sci. Forum 584-586 (2008) 605-609

[32]   Allain S., Bouaziz O.,Mater. Sci. Eng. A 496 (2008) 329-336

[33]   Hall E.O., Proc. Phys. Soc. Sect. B64 (1951) 747–753

[34]   Petch N.J., J. Iron Steel Inst. 174 (1953) 25–28

[35]   Dollar, M.; Bernstein, I.M.; Thompson, A.W., Acta Metall. 36 (1988) 311–320

[36]   Yahyoui H., Sidhom H., Braham C., Baczmanski A., Mat. and Des., 55 (2014) 888-897

[37]   Allain S., HDR report (2012)

[38]   Soler D, Childs TH, and Arrazola PJ (2015). A note on interpreting tool temperature measurements from thermography. Machining Science and Technology 19 (1):174_181.

[39]   Merchant ME (1944). Basic mechanics of the metal cutting process. Journal of Applied Mechanics 11 (A):168_175.

[40]   Usui E, Shirakashi T, Kitagawa T (1984) Analytical Prediction of Cutting Tool. *Wear* 100(1-3):129–151.

[41]   [NAT08] Integrated Computational Materials Engineering: A Transformational Discipline for Improved Competitiveness and National Security, ISBN: 0-309-12000-4, National Research Council, 2008.

[42]   [KON16] Industrial Needs for ICME A. W. A. Konter, H. Farivar, J. Post and U. Prahl, JOM 68 1 (2016) 59
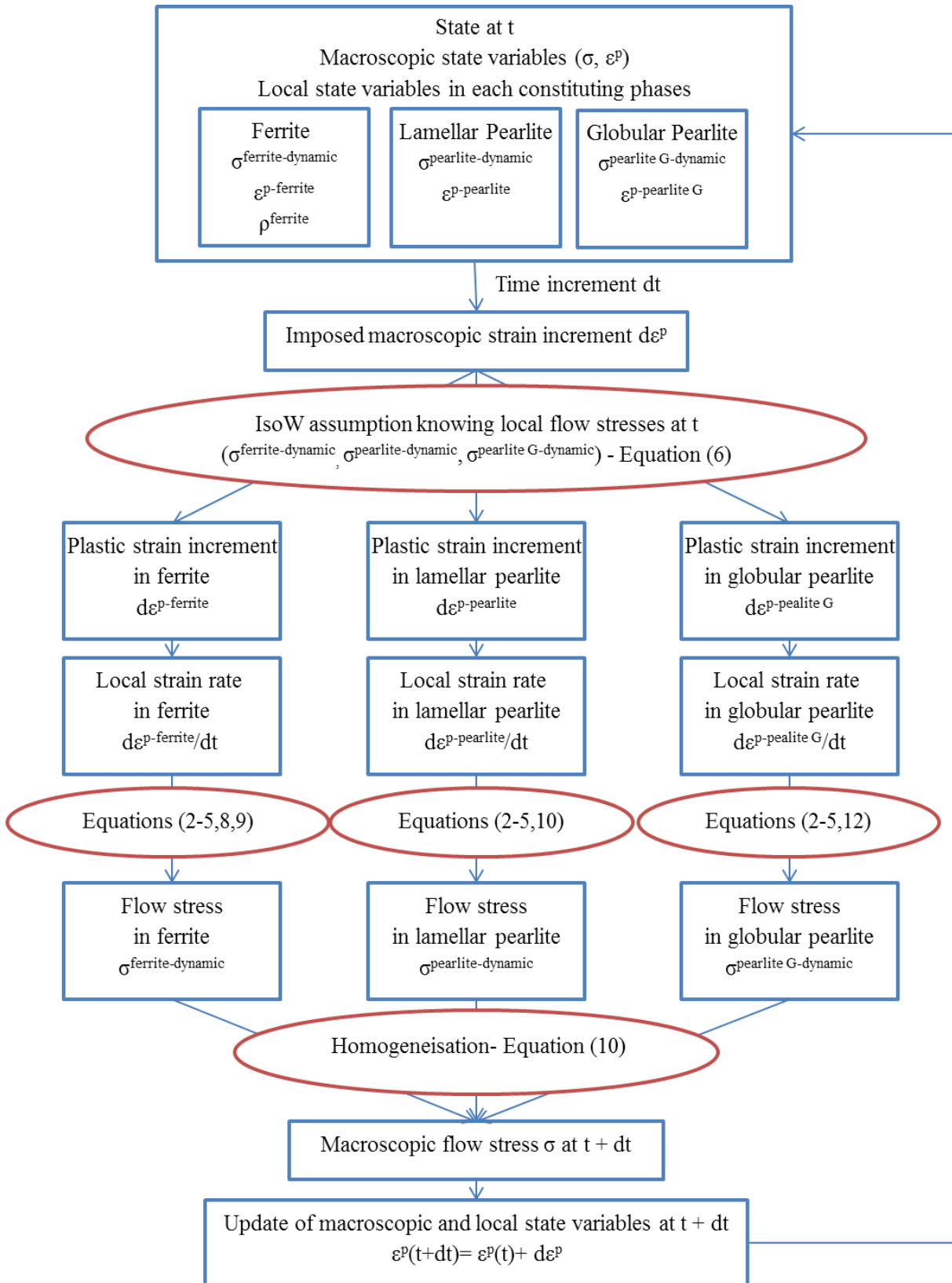
7. Appendices

7.1 Appendices WP2 (rheology)

### 7.1.1 Behavior curves for C45 grade from Gleeble test at different temperature and strain rate
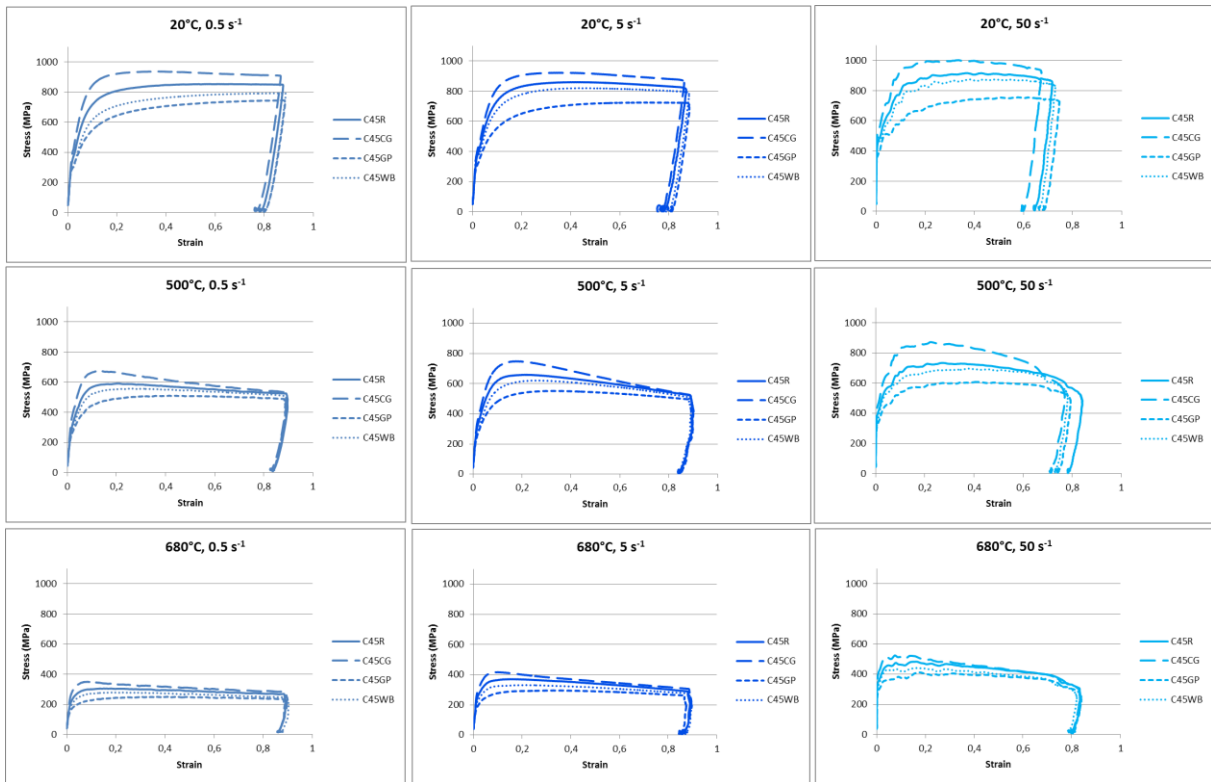
### 7.1.2 Plastic behavior curves for C45 grade from Hopkinson bars test at different temperature and strain rate

105
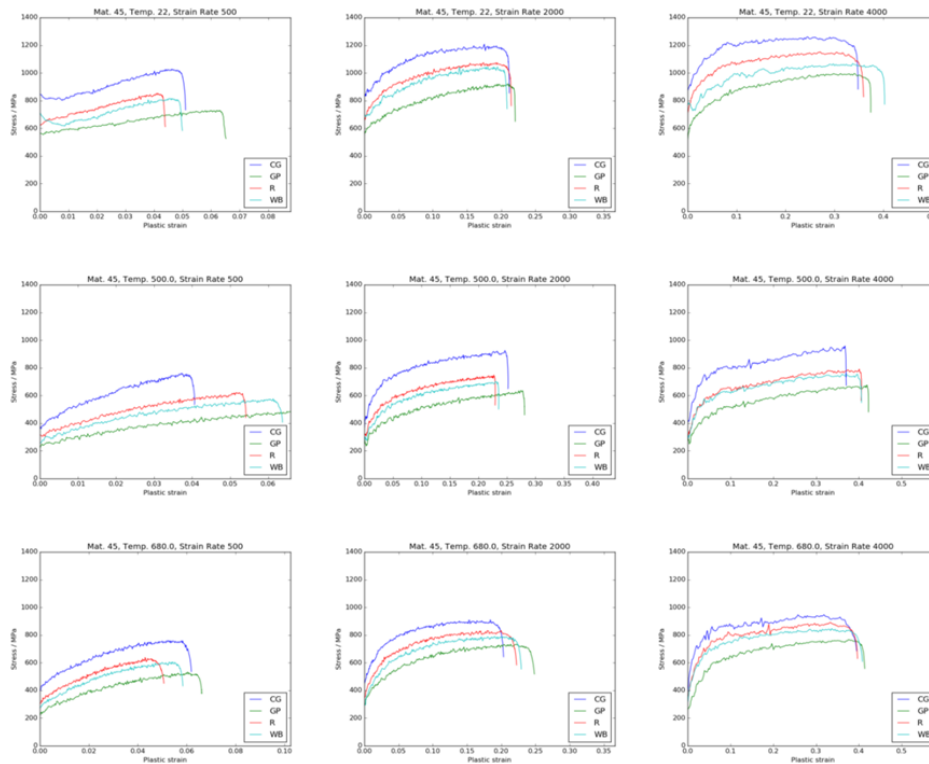
### 7.1.3 Solver algorithm to model the behavior law of P+F materials

State at t
Macroscopic state variables (σ, ε^p)
Local state variables in each constituting phases

Ferrite	Lamellar Pearlite	Globular Pearlite
$\sigma^{\text{ferrite-dynamic}}$	$\sigma^{\text{pearlite-dynamic}}$	$\sigma^{\text{pearlite G-dynamic}}$
$\varepsilon^{\text{p-ferrite}}$	$\varepsilon^{\text{p-pearlite}}$	$\varepsilon^{\text{p-pearlite G}}$
ρ^{ferrite}		

Time increment dt

Imposed macroscopic strain increment $d\varepsilon^p$

IsoW assumption knowing local flow stresses at t
$(\sigma^{\text{ferrite-dynamic}}, \sigma^{\text{pearlite-dynamic}}, \sigma^{\text{pearlite G-dynamic}})$ - Equation (6)

Plastic strain increment in ferrite
$d\varepsilon^{\text{p-ferrite}}$

Plastic strain increment in lamellar pearlite
$d\varepsilon^{\text{p-pearlite}}$

Plastic strain increment in globular pearlite
$d\varepsilon^{\text{p-pealite G}}$

Local strain rate in ferrite
$d\varepsilon^{\text{p-ferrite}}/dt$

Local strain rate in lamellar pearlite
$d\varepsilon^{\text{p-pearlite}}/dt$

Local strain rate in globular pearlite
$d\varepsilon^{\text{p-pealite G}}/dt$

Equations (2-5,8,9)

Equations (2-5,10)

Equations (2-5,12)

Flow stress in ferrite
$\sigma^{\text{ferrite-dynamic}}$

Flow stress in lamellar pearlite
$\sigma^{\text{pearlite-dynamic}}$

Flow stress in globular pearlite
$\sigma^{\text{pearlite G-dynamic}}$

Homogeneisation- Equation (10)

Macroscopic flow stress σ at t + dt

Update of macroscopic and local state variables at t + dt
$\varepsilon^p(t+dt) = \varepsilon^p(t) + d\varepsilon^p$

7.1.4 Results of the modelling for the C45 R grade at room temperature and at 500°C, for the different strain rate
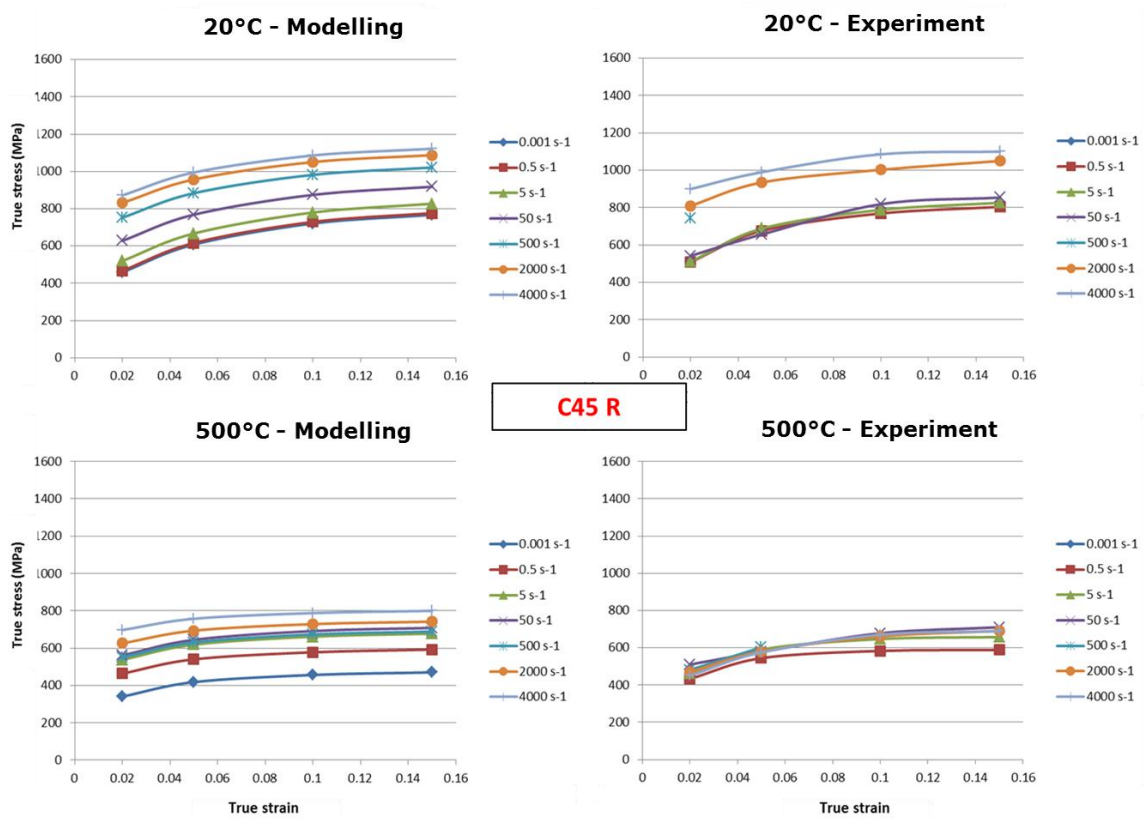
7.1.5 Results of the modelling for the 16MnCr5 CG grade at room temperature and at 500°C, for the different strain rates.
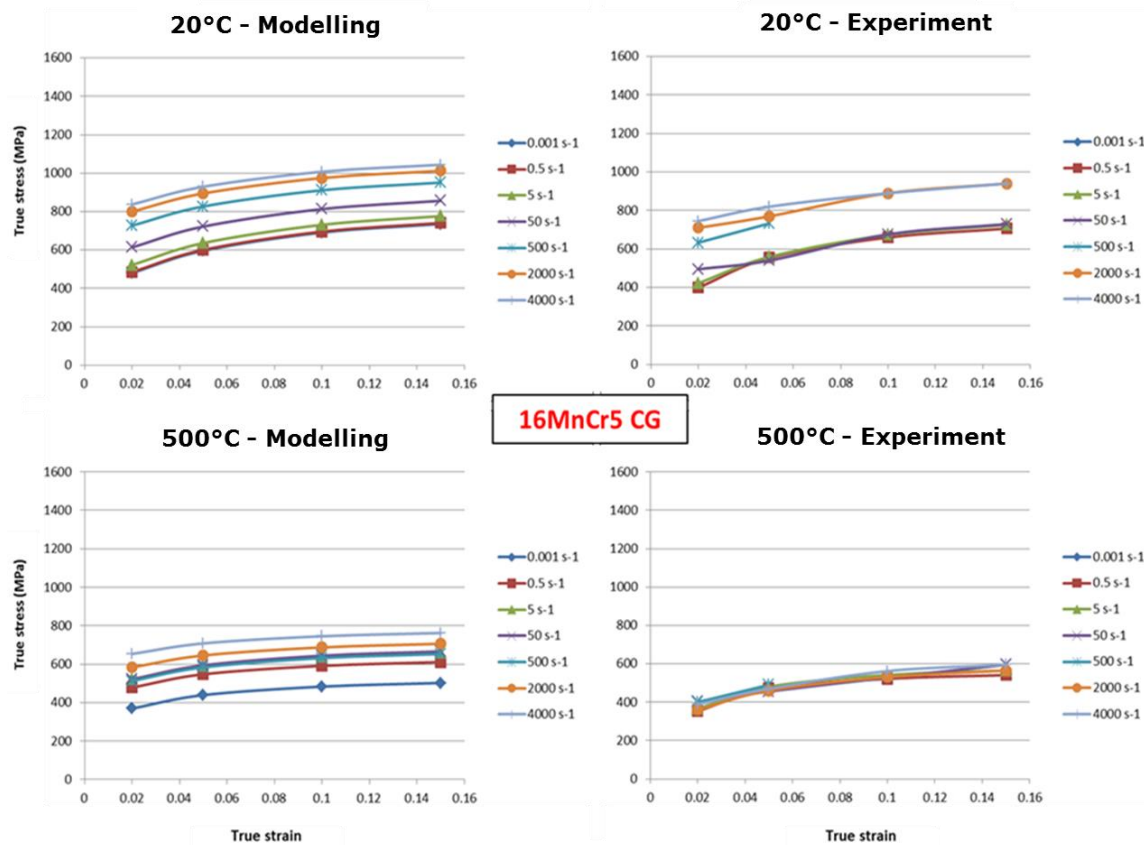
7.1.6 Comparison between the modelled and the experimental data for C45R grade at 500°C and 50 s^{-1}.
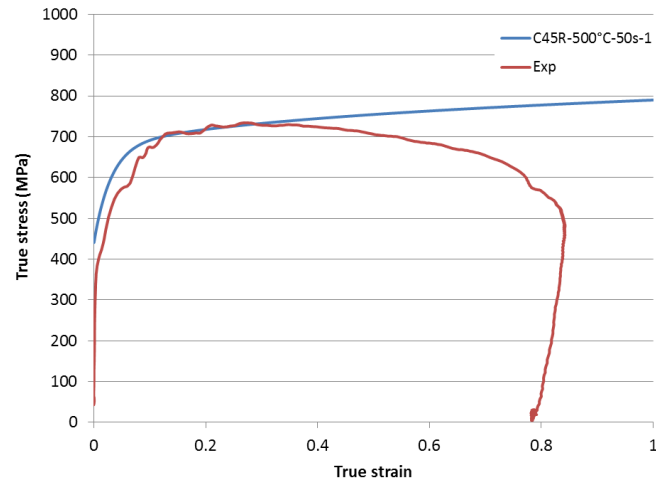
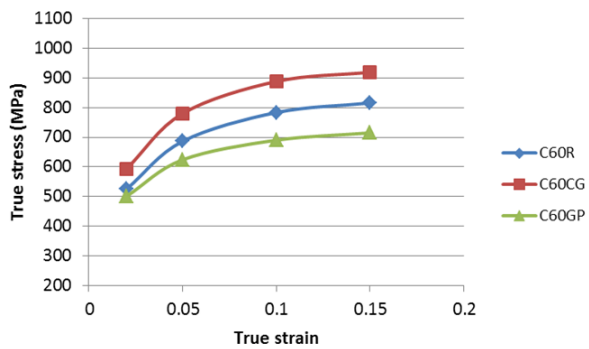### 7.1.7 Comparison between the modelled and the experimental results regarding the influence of variants for C45 (up) and C60 (bottom) at 20°C and 0.5 s^{-1}
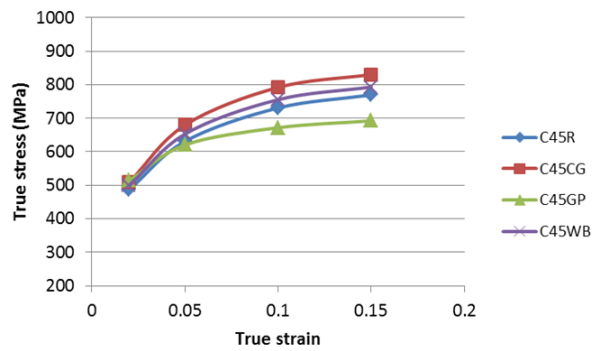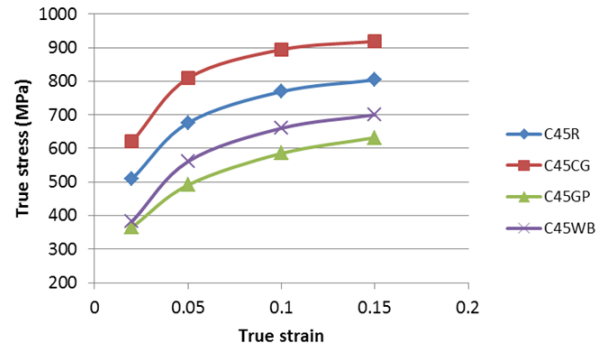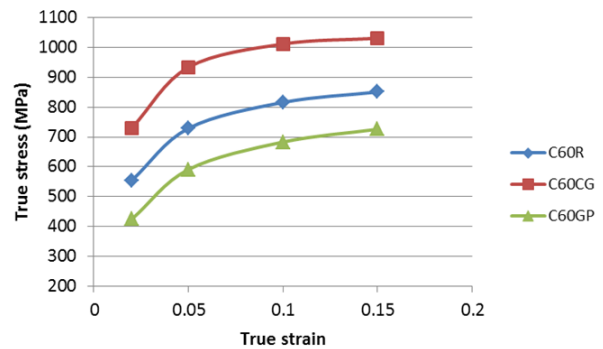
7.1.8 Summary of the parameters and constants used in the model - possible improvements

Group	Parameters /contant	Meaning	Type	Improvement
Microstructure	d	Ferritic grain size	Material constant	
	F	Lamellar pearlite fraction phase		
	F_G	Globular pearlite fraction phase		
	s	Interlamellar spacing		Evolution of s with the deformation
	$d^{\alpha G}$	Ferritic grain size inside globular pearlite		
	d_m	Size of carbides (cementite in globular pearlite)		
	F_m	Fraction of cementite		
Hardening	n_0	Critical density of geometrically necessary dislocations	Parameters calibrated on literature data	Can be adjusted
	λ	Shear bands density		Can be adjusted
	f	Dynamic recovery		Can be adjusted
	k_0	Latent hardening		Can be adjusted
	b	Burgers vector	Material constant	
	M	Taylor factor	Parameters calibrated on literature data	
	α	Forest hardening coefficient for ferritic phase		
	f_G	Dynamic recovery for globular pearlite	Parameters calibrated on this study	
	r	Saturating parameter of isotropic hardening		
	r'	Saturating parameter of kinematic hardening		
	K	Fitting parameter of hardening law for pearlite		
	g_1	Fitting parameter of hardening law for pearlite relative to the temperature dependence		The dependency to temperature could be adjusted with a non-linear formulation
	g_2	Fitting parameter of hardening law for pearlite relative to the temperature dependence		
	Θ^{IV}	Stage IV of hardening for pearlite		A non-linear formulation could be proposed
Dislocation dynamics	k_b	Boltzmann constant	Material constant	
	ν_0	Debye frequency		
	ρ_m	Mobile dislocation density		
Viscoplasticity **of pearlite** (low temperature)	V*	Activation volume of pearlite	Parameters calibrated on this study	
	ΔG_0	Activation energy of pearlite		
Viscoplasticity **of ferrite** (low temperature)	V*	Activation volume of ferrite		
	ΔG_0	Activation energy of ferrite		
DSA parameters **for pearlite**	σ^{max}	Maximal stress for DSA		
	ΔT	Temperature range for DSA		
	T_c	Temperature of DSA peak at low strain rate		
	cte1	Constant which describes the T evolution with the speed of DSA peak		
DSA parameters **for ferrite**	σ^{max}	Maximal stress for DSA		These parameters were fitted on F-P grades after identifying the parameters for pearlite; they could be identified on ferritic grades
	ΔT	Temperature range for DSA		
	T_c	Temperature of DSA peak at low strain rate		
	cte1	Constant which describes the T evolution with the speed of DSA peak		

7.2 Appendices WP3 (tribology)

7.2.1 Experimental set-up of ENISE

a. Description of the experimental setup

The tribometer is a specific device mounted in a NC lathe and developed to carry out frictional tests. The shows a detailed view of the setup and highlights the principle, sliding configuration and existing instrumentation.

The principle of this experimental set up is illustrated in the Figure 78. A cylindrical bar, made on the investigated material, is fixed in the chuck and by the tailstock (Figure 78a). A pin, having a spherical geometry, is pressed onto the cylindrical surface by means of a hydraulic jack (Figure 78c). An axial movement combined with the rotation of the bar leads to a helical movement (Figure 78f). The sphere–plane contact configuration has been chosen in order to reach a sufficient contact pressure and to avoid the risk of chip formation.
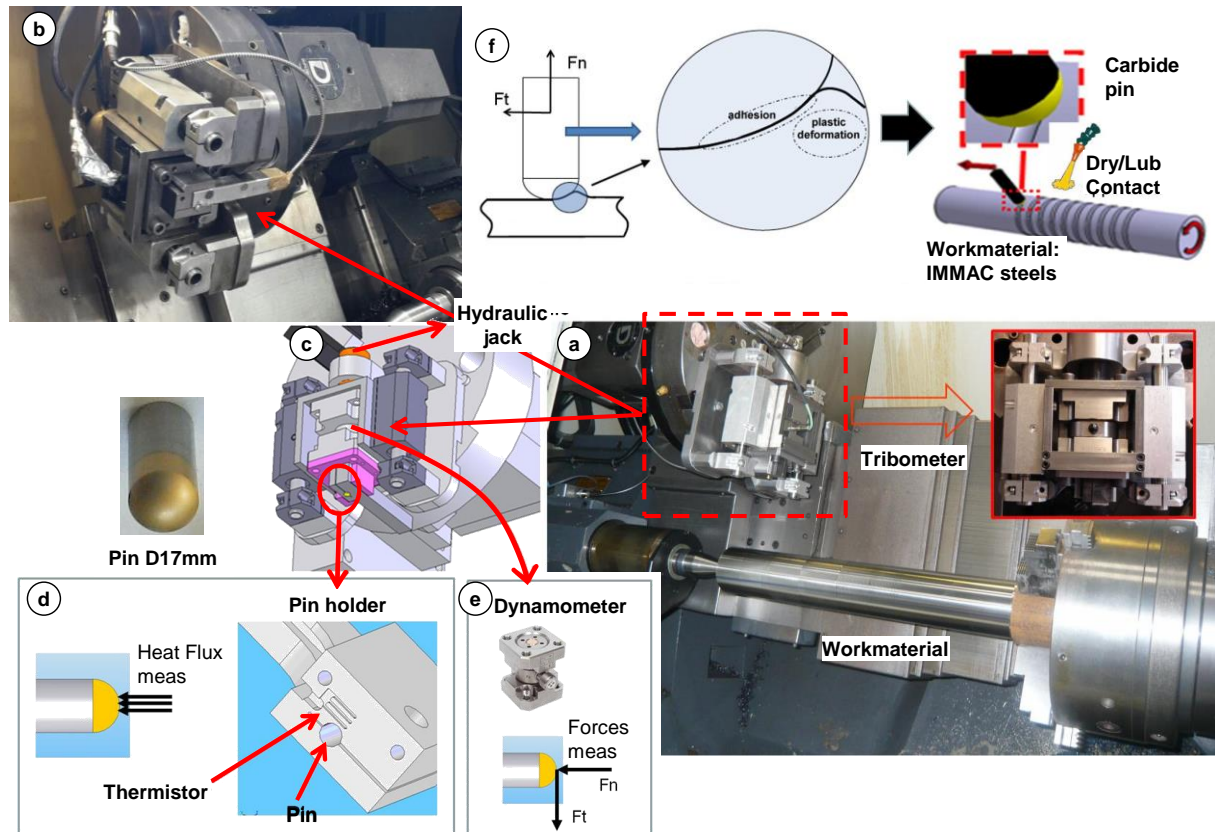
Figure 78: Detailed view of the setup: a) tribometer and workmaterial, b-c) view of the tribometer on the turret, d-e) existing instrumentation and f) close view on the sliding configuration.

After each frictional test, a cutting tool refreshes the scratched surface in order to prepare it for the following one. Each friction test has 10 seconds duration approximately and it has been replicated 3 times in order to estimate the uncertainty.

b. Work material and friction pins

The workmaterial has been provided in bars of Ø60-65 x 500mm and it was disposed on the lathe as seen in the Figure 78a. The tests were performed from the tailstock to the chuck.

Cutting tools are simulated through pins having a spherical geometry and made of cemented carbide with a similar grade to the one used for turning tools (10%Co – 90%WC) or in M35 HSS for the broaching operation. When needed a TiN layer was deposited by Physical Vapor Deposition (PVD). In order to eliminate the potential influence of surface roughness, pins have been polished to reach a low surface roughness (Ra < 0.3 µm) which is coherent with a typical surface roughness on a finely ground cutting tool. Each of them was cleaned in Acetone and Ethanol prior to the tests to remove any trace of grinding oil and polishing residues.

c. In-situ measurements

Each pin is maintained by an instrumented pin-holder (Figure 78d). The pin-holder is fixed onto a dynamometer in order to provide the apparent normal Fn and tangential force Ft (macroscopic forces) (Figure 78e). The apparent friction coefficient is provided by the ratio between the tangential and the normal forces.

$$\mu_{app} = \frac{F_t}{F_n}$$

During a test, the heat flux transmitted to the pin is quantified by means of an inverse methodology. The latter is based on a temperature measurement located in the pin-holder and on the identification on a heat transfer function specific to the system pin and pin-holder. This function provides the link between the average heat flux transmitted to the pin on a given contact zone and the temperature recorded in the pin-holder.

The following equation provides the total amount of energy dissipated in the contact (with μ: macroscopic friction coefficient – F_n: normal load – V_{sl}: sliding velocity):

$$\varphi_{tot} = \mu \times F_N \times V_{sl}$$

It is then possible to assess the heat partition coefficient representing the percentage of heat transferred from the interface to the pin:

$$\alpha = \frac{\varphi_{pin}}{\varphi_{tot}}$$

7.2.2 Experimental set-up of CRF

a. Description of the experimental setup

CRF used a "cylinder on disc" configuration to conduct the wear tests, with two different test rigs. A rotating disc, simulating the workpiece, is adjusted to the rotating shaft of the tribometer and a counterpart cylindrical pin simulating the machining tool is then pressed against the disk periphery (Figure 79). The steel variants bars Ø60mm were provided by ASCO and GERDAU, CRF and ASCO machined the disc specimens. Counterpart cylinders Ø8mm were provided by Gühring.

Two sets of testing conditions were applied and, as it can be seen from Figure 79 test rig used for test conditions nr.2 is equipped with a rigid lateral support that allows a better alignment of the stationary coated cylinder (pin) against the rotating disc. The two test conditions sets covered a velocity range from 26m/min to 147m/min corresponding to the drilling machining processes. Test duration was respectively 2.5 hours and 30 min. High contact pressure was applied (> 1 GPa) in all the tests. A single substrate and coating was employed for all the tribological experiments (WC-Co + TiAlN standard used for drilling tools at FCA). Accu-lube fluid was used to lubricate the contact area during the experiments with a 1 ml/min flow rate. Each steel variant was tested at least two times per each set of parameters, a third repetition was applied in case a too large discrepancy observed between the two first trials.
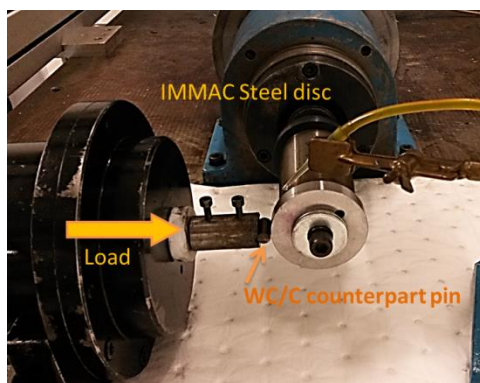
Close tribometer used for Test 1
(26 m/min)
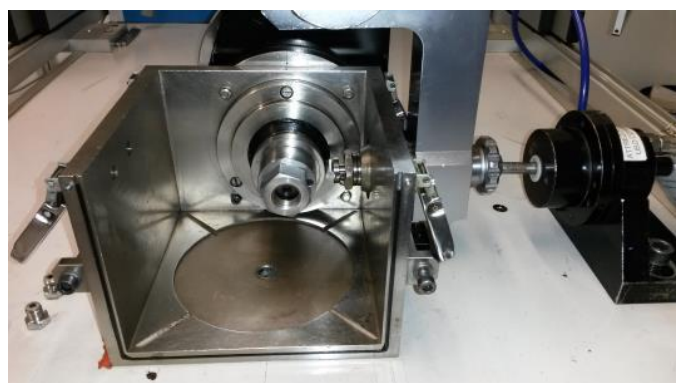
Close tribometer with rigid lateral support used – better
alignment – Used for Test 2 (147 m/min)

Figure 79: Test rigs used @ CRF

During the tests the Coefficient of Friction (in the following referred as CoF) was continuously recorded and after the tests the wear track width was measured by optical microscopy; in addition Test 2 wear scars were analysed by SEM/EDS to check the qualitative composition of the surface of the pin in and around the wear track and evaluate the abrasion/adhesion mechanisms occurred (Table 22).

7.2.3 Analyses of pin wear tendency at 300 m/min

The selected sliding velocity of 300 m/min is interesting as different worn areas can be seen whereas friction was really close from one variant to another.
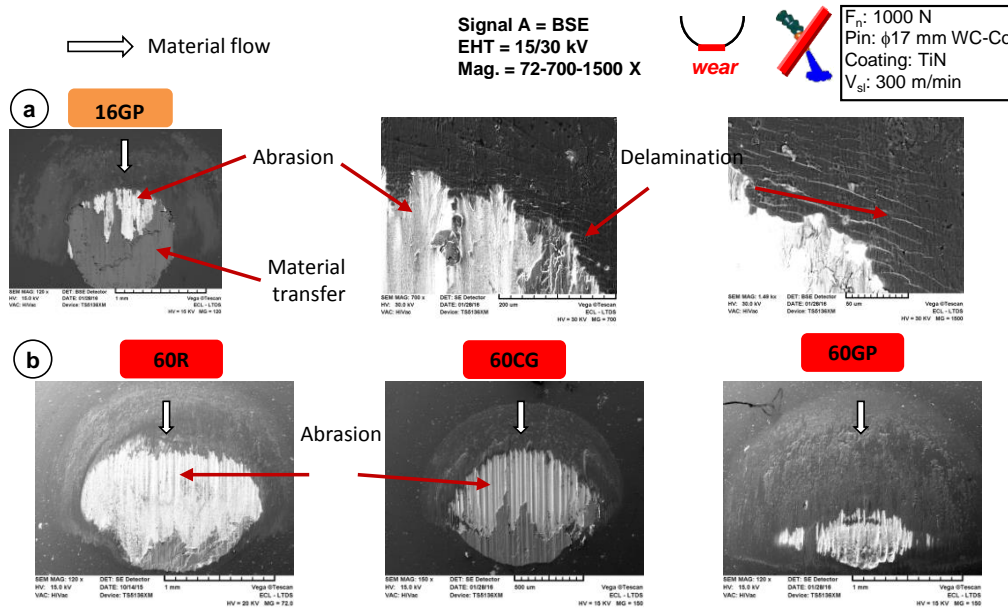
Figure 80: Wear mechanisms observed on some variants: a) 16 Globular Pearlite (GP), b) all the C60 variants.

7.2.4 Drilling oriented tests: pin contact zone analysis under MQL

STEEL GRADES	Structure Status			
	R	CG	GP	WB
27MnCr5				
C45				

Table 22: EDX maps of the friction pins obtained at 147 m/min (Green → TiAlN coating; Blue → substrate ; Red → adhered steel ; Yellow → lubricating fluid traces)

7.2.5 Mechanical and thermal contact models

Results of first compaign (WC-CO + TiN coating pins) were plotted versus several material parameters Figure 81. The large deviation observed on the interlamellar spacing did not enable to properly identify a friction model pendent on this parameter. The most relevant parameter appeared to be the ferrite-pearlite ratio.
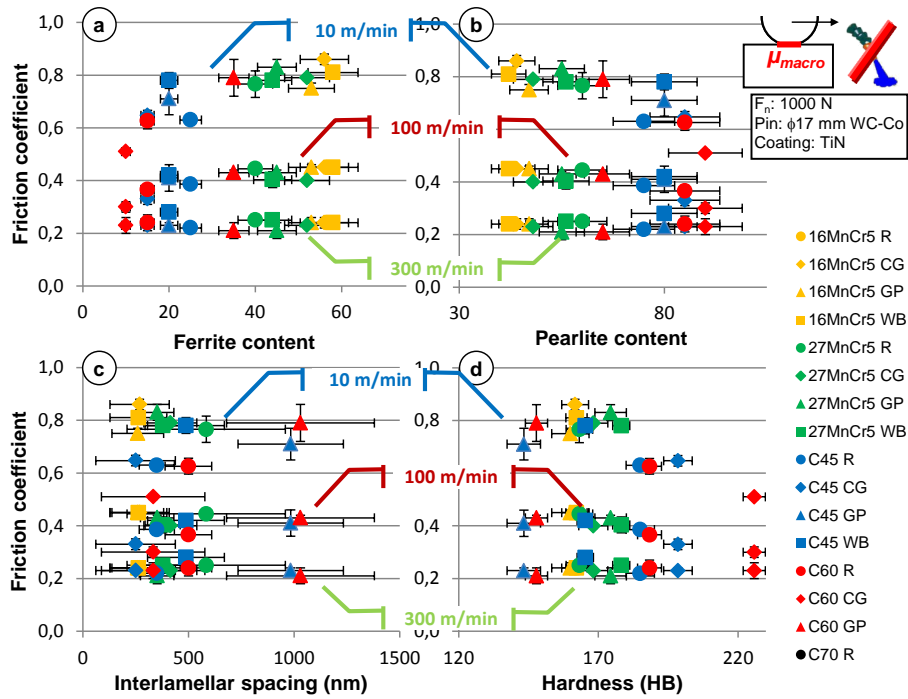
Figure 81: Friction coefficient plotted against ferrite-pearlite microstructural parameters: a) ferrite content, b) pearlite content, c) interlamellar spacing and d) macro hardness.

7.2.6 Mechanical and thermal contact models – Comparison

The Figure 82 shows the comparison between the experimental data and the friction values provided by the developped contact models.
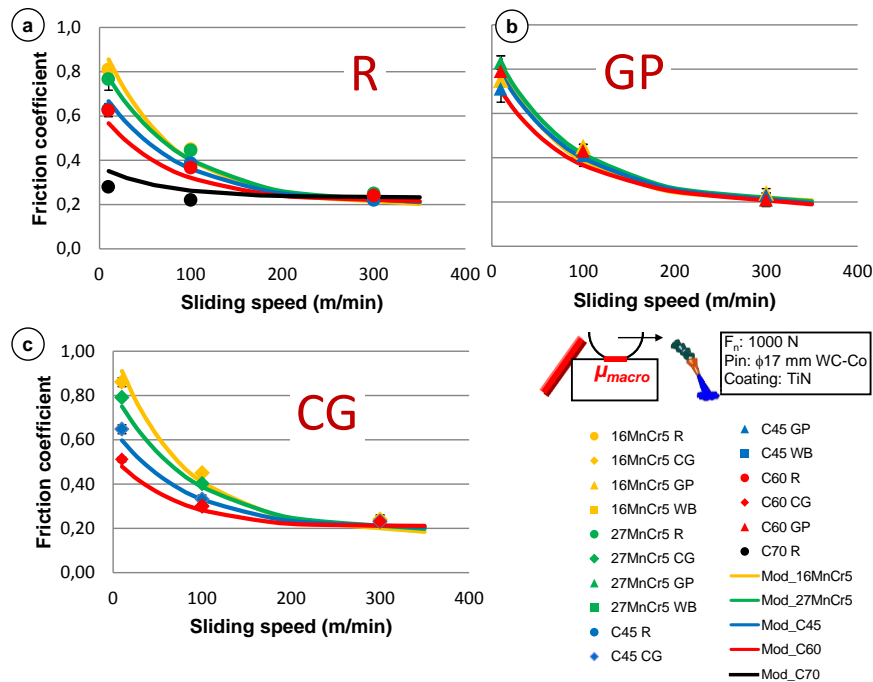
Figure 82: Comparison between the experimental data (items) and the friction coefficients computed by the proposed friction model (lines) focusing on a) the standard variants (R), b) the globular pearlite variant (GP) and c) the pearlite coarse grain variants (CG).

7.3 Appendices WP5 (turning)

7.3.1 Schematic representation of the ALE turning model
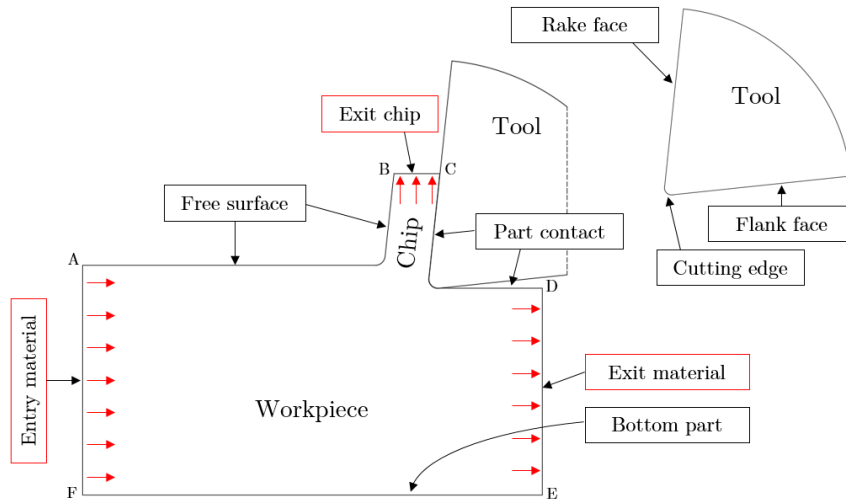
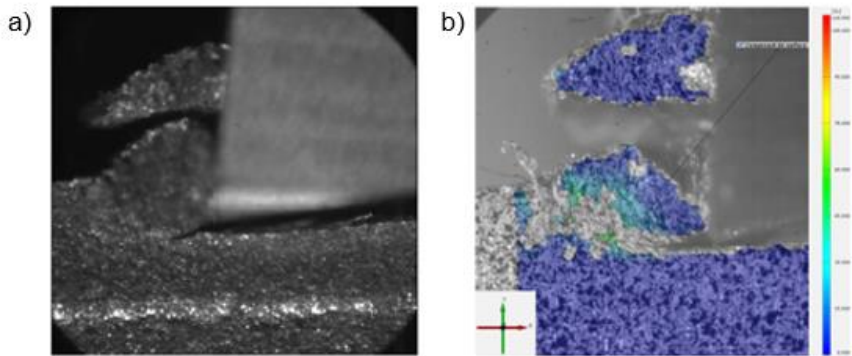#### 7.3.2 Mechanical and thermal boundary conditions of the ALE model
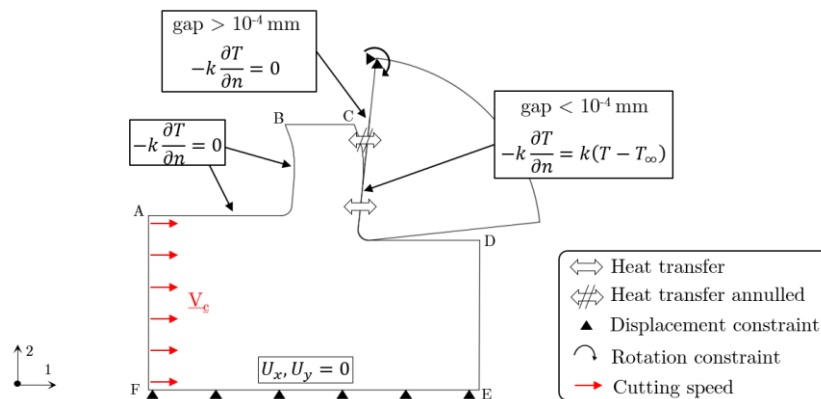
7.3.3 Discretized mesh of the ALE model
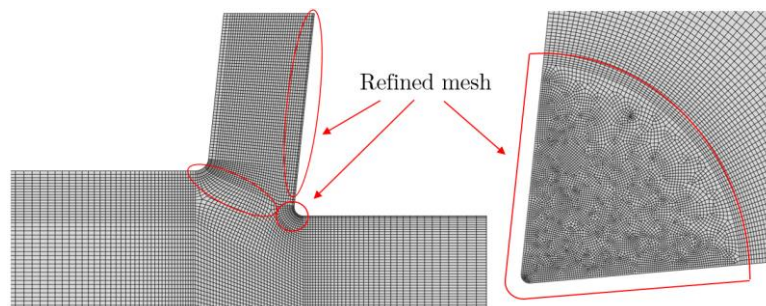
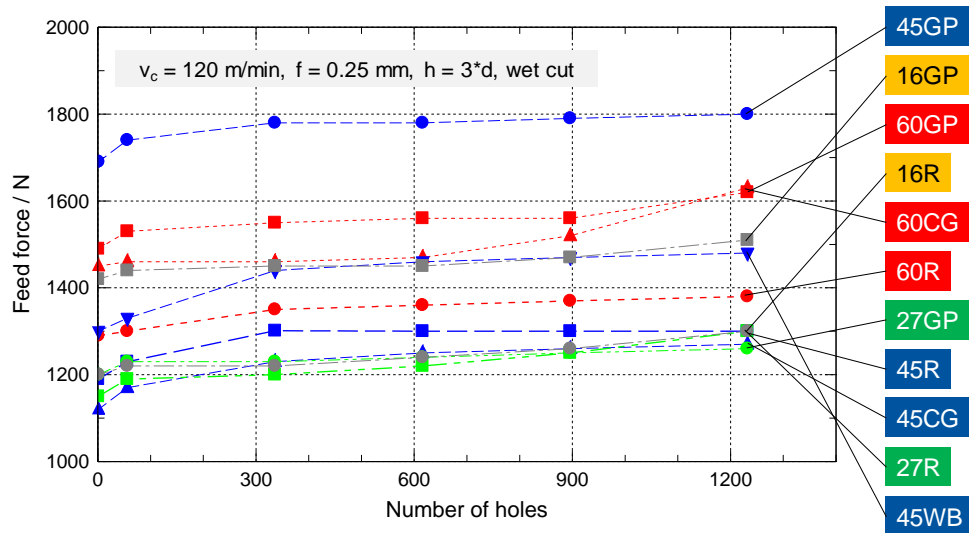### 7.3.4 Orthogonal cutting set-up
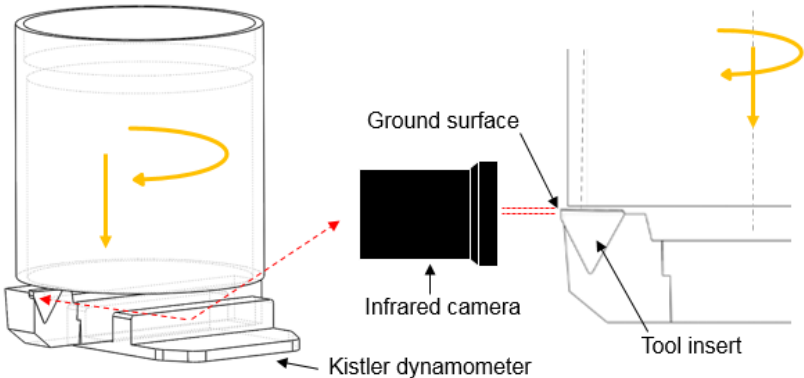
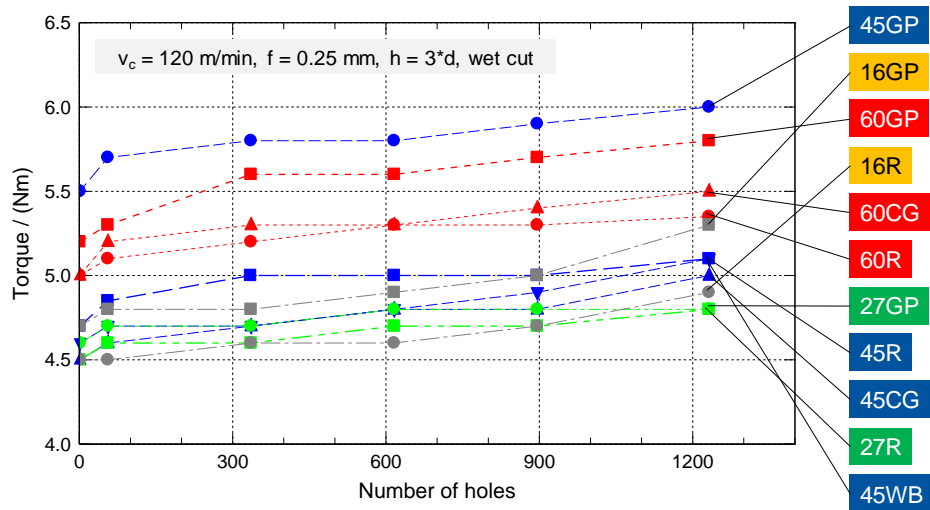### 7.3.5 Chip forming of the cutting orthogonal process

a) Image obtained with high-speed camera; b) Strain measurement attempt in C60R steel variant
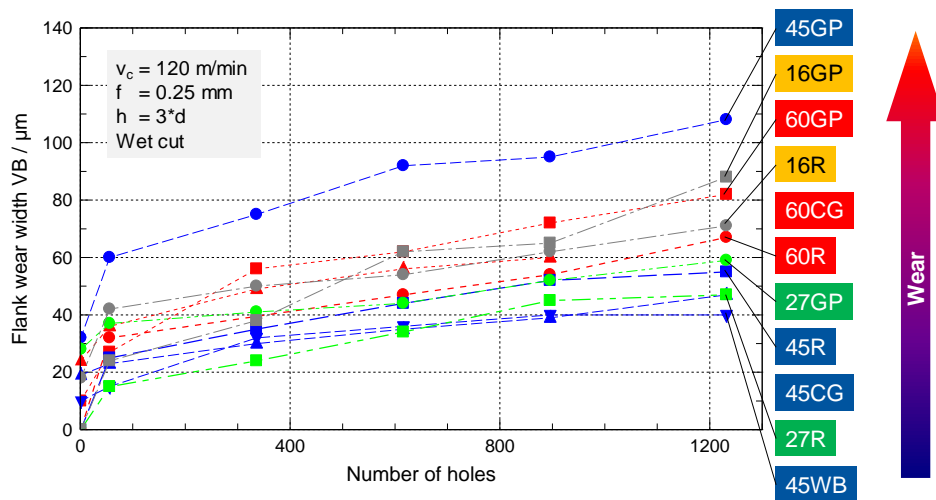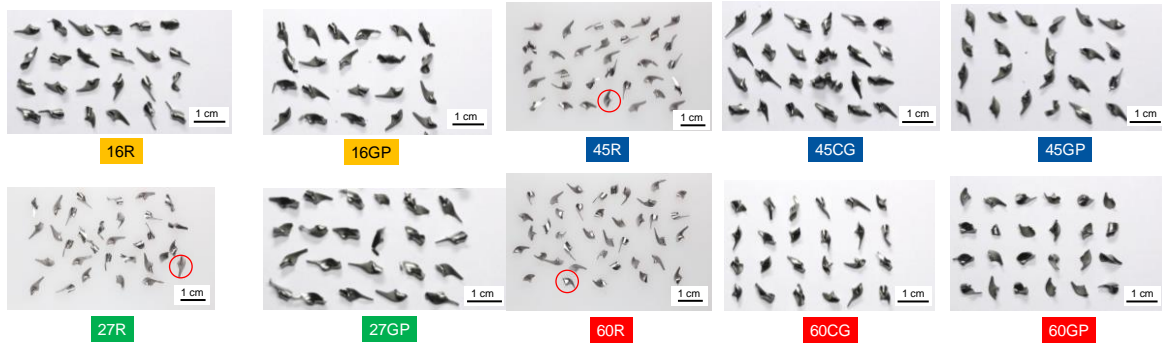
7.4 Appendices WP6 (drilling)

7.4.1 Feed force over the number of the drilled holes

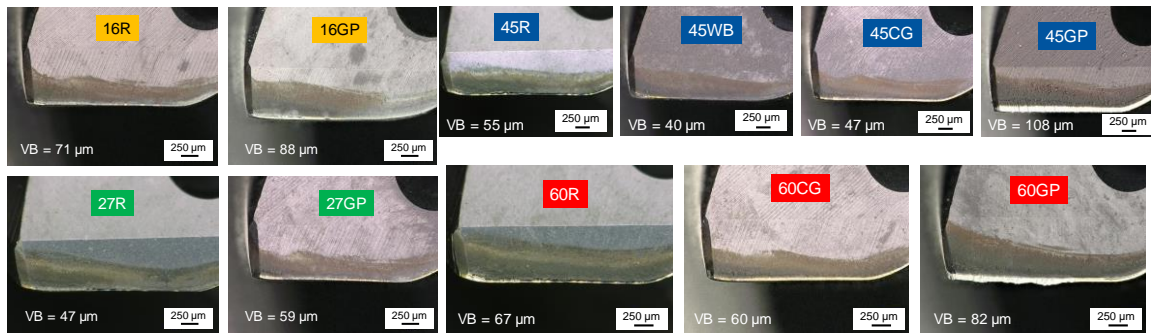### 7.4.2 Cutting torque over the number of the drilled holes

7.4.3 Tool wear development when drilling

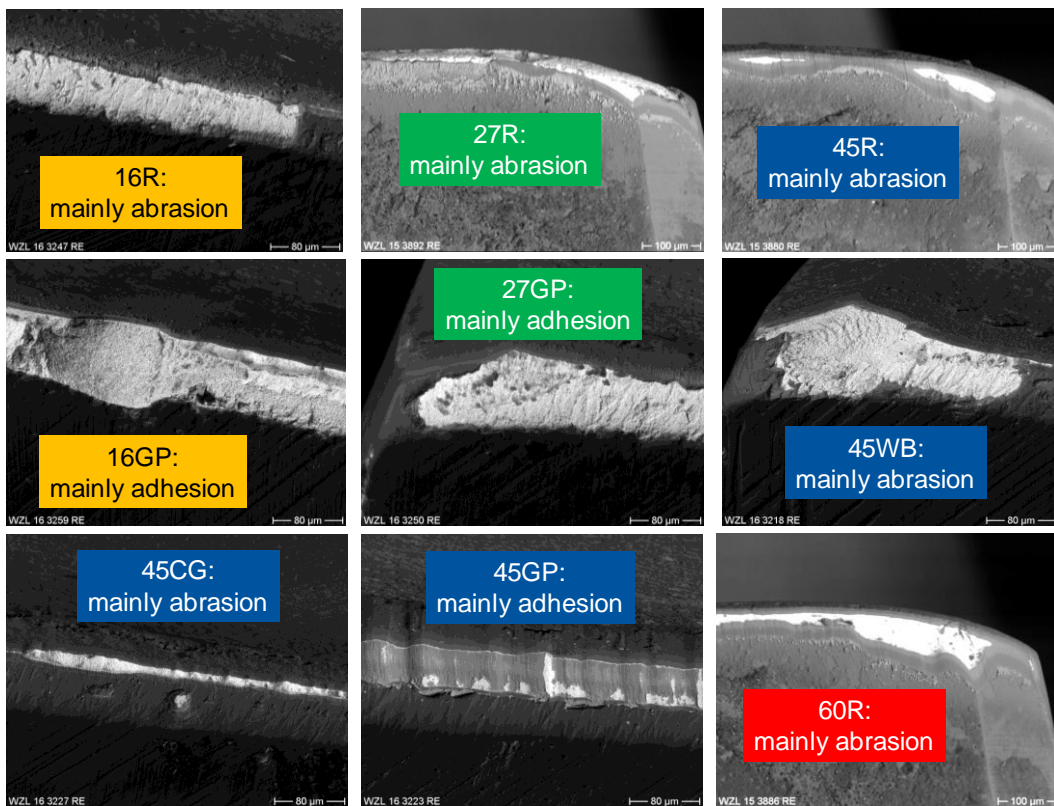## 7.4.4 Chip form when drilling the studied steel variants

16R | 16GP | 45R | 45CG | 45GP

27R | 27GP | 60R | 60CG | 60GP

7.4.5 Tool wear on the cutting edge after hole 1232

16R — VB = 71 µm | 16GP — VB = 88 µm | 45R — VB = 55 µm | 45WB — VB = 40 µm | 45CG — VB = 47 µm | 45GP — VB = 108 µm

27R — VB = 47 µm | 27GP — VB = 59 µm | 60R — VB = 67 µm | 60CG — VB = 60 µm | 60GP — VB = 82 µm

(v_c = 120 m/min, f = 0.25 mm, h = 3*d, wet cut)

7.4.6 Tool wear mechanism after hole 1232

16R: mainly abrasion | 27R: mainly abrasion | 45R: mainly abrasion

16GP: mainly adhesion | 27GP: mainly adhesion | 45WB: mainly abrasion

45CG: mainly abrasion | 45GP: mainly adhesion | 60R: mainly abrasion

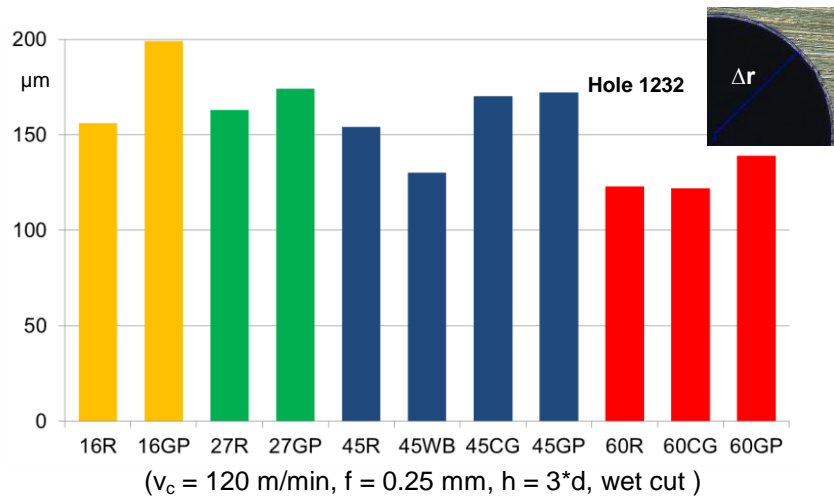(v_c = 120 m/min, f = 0.25 mm, h = 3*d, wet cut)

7.4.7 Surface parameters R_a, R_z when drilling 16MnCr5, 27MnCr5, C45, C60

(v_c = 120 m/min, f = 0.25 mm, h = 3*d, wet cut)

7.4.8 Radial burr formation Δr when drilling 16MnCr5, 27MnCr5, C45, C60

(v_c = 120 m/min, f = 0.25 mm, h = 3*d, wet cut)
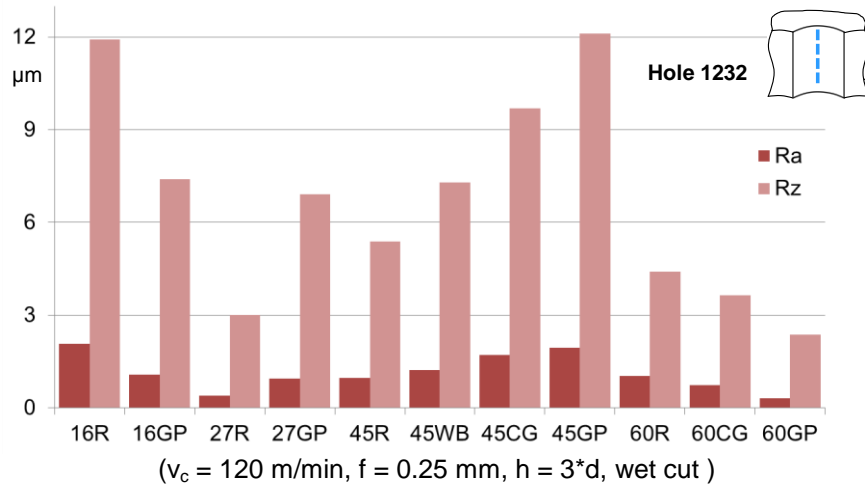
7.4.9 Hole cylindrical form when drilling 16MnCr5, 27MnCr5, C45, C60

(v_c = 120 m/min, f = 0.25 mm, h = 3*d, wet cut)
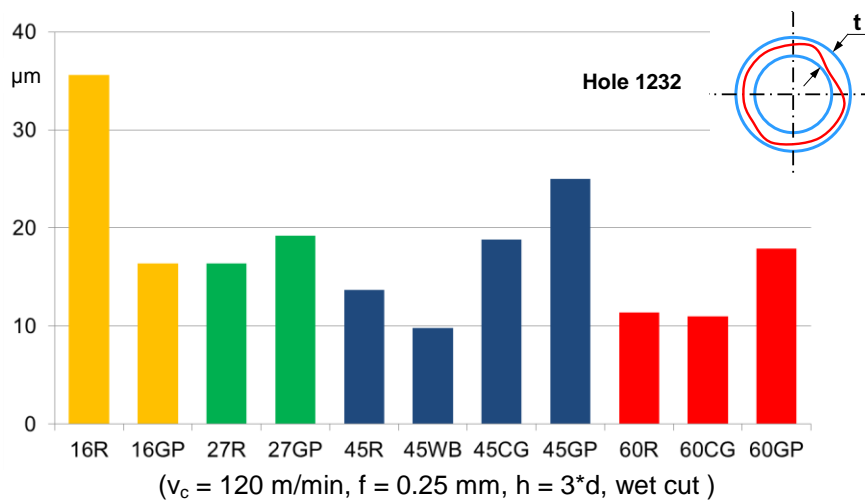
7.4.10 Machinability classification by means of the weighted point evaluation method (for 1232 drilled holes)

Evaluation criterion	Weighting factor	16 R	16 GP	27 R	27 GP	45 R	45 WB	45 CG	45 GP	60 R	60 CG	60 GP
Feed force and torque	10	7	3	8	8	7	6	5	1	4	3	2
Chip form	10	2	1	3	2	7	7	5	6	7	7	8
Tool flank wear	10	3	2	7	6	6	8	7	1	4	1	3
Surface parameter R_z, Ra	5	1	3	7	3	4	3	2	1	5	6	8
Radial burr formation Δr	5	5	1	4	2	5	7	2	2	8	8	6
Hole cylindrical form t	5	1	4	4	3	6	8	3	2	7	7	3
Total utility value (TUV)		155	100	255	200	275	300	205	105	250	215	215
Ranking of the machinability		8	10	3	7	2	1	6	9	4	5	5

Steel grade with the higher machinability

Legend:

C_j, j = 1 - 3:   Investigated cases (cutting conditions)

Weighting factor (W_i):   1 (less important) to 10 (very important)

Utility value (UV_{ji}):   1 (worst case) to 8 (best case)

$$TUV_{,j} = \sum_{i=1}^{3} W_i \cdot UV_{ji}$$

7.5 Appendices WP7 (broaching)

7.5.1 Experimental set-up

Details of the first broaching configuration and implementation of the high speed imaging technique.
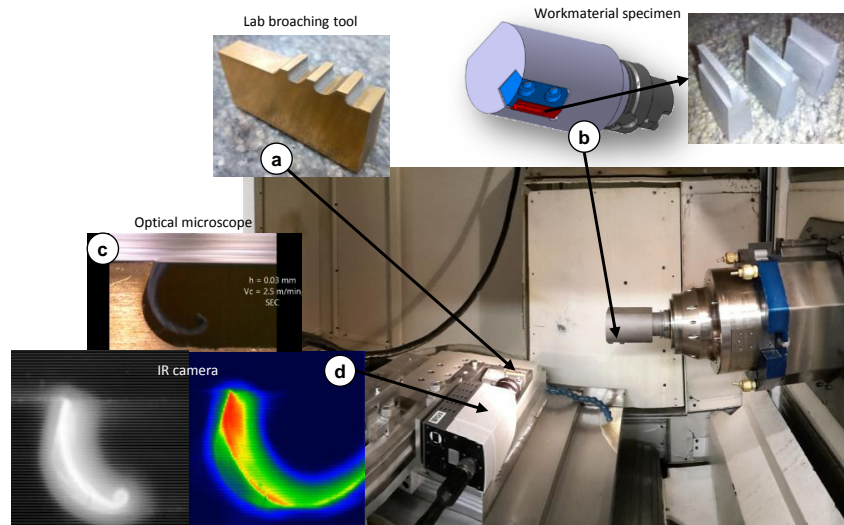

Figure 83: Overview of the experimental setup with a) the lab broaching tool, b) the workpiece specimen, c) imaging with a simple microscope and d) view from the IR camera.

The broaching tool is simplified to a single row of teeth. A simple specimen is also manufactured from each variant and is considered as the workpiece. It is fitted on a specific holder in the spindle whereas the broaching tool is fixed onto the machine table. A strain gauge dynamometer was used to record online the machining forces. With this configuration, it is also possible to set a camera that will focus on the phenomena occurring in the cutting zone. Figure 83 shows a detailed view of the set-up with the tool (a), specimen (b) and camera (c-d).

Figure 83c shows for example a view of the chip formation during broaching obtained at low cutting speed (2.5 m/min) with a simple microscope. Figure 83d shows what can be observed when an infrared camera is employed: on the left, the gray level map can be used to extract tool-chip contact length and chip curvature whereas on the right, a luminance map can be analysed to identify heat generation zones.

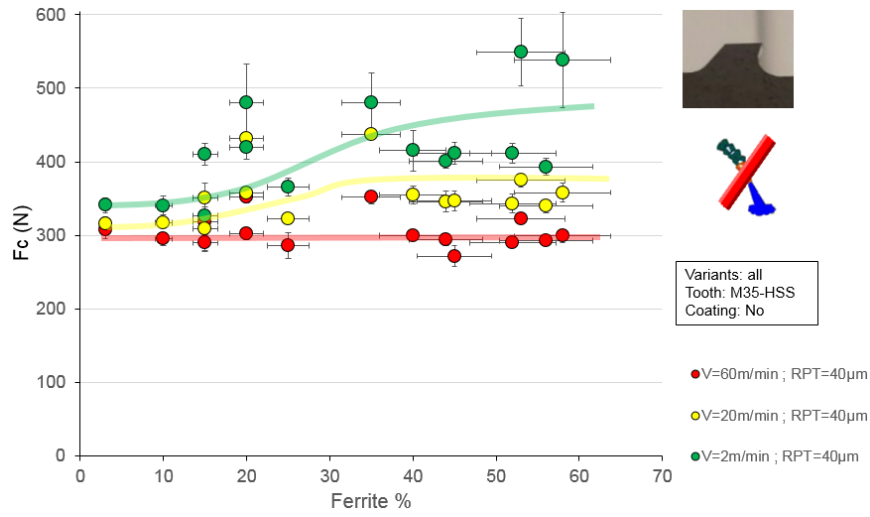### 7.5.2 Results of the full experimental campaign
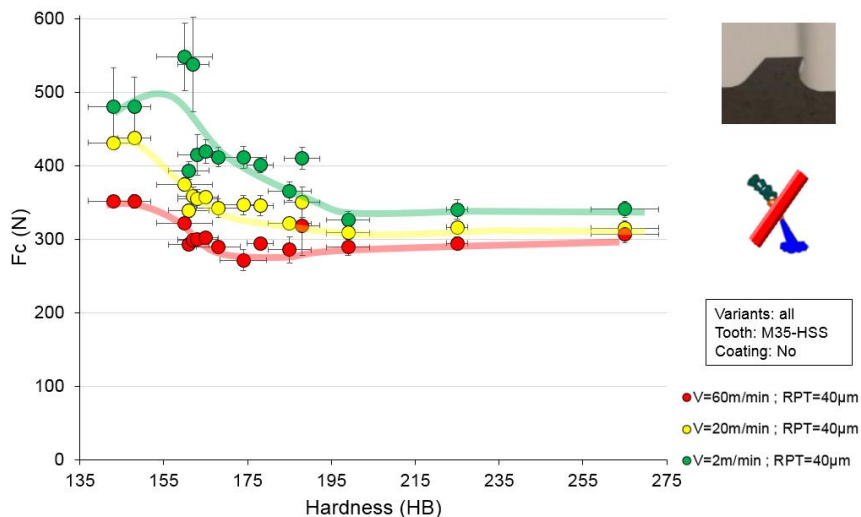
Figure 84: Broaching cutting forces versus hardness and ferrite content when changing speed.
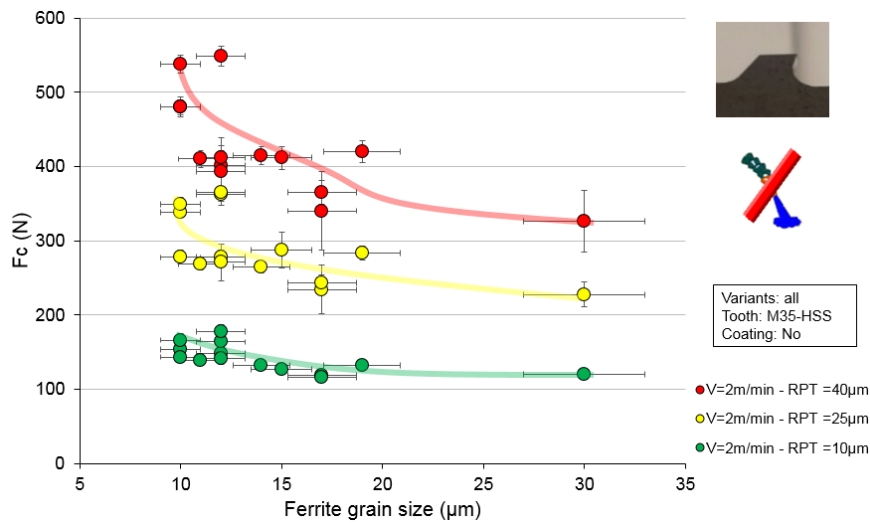

Figure 85: Broaching cutting forces versus ferrite grain size when changing rise per tooth.

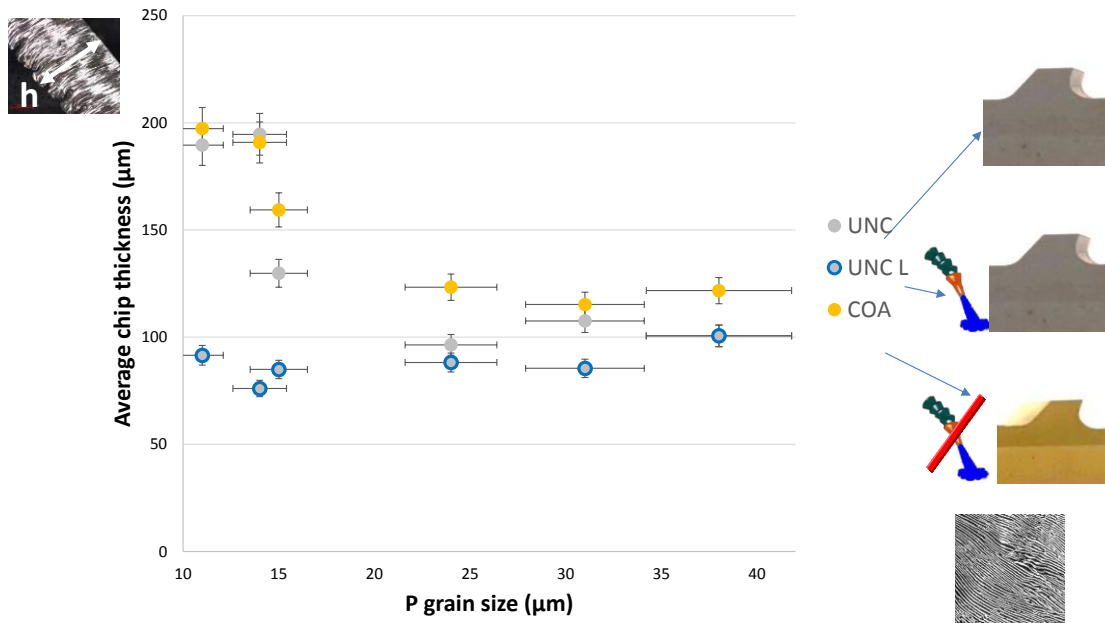### 7.5.3 Additional results – Cutting mechanisms

Figure 86 : average chip thickness versus perlite grain size.

7.5.4 Specific scale effects when broaching a FP steel

According to the low rise per tooth (RPT) existing in broaching, one cannot neglect the fact that the material is being cut at the scale of the grain size. Thus, it is even more difficult to consider the workmaterial as homogeneous.
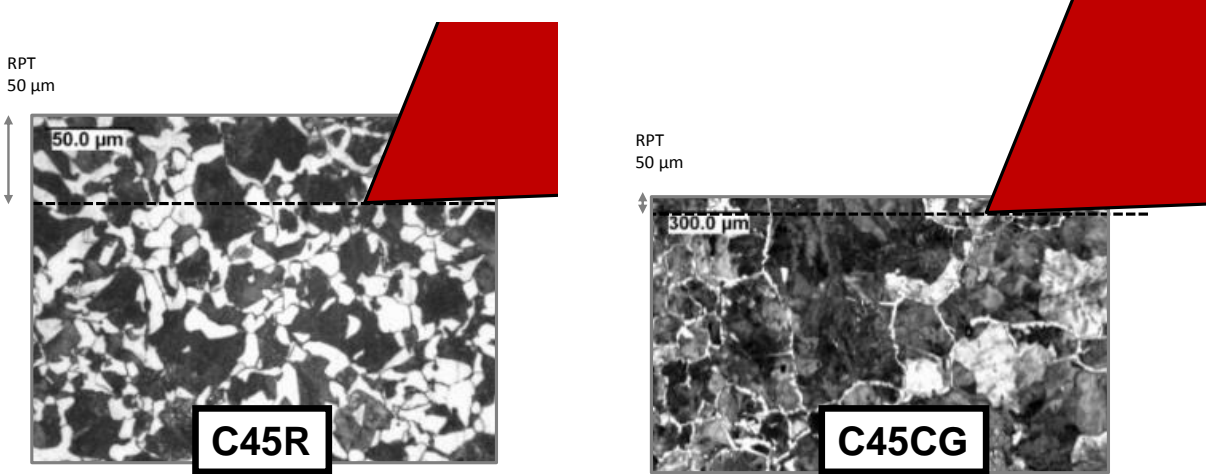

Figure 87 : illustration of the scale effects to consider when cutting a) a standard C45R and b) a coarse grain C45CG with a RPT of 50µm

Getting in touch with the EU

In person

All over the European Union there are hundreds of Europe Direct information centres. You can find the address
of the centre nearest you at: https://europa.eu/european-union/contact_en

On the phone or by email

Europe Direct is a service that answers your questions about the European Union. You can contact this service:

– by freephone: 00 800 6 7 8 9 10 11 (certain operators may charge for these calls),

– at the following standard number: +32 22999696 or

– by email via: https://europa.eu/european-union/contact_en

Finding information about the EU

Online

Information about the European Union in all the official languages of the EU is available on the Europa website
at: https://europa.eu/european-union/index_en

EU publications

You can download or order free and priced EU publications at:
https://publications.europa.eu/en/publications. Multiple copies of free publications may be obtained by contacting Europe Direct or your local information centre (see https://europa.eu/european-union/contact_en).

EU law and related documents

For access to legal information from the EU, including all EU law since 1952 in all the official language versions,
go to EUR-Lex at: http://eur-lex.europa.eu

Open data from the EU

The EU Open Data Portal (http://data.europa.eu/euodp/en) provides access to datasets from the EU.
Data can be downloaded and reused for free, for both commercial and non-commercial purposes.

Production sectors like automotive, mechanical engineering are faced strong competitive constraints from North America and Asia. To keep the European countries competitive, investigations in new research areas and innovation is essential. Integrated Computational Materials Engineering (ICME) is one of most attractive emerging discipline for research and innovation because it can accelerate materials development, unify design and manufacturing, help to create new technology area, and hence provide significant economic benefit. IMMAC project dealt with the use of innovative ICME-Tools in basic research for the machinability evaluation of ferrite-pearlite (FP) steels, including material modelling, cutting simulation and optimization. The objective of IMMAC project is to develop a numerical approach to better design the machinability-improved FP grade tailored to a given machining operation, and more broadly for a given application (type of components). The cutting operations studied are turning, drilling and broaching, mainly used in automotive or engineering components. To this end, a better understanding of thermal stress-strain behaviors, contact mechanisms and thermal properties of FP microstructures and material cutting tool have been achieved. The main parameters of FP microstructure driving the machinability performances were identified for each cutting operation. Moreover, an empirical formulation, only for the drilling, has been developed based on the microstructure parameters. Related model parameters identified through the rheological and tribological tests were used in numerical models to predict qualitative machinability performances of FP steels variants. With the help of numerical and empirical models, an optimized microstructure for crankshaft application could be predicted. Component oriented machining tests have confirmed this microstructure solution.

Studies and reports